QATAR UNIVERSITY

COLLEGE OF ENGINEERING

CRASHWORTHINESS CHARACTERISTICS OF GFRP OVERWRAPPED PVC COMPOSITE TUBES

BY

RAHIB AHMED KHAN

A Thesis Submitted to

the College of Engineering

in Partial Fulfillment of the Requirements for the Degree of

Masters of Science in Mechanical Engineering

January 2021

COMMITTEE PAGE

The members of the Committee approve the Thesis of

Rahib Ahmed Khan defended on 07/12/2020.

Prof. Elsadig Mahdi Saad
Thesis Supervisor

Dr. John-John Cabibihan
Program Coordinator

Dr. Asan G. A. Muthalif
Committee Member

Dr. Tahir I. Khan
Committee Member

Approved:

Khalid Kamal Naji, Dean, College of Engineering

ABSTRACT

KHAN, RAHIB, A., Masters: January: 2021, Masters of Science in Mechanical Engineering

Title: Crashworthiness Characteristics of GFRP Overwrapped PVC Composite Tubes

Supervisor of Thesis: Elsadig M. Saad

This thesis investigates the effect of various factors on the crashworthiness characteristics of GFRP overwrapped PVC tubes. PVC tubes overwrapped in GFRP at four different fiber orientations, 45°, 55°, 65°, and 90°, respectively, were subjected to quasi-static axial compression tests. For the GFRP/PVC samples of different fiber orientations with standard circular tube geometry, load-bearing capacity, crush force efficiency, and energy absorption capability generally improved with increasing fiber orientation. The first proposed design change to the conventional circular composite tube geometry increased specific energy absorbed by an average of 32.52%, while load-bearing capacity was also maintained. However, it also resulted in a noticeable decrease in crush force efficiency. For the second proposed design change to the conventional circular composite tube geometry, the advantage of increased specific energy absorption, seen for the first design change, was retained. At the same time, a sizeable 43.82% average increase in crush force efficiency was also observed. The combination of the two proposed design changes as compared to chamfer triggers was proven to be comprehensively more effective. Finally, foam cores of four different geometries were used to fill the composite tube with the best performance from all previous tests. As compared to the core-less samples, the composite tubes with cores had noticeably higher load-bearing capacity and energy absorption capabilities. However, their crushing failure was not as stable.

DEDICATION

This thesis is dedicated to my parents, Safdar and Sajida, and sister, Farnaaz. They were always there to motivate me when I found it challenging to move forward.

Without them, I would not be where I am today.

ACKNOWLEDGEMENTS

This project was carried out in the Mechanical and Industrial Department of Qatar University, and the author is incredibly grateful to the university and all faculty members who supported the author while working on this project.

The author would especially like to thank the thesis supervisor, Dr. Elsadig, for his guidance and support. The author would also like to thank Dr. Farayi and Dr. Cabibihan for helping to complete this thesis.

TABLE OF CONTENTS

LIST OF TABLES

LIST OF FIGURES

CHAPTER 1. INTRODUCTION

This chapter contains a brief introduction to the investigated problem, detailed objectives, and the study's significance. Also, the general outline of this thesis will be presented in this chapter.

1.1. Background

In passenger vehicles, “crashworthiness” refers to a structure’s capacity to absorb the impact energy from collisions and, in so doing, increase the survivability of the occupants [1]. Crashworthiness explicitly involves controlling this absorption through failure mechanisms and modes so that a stable load profile is obtained during the absorption process [2]. Current legislation (United States) for vehicles necessitates that they are designed such that, if a collision occurs at speeds of up to 15.5 m/sec (35 mph) with a solid, fixed object, the passengers in the vehicle should not be subjected to a resulting force that could produce a net deceleration higher than 20g [3].

The ability to make composites specific to requirements, as well as their comparatively high stiffness to weight and strength to weight ratios, fatigue resistance, and corrosion resistance, makes them very appealing for crashworthiness applications. The challenge is to use specific geometry and materials features to facilitate more excellent safety while concurrently decreasing the weight, without exceeding what would be considered acceptable adverse effects in terms of the overall economics of fabrication and production. In crashworthiness applications, composites are most commonly utilized in tubular structures, which are strategically incorporated into vehicular frames to act as

energy-absorbing devices [4, 5, 6]. The composite tubes employed are also frequently composite tubes with a circular cross-section due to the inherent stability and ease of manufacturing this particular geometry [7]. In recent years, extensive studies have been conducted to investigate the failure mechanism of composite tubes using approaches based on material properties and geometry. Studies done by Abosbaia et al. [8] have shown that segmented composite tubes manufactured from carbon fabric fiber and cotton fabric fiber exhibited satisfactory energy absorption capability and stable load-carrying capacity. Geier et al. [9] reported that axially compressed fiber's buckling behavior is influenced by the sequence of stacking within the laminates. A more detailed study done by Will et al. [10] showed that the sequence of laminate stacking affects the total area of delamination, the location of delamination, and the shear fracture area. Mamalis et al. [11] extensively investigated the crashworthy capability of composite material structures and found that carbon fiber/epoxy shells generally absorb more energy than glass fiber/epoxy or aramid fiber/epoxy specimens. They also stated that specific energy tends to vary with ply orientation. The effect of changing the vertex angle on the energy absorption capability of axially crushed kenaf/epoxy composite elliptical cones was experimentally examined by Alkateb et al. [12]. The vertex angle of the manufactured tubes was varied from 0° to 24° in 6° increments, where the elliptical cone with a vertex angle of 0° was an elliptical tube. The results showed that load carrying capacity and energy absorption capability generally increased with increasing vertex angle. Palanivelu et al. [13] carried out quasi-static compression experiments on composite tubes with nine different geometries. The tested composite tubes were manufactured from unidirectional E-glass fabric and polyester resin using the hand lay-up method. For each geometry, a total of 4 different composite tube

configurations were tested using two varying thicknesses and two different triggering mechanisms. It was found that the conical circular and circular cross-section geometry composite tubes exhibited the best load carrying capacity and energy absorption capability. The sample with the highest crush force efficiency was also a composite tube with a circular cross-section. A substantial proportion of composite applications involve glass fiber reinforced polymers (GFRPs) as composites with other reinforcing material types are often considerably more costly [14, 15]. According to a report on the composites market published by AVK Industrievereinigung Verstärkte Kunststoffe e.V., one of the most significant European associations in the field of composites, the European GFRP market share alone was estimated to be a total volume of 1.141 million tonnes in 2018, accounting for over 90 % of Europe's composite usage in the year. GFRPs still remain the most dominant type of composite in the world's composite market today [16, 17].

While studies have been carried out on the effect of fiber orientation on the crashworthiness characteristics of axially crushed composite tubes, they are still insufficient, especially considering the different constituent materials of the composites and manufacturing methods that may be utilized in these investigations. Therefore, there is a need for more research to enrich the scientific knowledge in this area. Although a considerable amount of work has been done concerning the effect of using different geometries of composite tubes, there is little work done that looks into further improving the performance of existing conventionally used geometries by making custom-made changes to the standard design of the geometry. Instead, several trigger mechanisms are commonly used to enhance the crushing performance of composite tubes. It has been

established that utilizing trigger mechanisms as artificially created failure initiation sites effectively reduces the initial peak crushing force while also ensuring energy absorption is maximized. Without triggering mechanisms, composite tubes' crushing failure usually results in a load profile with an undesirably high initial peak force, followed by a catastrophic drop in load-bearing capacity [18]. The proposed design changes in this study are custom-made for composite tubes with an inner tube and serve as a competitive alternative to conventional trigger mechanisms. The inclusion of foam cores is another method that has been used to strengthen the crashworthiness characteristics of composite tubes [19].

The composites used in the research work, which were manufactured using E-glass fiber as the reinforcement material and epoxy resin as the matrix material, are widely used in the industry. This research focuses on the crashworthiness performance of circular tubes subjected to quasi-static axial crushing. This research aims to study the influence of fiber orientation on crashworthiness properties of cylindrical PVC tubes that have been overwrapped with GFRP using a winding machine. Furthermore, slight changes have been made to the design of conventionally used circular composite tubes to improve further the crashworthy characteristics of the GFRP overwrapped PVC pipes tested. The effectiveness of the proposed design changes is also compared to that of a standard chamfer trigger mechanism. Attention is also given to determine the best performing design between core and core-less composite tubes. Foam material is used to fill the core composite tubes whereas the core-less composite tubes have no filler material in the center.

1.2. Project Objectives

The goals of this study are as follows:

1. To examine the influence of wrapping PVC tubes in GFRP composite on the tubes' crashworthiness performance under quasi-static axial crushing.
2. To study the influence of different fiber orientations on the crashworthiness characteristics of GFRP overwrapped PVC composite tubes under quasi-static axial crushing.
3. To investigate the effects of making slight changes to the conventionally used circular cross-section composite tubes, which allow for the effective utilization of the PVC inner tube and suppression of the initial peak load on the crashworthiness characteristics of GFRP overwrapped PVC tubes.
4. Chamfer triggers of the same fiber orientation as the best performing fiber orientation were compared to the two proposed design changes' combined effect.
5. To examine the differences between core and core-less tubes subjected to quasi-static axial crushing loads and compare their crashworthiness characteristics.

1.3. Significance of the Study

This research's primary focus concentrates mostly on obtaining the composite tube with the best overall crashworthiness characteristics. This is done by maneuvering the fiber orientation of the reinforcement and using the best longitudinal cross-sectional design.

Some practical aspects of using composite materials for crashworthiness applications have been mainly in the automobile and aerospace industry. As both industries

were in full bloom coming into the 21st century, more and more composite materials have been incorporated into automobiles and aircraft [20, 21]. An example of the composite tube applications is its integration into the engine's structure and luggage compartments of automobiles. These composite structures serve as an energy-absorbing device if the car is hit from the front or behind [22, 23]. The ultimate goal is to decelerate the car without injuring the passenger. This is done by crushing the composite in a controllable manner.

Another practical application of composites is its incorporation into the design of modern aircraft. Over the past decades, composites have been regularly used in military aircraft and have seen increased use in large passenger aircraft design. Remarkably, both Boeing's B787 Dreamliner and Airbus's A350XWB composites account for approximately 50% of the construction materials by weight. Composites also allow for aircraft's airframes to be considerably lighter, thereby resulting in greater fuel efficiency [24, 25].

In the end, the challenge is in how to increase the energy absorption capabilities of composite structures without sacrificing the ease of manufacturing and making a cost-effective crashworthy structure suitable for mass-production [26]. It is also crucial that energy absorption occurs in a gradual, stable manner without catastrophic failure and significant fluctuation in load-bearing behavior.

1.4. Thesis Layout

This thesis is divided into five chapters. In the next chapter, Chapter 2 gathers information from related sources regarding the behavior of composite tubes, testing procedures, energy absorption capacity, crushing behavior, and failure mechanisms of composite material. Chapter 3 presents a systematic and detailed description of the methodology used to carry out this research. The results from the various experiments carried out are presented, discussed, and analyzed in Chapter 4. Finally, the findings of this research are presented in Chapter 5.

CHAPTER 2. LITERATURE REVIEW

In this chapter, essential terms related to the research carried out for this thesis are explained, and literature concerning similar work that was previously done is reviewed. Accordingly, information is given on composite materials and their structure, fiber-reinforced composites, matrix materials, fabrication of composites, core materials, parameters that will be calculated from experimental readings, and the failure modes and energy absorption mechanisms of thin-walled composites.

2.1. Composite Materials

Composite materials refer to combining two or more constituent materials on a macroscopic scale to form a third material with characteristics different from the original individual materials. However, as opposed to materials that are combined on a microscopic scale, such as alloys of metals, in the macroscopic examination of composite material, the components can be identified by the naked eye. In materials combined on a microscopic scale, the resulting material appears macroscopically homogeneous for all practical purposes [27].

The constituent material of a discontinuous and comparatively stiffer composite is referred to as the reinforcement, whereas the component material that is continuous and relatively less stiff and weaker is called the matrix material. The reinforcement material usually exists in the form of fibers or particulates. Sometimes, due to chemical interactions or other processes during composites' manufacture, an added distinct material, known as

the interphase, forms between the reinforcement and the matrix [28]. Figure 1 shows a schematic illustration of the phases of typical composite material.

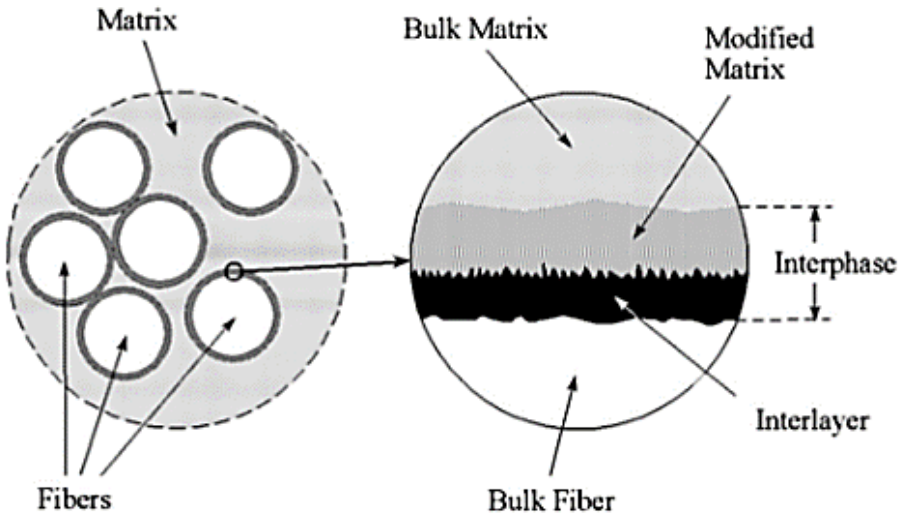

Figure 1. Schematic illustration of the phases of composite material [29]

A composite's properties rely on the properties of its constituent materials, their geometry, and the arrangement of its phases. An essential parameter of composite materials is its volume (or weight) fraction of reinforcement or fiber volume ratio [30].

One of the advantages of composites is that, if well designed, they usually possess the most desired qualities of their constituents and often some qualities that neither of the constituents demonstrates. The properties that can be enhanced by manufacturing a composite material from its constituents include strength, stiffness, corrosion resistance, attractiveness, thermal insulation, and acoustical insulation [27, 31].

2.2. Fiber-Reinforced Composites

The phenomenon of the material's actual strength being considerably less than its theoretically predicted strength is a common occurrence. This disparity in strength values is believed to occur due to imperfections or inherent flaws in the materials' structure. If an attempt is made to reduce or eliminate these flaws, this can potentially enhance a material [32, 33]. Some flaws are especially detrimental to a material's strength, such as cracks perpendicular to the material's forces. When contrasted to the strength of significantly larger material, human-made filaments or fibers of nonpolymeric materials demonstrate considerably greater strength along their lengths, as materials of larger size may contain several flaws.

In contrast, flaws are minimized in fibers owing to their small cross-sectional dimensions [34]. For polymeric materials, the molecular structure's correct orientation allows the material to demonstrate high strength and stiffness [35]. The properties of some standard types of fibers and some commonly used materials are shown in Table 1.

Table 1. Properties of Fibers and Conventional Bulk Materials [36]

Material	Tensile Modulus (E) (GPa)	Tensile Strength (σ_u) (GPa)	Density (ρ) (g/cm^3)	Specific Modulus (E/ρ)	Specific Strength (σ_u/ρ)
Fibers					
E-glass	72.4	3.5[a]	2.54	28.5	1.38
S-glass	85.5	4.6[a]	2.48	34.5	1.85
Graphite (high modulus)	390.0	2.1	1.90	205.0	1.1
Graphite (high tensile strength)	240.0	2.5	1.90	126.0	1.3
Boron	385.0	2.8	2.63	146.0	1.1
Silica	72.4	5.8	2.19	33.0	2.65
Tungsten	414.0	4.2	19.30	21.0	0.22
Beryllium	240.0	1.3	1.83	131.0	0.71
Kevlar 49 (aramid polymer)	130.0	2.8	1.50	87.0	1.87
Conventional Materials					
Steel	210.0	0.34–2.1	7.8	26.9	0.043–0.27
Aluminum alloys	70.0	0.14–0.62	2.7	25.9	0.052–0.23
Glass	70.0	0.7–2.1	2.5	28.0	0.28–0.84
Tungsten	350.0	1.1–4.1	19.30	18.1	0.057–0.21
Beryllium	300.0	0.7	1.83	164.0	0.38

Part of the reason that glass fibers have high strength is that their surface is almost entirely free of defects, while the strength of graphite and aramid fibers is more due to the superior orientation of their internal structure [37, 38]. E-glass fibers are considered incredibly essential reinforcement fibers due to their relative affordability. However, in terms of outstanding stiffness values, boron, graphite, and the aramid polymer fibers are the most preferred. Amongst these, graphite fibers are the most flexible as their structure has high variability [39, 40].

Due to their microscopic cross-sectional size, fibers usually are not used on their own for engineering applications. Instead, they are combined with matrix materials to

produce fibrous composites. The matrix helps to hold the fibers together, relays forces experienced to the fibers, and serves as environmental and wear protection [36].

2.2.1. Glass Fibers

The majority of polymer matrix composites use glass fibers as the reinforcing material. Glass fiber is preferred due to its relative affordability while still having considerable strength. In terms of disadvantages, glass fibers have low resistance to wear and tear, which can, at times, adversely affect the material's strength [41]. Also, they display less than acceptable adherence to polymer matrix resins, especially when moisture is present. Coupling agents, such as silanes, can promote the adherence of glass fibers [42]. Finally, in comparison to other high-quality reinforcing fibers such as boron, carbon, and Kevlar, glass fibers do not have a modulus that is as high [36].

In high-end composite applications, glass fibers are barely used due to the previously stated disadvantages. Instead, they are frequently used as the reinforcing material in low to medium-end applications [43, 44]. Glass fibers are manufactured through the extrusion of molten silica (SiO) mixed with various oxides. This mixture is extruded through the holes in a platinum alloy bushing [30]. Glass fibers can be further divided into two broad categories, relatively affordable multipurpose fibers, and superior high-performance fibers. As much as 90% of produced glass fibers are multipurpose products. These fibers are commonly referred to as E-glass fibers. All glass fibers are usually manufactured to ASTM standards [45].

Superior high-performance glass fibers include S-glass, D glass, A-glass, ECR-glass, ultrapure silica fibers, hollow fibers, and trilobal fibers. All these fibers have at least 10 to 15% greater strength than E-glass at room temperature. However, their actual value is that they can withstand higher temperatures than E-glass when being utilized. High-performance glass fibers are commonly employed in military applications. In these applications, manufacturing standards are considerably more stringent than usual [46, 47, 48].

When produced for commercial use, glass fibers come in different forms according to the intended application. Fiberglass rovings consist of continuous glass fiber filaments grouped together. According to the desired yield (in meters per kilogram), commonly used rovings are manufactured by winding together single strands of glass fiber (in meters per kilogram) [49]. Usually, rovings are produced from fibers with a diameter of 9 -13 μm. General roving yields range from approximately 3600 to 4500 m/kg and typically consist of 20 strands. Rovings can be utilized directly for pultrusion, filament winding, and prepregs production [36].

Fiberglass rovings can be as long as several kilometers depending on their intended use. Rovings are commonly woven into a massive, rough fabric to be employed in cases where a considerable increase in thickness is required over extensive areas. This trait is incredibly convenient when using glass fiber to produce boats, other marine products, and numerous kinds of tooling [50, 51].

2.3. Matrix Materials

Due to their microscopic cross-sectional area, fibers are generally not utilized directly. Furthermore, when fibers exist alone, they cannot efficiently transmit loads from one fiber to another to effectively share the load. This drastically restricts their direct utilization in engineering applications where large forces need to be withstood. This restriction can be overcome by embedding fibers in a matrix material, thus forming a composite [52]. The material used as a matrix strongly influences the resulting composite's mechanical properties, including the composite's transverse modulus and strength, shear properties, and properties under compression. The material used as a matrix often limits the temperature at which a composite can be used [53, 54]. Temperature ranges for the use of composites manufactured from various matrices are shown in Figure 2.

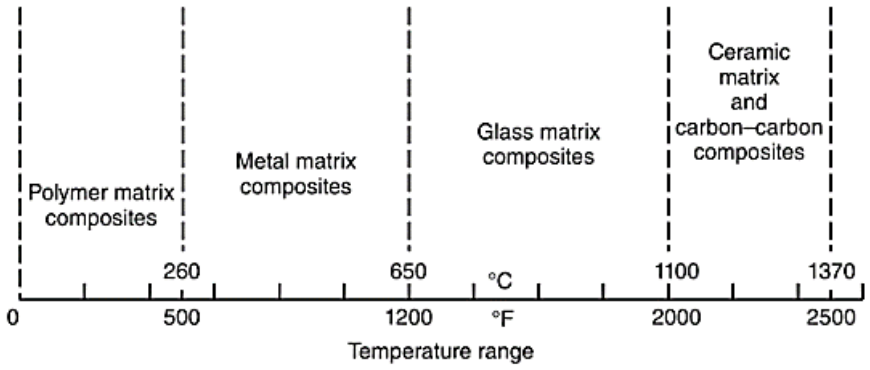

Figure 2. Service temperature range for composites formed from various matrix materials [36]

The physical and chemical traits of the matrix material, such as melting temperature, viscosity, and how easily it reacts with fibers, must be considered when selecting a composite's fabrication process [55]. The majority of fiber composites use

polymers as their matrix material. The main advantages of polymers are their affordability, ease of processing, high chemical resistance, and low relative density. Their disadvantages include their comparatively low strength, low modulus, and low service temperature. Polymers will break down if exposed to ultraviolet light and special solvents for a prolonged period [56, 57]. Polymers are separated into thermoplastics and thermosets, depending on their behavior and structure. Polymers that soften or melt when heated are classified as thermoplastic polymers. They are linear or branched-chain molecules with high strength intramolecular bonds, but low strength intermolecular bonds [58]. The melting and solidification of thermoplastic polymers are reversible, and therefore they can be reshaped as required using heat and pressure. The structure of these polymers can be either semi-crystalline or amorphous. Some examples of thermoplastic polymers are polyethylene, polystyrene, nylons, polycarbonate, polyacetals, polyamide-imide, polyether-ether ketone (PEEK), polysulfone, polyphenylene sulfide (PPS), and polyetherimide [59]. Thermosetting plastics consist of cross-linked structures that have covalent bonds connecting its molecules. As opposed to thermoplastic polymers, when thermosetting polymers are heated, they break down. Therefore, once these polymers solidify through a curing process, they cannot be remolded. Typical thermosetting polymers include epoxies, polyesters, phenolics, ureas, melamine, silicone, and polyimides [60].

Of the various polymeric matrix materials, polyester and epoxy are generally preferred when manufacturing composites using high-end reinforcing fibers. They are both

thermosetting polymers. Their preference is mainly due to the ease with which they can be processed and their high chemical resistance [36].

2.3.1. Epoxy Resins

Epoxy resins are organic liquids with a relatively small molecular mass that incorporate several epoxide groups, consisting of three-membered rings formed from one oxygen and two carbon atoms. Epoxides are generally produced through the reaction of epichlorohydrin with bisphenol-A. Cross-linking occurs due to the introduction of chemicals that react with the epoxy groups between neighboring chains.

Epoxy resin prepolymers are a product of the chemical reaction below (Figure 3):

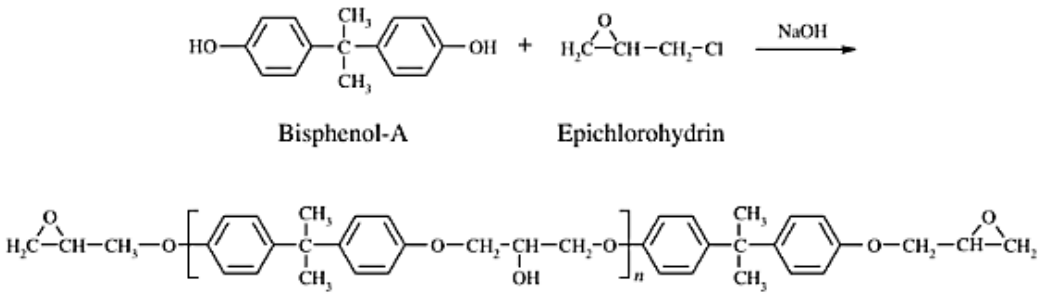

Figure 3. Chemical reaction to produce epoxy resin prepolymer [36]

It is combined with a curing agent resulting in a cross-linked polymer's formation with a strong network to polymerize the epoxy prepolymer. Generally, the curing of epoxy systems takes place at room temperature. Although the curing agent selected also plays an integral part in whether a room-temperature or higher temperature cure is necessary. Many times added heat could accelerate curing and help attain a better cure [61, 62]. After curing,

the epoxy resin characteristics are dependent on the chemical structure of its epoxy prepolymer, which may be altered to a large extent, together with the selected curing agent. General characteristics of cast epoxy resin are shown in Table 2. Generally, epoxy resins are preferred over polyesters due to their ability to adhere to a broader selection of fibers, higher resistance to dampness, and more excellent chemical resistance [36].

Table 2. Properties of a Typical Cast Epoxy Resin (at 23°C) [36]

Density, g/cm^3	1.2–1.3
Tensile strength, MPa	55–130
Tensile modulus, GPa	2.75–4.10
Thermal expansion, 10^{-6}/°C	45–65
Water absorption in 24 h, %	0.08–0.15

2.3.2. Metals

As an engineering material, metals have considerable flexibility. They are often favored as a matrix material in composites due to their incredible strength, large modulus, sizeable toughness, impact resistance, and their ability to withstand extreme temperatures. Metal matrices are often preferred over polymer matrices in applications where environmental conditions, such as temperature, are severe. However, the use of metal as composite matrix material is sometimes limited by its comparatively large density, the considerable temperatures required during processing, its reactivity with fibers, and vulnerability to corrosion [63, 64].

Aluminum and titanium are the metals most frequently selected for use as a matrix material. From metals, they both have relatively small densities (aluminum, 2.7 g/cm^3; titanium, 4.5 g/cm^3) and have a large variety of useful alloys. In composites, carbon fibers typically utilize aluminum alloys as their matrix material. Unfortunately, at manufacturing temperatures of 500°C or more, carbon may react with aluminum, which can significantly degrade the composite's mechanical characteristics. To counter this, protective coatings can be applied to carbon fibers, which also enhance the fiber wetting by the aluminum alloy matrix. Comparatively, titanium alloys generally possess more excellent strength-weight ratios. Titanium alloys also have exceptional corrosion resistance. However, these advantages are often outweighed by their considerably higher cost [36, 65].

2.4. Fabrication of Composites

Products are manufactured from materials like plastics and metals through molding and shaping processes. These materials are initially extracted or created and then processed using various methods such as forging, sheet forming, and injection molding. On the other hand, products manufactured from composites are often created at the same time as the composite material is formed. For example, the filament winding is used to produce a composite pipe composed of polymer and glass fibers.

The fabrication process selected to form a composite is mainly dependent on the matrix's chemical nature (e.g., whether it is a thermoset or thermoplastic for polymers) and the temperature requirements when forming, melting, or curing the matrix. The most

common use thermosetting resins in order of their preference are polyester resins, vinyl ester resins, and epoxy resins [66, 67].

The prepolymers required for producing thermosetting resin systems generally exist in a liquid state. After chemical reactions to form their polymers, they then become solids. In the course of this chemical reaction, prepolymer molecules are combined, forming polymer networks. This cross-linking process is referred to as polymerization. Polymerization is carried out by catalysts or curing agents selected according to the required combination of time and temperature needed to produce a particular product. Curing and hardening that occurs during this process are usually irreversible. Further heating will only result in the breakdown of the product.

Fabrication processes for forming composites using thermosetting resin as a matrix can be roughly separated into wet-forming processes and processes that make use of premixes or prepregs. For wet-forming processes, the resin is still a liquid when the final product is initially formed, and hardening occurs after a curing process. This includes processes such as hand lay-up, bag molding, resin-transfer molding, filament winding, and pultrusion [36, 55, 68].

2.4.1. Filament Winding

Filament winding is commonly employed when manufacturing surfaces of revolution like pipes, tubes, cylinders, and spheres and is typically utilized to produce sizeable tanks and pipes for use in chemical industries [69]. The quick and precise laying

down of continuous reinforcement in predetermined patterns is the essence of filament winding. This continuous reinforcement is usually in the form of rovings that are fed from a multitude of creels. Creels are shelves that hold the roving packages and are designed to pull the roving from these packages at the required intervals. These rovings then travel through a resin bath, after which they are gathered into a band of the desired width and consequently wound on top of a rotating male mandrel. The winding angle of the continuous reinforcing materials and its placement is controlled using specialized intricate machinery that travels at speeds according to the mandrel rotation. The reinforcement is continuously overwrapped in neighboring bands of a fixed width until it eventually covers the mandrel surface in its entirety. For this technique, the winding tension, the wind angle, and the resin composition can be controlled as necessary for each layer until the composite of required thickness and resin composition is formed [70, 71]. An illustration of the filament winding operation is shown in Figure 4.

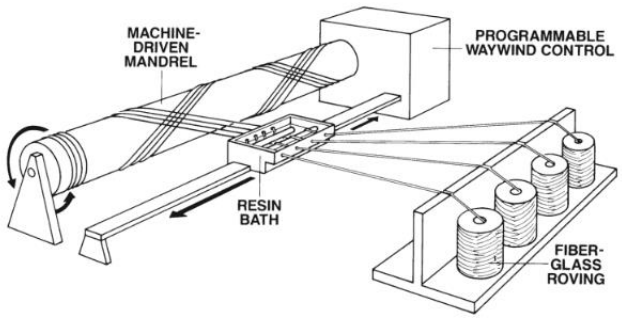

Figure 4. Filament winding machine [36]

The filament winding angle employed in the production of pipes or tanks is dependent on the strength and performance specifications required and, therefore, may

change from longitudinal through helical to circumferential as needed. These filament winding patterns are illustrated in Figure 5.

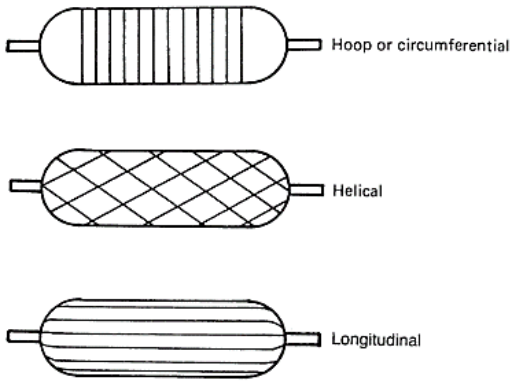

Figure 5. Typical filament winding patterns [36]

The advantages of the filament winding method include [36]:

1. It can be automated and generally has a large production rate.

2. The strength of products is optimized due to precise fiber placement.

3. The size of the products is flexible.

The limitations of the filament winding process include:

1. For products that require reverse curvature, the winding is complicated.

2. Low angle winding (parallel to the axis of rotation) is challenging.

3. For complex (double curvature) products, complexity can be too great.

2.5. Trigger Mechanisms

The crushing failure of composite tubes often results in a load profile with an undesirably high initial peak force, followed by a catastrophic drop in load-bearing

capacity. As a direct result, this means that crushing force efficiency values will be lowered, indicating unstable failure. As energy-absorbing devices are commonly applied in transportation to minimize injuries that passengers will receive during collisions, it is preferable for failure to be as stable as possible. Also, it is advantageous for energy absorbers to have a lower initial peak crushing force. Trigger mechanisms are an essential tool through which energy absorbers' overall safety and performance can be improved. It has been established that utilizing trigger mechanisms to create failure initiation sites artificially can effectively reduce the initial peak crushing force while also ensuring energy absorption is maximized. However, it is also necessary that a suitable trigger mechanism is chosen as some triggers will perform better than others for a given composite configuration. Trigger mechanisms can either be integrated into the composite tube or externally applied using a plug type trigger. For integrated triggers, the top edge of the composite tube is usually machined to the selected trigger type's geometry. Some of the integrated trigger mechanisms that have been previously investigated include chamfer triggers, tulip triggers, steeple triggers, and notch triggers. Most trigger mechanisms work by reducing the leading edge's cross-sectional area that first experiences compression, resulting in large stress concentrations in this region and a subsequent drop in the initial peak crushing force [72].

2.5.1. Chamfer Triggers

Chamfer triggers are usually integrated into a composite tube by machining away the tube's outer top edge so that there is a slanted edge from the inner edge of the tube to the outside surface of the tube. This type of trigger is widely used as the machining

involved is relatively simple. Chamfer triggers can be machined at various angles, and the chamfer angle has a significant effect on its performance. Figure 6a) shows a circular composite tube with a 45° chamfer trigger. In a study by Palanivelu et al. [73], a 45° chamfer trigger was shown to be more effective than a tulip trigger for enhancing the crushing performance of the circular pultruded composite tubes tested.

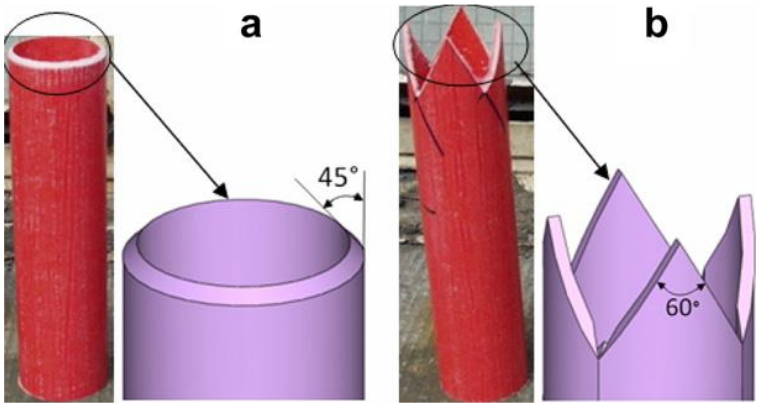

Figure 6. Circular tubes with a) a 45° chamfer trigger and b) a tulip trigger [73]

2.5.2. Tulip Triggers

For tulip triggers, the top of the composite tube is usually split into four sections when machining. Each section is machined so that there is a point at the top of the center of the section, which then slopes downwards to the corners of the section. For this type of trigger, outward splaying failure often occurs. A circular tube with a tulip trigger can be seen in Figure 6b). Palanivelu et al. [73] found that a tulip trigger is more effective than a 45° chamfer trigger for enhancing the crushing performance of the square pultruded composite tubes tested.

2.5.3. Steeple and Notch Triggers

Chamfers are machined on both the top of a composite's inner and outer edges, forming a sharp edge in the center. On the other hand, to form a notch trigger, straight sections of the top of a composite are cut out to form notches that have a slanted edge on one side and a vertical edge on the other. Both of these types of triggers are prevalently found in flat plate composites [74]. Figure 7 shows an illustration of flat plate composites with steeple and notch triggers, respectively.

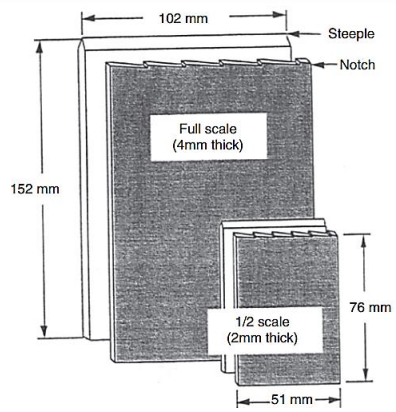

Figure 7. Flat plate composites with steeple and notch triggers [74]

2.6. Core Materials

From engineering theory, it can be determined that the flexural stiffness is proportional to the cube of its thickness. Therefore, in a composite material, a core's existence can enhance the composite's stiffness by effectively 'thickening' it. Commonly, low-density materials are used for cores, as this allows for a significant increase in stiffness while minimizing the additional weight of the composite. Furthermore, the core material needs to be capable of withstanding compressive loads without experiencing premature

failure. When the composites are relatively thin, cores also help prevent failure due to wrinkling and buckling modes [75, 76].

2.6.1. Foam Cores

Foams materials are commonly used as cores due to their comparatively low densities. These materials are produced from several human-made polymers such as polyvinyl chloride (PVC), polystyrene (PS), polyurethane (PU), polymethacrylate, polyetherimide (PEI), and styrene-acrylonitrile (SAN). Foam materials are manufactured with a wide range of densities, from as low as 10 kg/m^3 to as high as 300 kg/m^3. For composite structures, the preferred foams have densities ranging from 40 to 200 kg/m^3. Foam materials are also manufactured with varying thickness, generally from 5 mm to 50 mm [77].

The main factors that determine the energy absorption capability of foam material include:

a) The foam's relative density.

b) How material is distributed within the foam.

c) The deformation mechanisms of the foam material (elastic or plastic).

d) The flow of the cells within the foam under compression.

Several researchers have investigated the effects of using foam to fill hollow structures to enhance the structure's energy absorption capability. Investigations carried out by Thornton are of particular importance as they show that foam filling can

considerably improve the overall failure mode of a fiber-reinforced polymer tube. It was also shown that, in some cases, the use of foam cores could promote crushing stability [78].

2.6.1.1. PVC Foam

Polyvinyl chloride (PVC) foams are commonly employed as core materials to produce high-quality composite structures. This closed-cell material is a hybrid of PVC and polyurethane but is usually referred to as 'PVC foam.' PVC foams have useful static and dynamic properties and are notably resistant to moisture. They can also be used in an extensive range of service temperatures from -240°C to +80°C and have high chemical resistance. While PVC foams are typically flammable, there are some fire-retardant varieties and, therefore, may be utilized in fire-critical applications, for example, in the manufacture of some components of trains. PVC foam can be used as a core in conjunction with fiber-reinforced polymer skins safely, as it is quite resistant to styrene, and, therefore, its use is widespread in the industry. This material is usually commercially available in sheet form, either straight or grid-scored, to easily permit the material to be formed according to the required shape.

2.6.1.2. Polystyrene Foams

Polystyrene foam is used intensively in sails and surfboards productions due to its considerably low density (40kg/m^3), affordability, and the fact that it is easy to machine. However, because some of its other mechanical properties are below satisfactory levels, it is rarely utilized for high-end applications. In particular, this foam cannot be employed in combination with polyester resins due to its high reactivity with the resin's styrene.

2.6.1.3. Polyurethane Foams

Polyurethane (PU) is formed when polyols react with isocyanate to form a polymer made up of organic units linked together by urethane groups. The properties of polyurethane foams can be varied by changing the functionality of polyol. Uses of polyurethane foam depend on whether it is manufactured with a preference for flexibility or rigidity. Flexible polyurethane foam is commonly utilized as cushioning for bedding, furniture, and automotive interiors. This type of PU foam is available in different shapes with varying firmness. On the other hand, rigid PU foam is a trendy insulating material. This foam is often used when insulating buildings and helps to maintain temperature and reduce noise levels.

2.6.1.4. PMI (Polymethacrylimide) Foams

PMI (poly-methacrylimide) foam offers considerably high overall strength and stiffness when compared to other foam cores at a specific density value. Other useful properties of this foam material include its significant dimensional stability, closed-cell configuration, and fatigue resistance. This foam material also undergoes curing at high temperatures, which means it can be used within an extensive temperature range. The overall cost of this material and its performance traits ensure that this material is usually mainly utilized in high-performance aircraft composite components, such as the rotor blades of helicopters, airfoils, and the stringer profiles planes.

2.6.1.5. Styrene Acrylonitrile (SAN) Co-polymer Foams

SAN foam exhibits similar behavior as compared to the rigid cross-linked PVC cores. Their static characteristics are comparable to cross-linked PVC foams while having significantly greater elongation and toughness. Therefore, they can withstand higher impact levels. As a result, SAN foams are increasingly being used in place of linear PVC foams in many cases. This is also in part because they have better temperature performance. Despite this, heat can still be used to reform these foams, which helps manufacture curved components. Some SAN foams with increased thermal stability can be utilized with low-temperature prepregs being cured, as they will not interfere with ongoing chemical reactions [79, 80].

2.7. Quasi-static Testing

The sample under testing is compressed during quasi-static testing at a steady rate using a conventional universal testing machine. The test structure is axially compressed between flat, steel plates that are parallel to each other. The bottom plate is kept static while the top plate moves downwards at a constant crosshead speed. Typically, for quasi-static testing, the compression speed ranges from 1 to 11 mm/s. Quasi-static testing may not accurately replicate actual crash conditions, as in a real-life collision, the structure being crushed experiences a decrease in crushing speed from the initial speed of impact until the structure finally comes to a stop [81]. However, to grasp dynamic behavior, it is illuminating first to investigate the deformation of composite tubes under a quasi-static load so that strain rate dependence can be ignored, and other factors can be investigated. Composite tubes that act as collapsible energy-absorbing devices in automobiles' structures

are usually supported at one end (i.e., the point of attachment) by a structure with higher strength. Therefore their behavior may display some similarities to that exhibited in quasi-static axial crushing [82].

The main advantages of quasi-static testing include the following [83]:

a) Test conditions can be easily controlled

b) Quasi-static test equipment is much cheaper than the equipment required for impact testing because impact tests happen exceptionally quickly in comparison. Consequently, quasi-static testing can allow for greater ease when studying composites' failure mechanisms due to the slower crushing speed.

The main disadvantage of quasi-static testing is that results may not accurately represent actual crash conditions.

2.8. Quantitative Energy Absorption Performance Indicators

The energy absorption performance of composite structures may be assessed both qualitatively and quantitively. Qualitative assessment can include the structure's overall crushing behavior, the composites' force-displacement properties, and failure mechanisms exhibited by the structure. Quantitative analysis, on the other hand, includes quantifying crashworthiness characteristics that allow one to have an idea of the structure’s energy-absorbing capabilities [84]. Some critical parameters that reflect a structure’s crashworthy characteristics are detailed below, while Figure 8 shows some of the necessary quantities needed from the load-displacement curve while calculating these parameters.

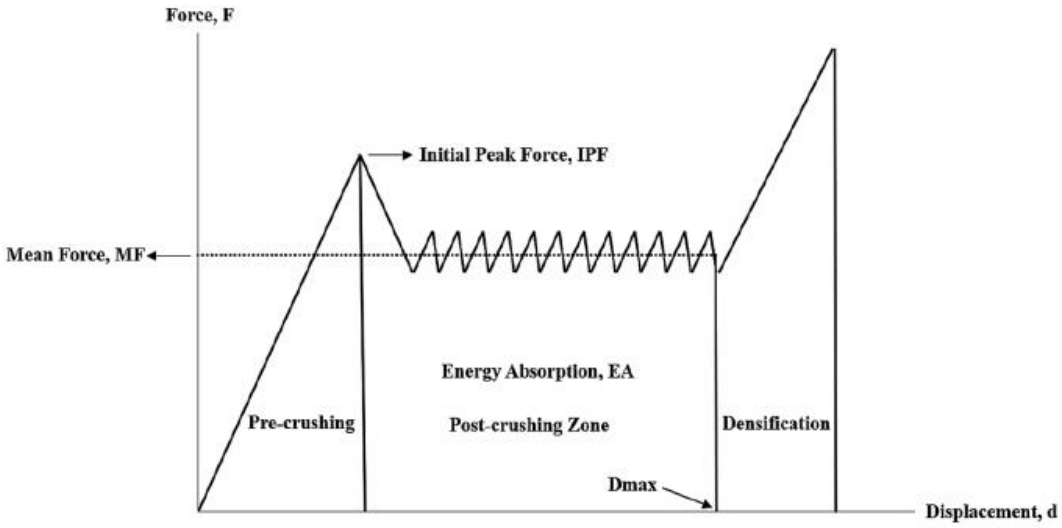

Figure 8. The general shape of the load-displacement curve for composite tubes [85]

2.8.1. Initial Peak Force

The initial peak force (IPF) is the force needed to commence plastic tube deformation. It is preferable for the IPF to below as this will help reduce the possibility of passengers being injured by lowering the size of reaction forces experienced in situations where safety is essential such as car and train collisions [86].

2.8.2. Energy Absorption and Specific Energy Absorption

Energy absorption is commonly quantified to evaluate composite structures' ability to absorb crushing energy that results from collisions. This quantity is represented graphically as the area under the force-displacement curve. In mathematical terms, the energy absorbed is represented as follows [87]:

$$EA = \int_0^{Dmax} Fds \quad (1)$$

Where F is the compressive load. The specific energy absorption (SEA) gives a measure of the absorbed energy to the structure's mass:

$$SEA = \frac{EA}{m} \quad (2)$$

Where m is the mass of the structure under compression

2.8.3. Mean Crushing Force

The mean crushing force (MF) is the average force that a composite structure experiences under compression. This quantity is customarily calculated while excluding forces experienced in the densification stage [84]:

$$MF = \frac{EA}{Dmax} \quad (3)$$

Where $Dmax$ is the displacement of the composite structure at the beginning of the densification stage.

2.8.4. Crush Force Efficiency

Crush force efficiency (CFE) quantifies the ratio of the mean force experienced by the composite to its initial peak crushing force [85]:

$$CFE = \frac{MF}{IPF} \quad (4)$$

An ideal situation in terms of energy absorption would be achieved when CFE has a value of 1, as this would mean that the initial peak crushing force would be sustained through the entire post-crushing stage so that it is approximately equal to the mean crushing force [85].

2.8.5. Instantaneous Crush Force Efficiency

Although the CFE gives an idea of crushing the overall stability for compression tests, it may still have a value for 1, even if the load wildly fluctuates, as long as this fluctuation is evenly distributed about the mean. Therefore, a novel variable is proposed, which will give an idea of what percentage of the load is within a certain threshold compared to the mean force. The instantaneous crushing force is a continuous variable instead of the crushing force efficiency, which is a discrete variable. It is calculated using only the load values of the post-crushing stage by dividing the mean force by the instantaneous force at each displacement value in this stage i.e.

$$iCFE = \frac{MF}{F_i} \quad \text{, for the post} - \text{crush stage} \quad (5)$$

The results are then plotted against displacement and how close each force is to the mean force. If the instantaneous crushing force efficiency for a load is 1, then this indicates that the force is equal to the mean force. The instantaneous crush force efficiency for each of the tested composite tubes was plotted to extract a discrete quantity from this variable

in the thesis, and then the percentage of the plotted curve within 0.1 of the value 1 was determined. This percentage gives an idea of how large a section of the post-crushing stage is within an acceptably small threshold from the mean value. If a composite tube has a crushing force efficiency close to 1 and a high percentage value for instantaneous crushing force efficiency with a 0.1 threshold of 1, this will indicate a remarkably stable failure for the post-crushing stage.

2.9. Failure Modes and Energy Absorption Mechanisms of Composites

The crushing behavior exhibited by composite structures when subjected to quasi-static axial compression can broadly be categorized as either stable or unstable failure. Unstable failure is distinguished by an initial peak load, after which there is a steep drop in the load-bearing capacity of the composite. Following this type of failure, the composite can no longer sustain a sizeable compression load. On the other hand, when a stable failure occurs, the compressive load initially increases until an initial peak load. After this, although slightly damaged, the composite is still able to support a sizeable amount of compression without a drop in load-bearing capacity while experiencing further displacement. Stable failure results in a higher energy absorption ability and thus is the objective of crashworthy structures. It is necessary to comprehend the failure mechanisms associated with stable failure and unstable failure [88].

The geometric dimensions of composite tubes play an essential role in determining whether they will experience stable or unstable failure. The length to diameter (L/d) ratio of a composite tube explains how slender the tube is and can help determine if the

composite will undergo global buckling (Figure 9). Tube dimensions are usually selected to avoid global buckling as this type of composite tube collapse mode results in deficient energy absorption. Likewise, the ratio of a composite tube's diameter to its wall thickness (D/t, for circular composite tubes) or the ratio of composite tube's length of a side to its wall thickness (S/t, for square, equilateral triangle composite tubes) are significant [89].

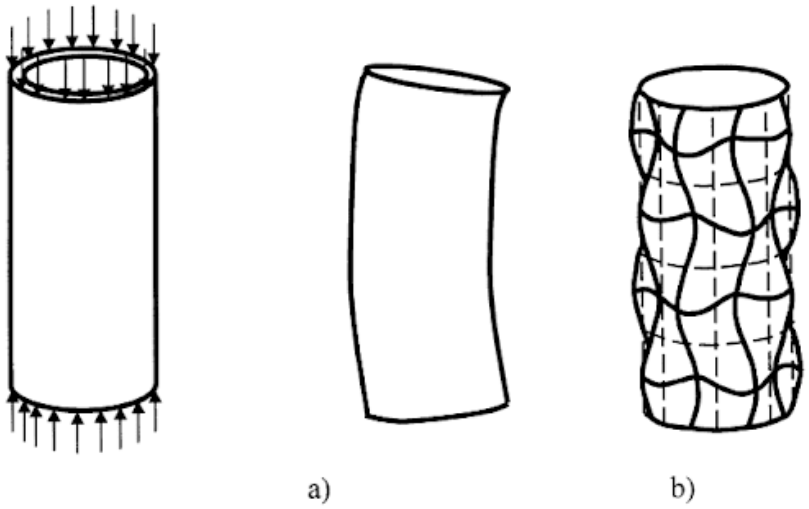

Figure 9. Illustrations of: a) global buckling and b) local buckling of a composite tube under axial compression [90]

According to Mamalis et al. [88], the failure modes commonly explicitly observed in thin-walled cylindrical composite tubes when subjected to quasi-static axial compression can be broadly divided into three different modes; referred to as Mode-I, Mode-II, and Mode-III. In Mode-I, failure occurs due to the progressive crushing, accompanied by micro fragmentation, of the composite tube. The distinguishing trait of this particular failure Mode-Is long interlaminar, intra-laminar, and axial cracks that exceed the length of the composites' laminate thickness. These cracks divide the fibers into bunches, commonly

known as fronds [91]. These fronds spread radially outwards and inwards from the surface of contact between the composite tube and the compression platen, causing the appearance of the crushed cylindrical composite sample to resemble a mushroom. The curved fronds' radius changes depending on the fiber, matrix, and laminate properties of the composite. Sigalas et al. [92] identify the forces that emerge in the crush zone in the course of frond formation as follows: compressive loads experienced by fronds and debris wedge, abrasion forces as the fronds scrape across the load plates, abrasion forces between the fronds and the debris wedge, abrasion forces that exist between the lamina of the composite and fronds as they twist through the radii of curvature and hoop forces that occur as a result of the inner and outer fibers attempting to resist longitudinal crack propagation. There are several means by which composites that experience this failure mode attempt to dissipate the resulting energy, including energy absorbed due to the formation of cracks in the longitudinal wall, energy absorbed due to delamination and the process of forming fronds, energy used in curving the fronds, energy absorbed due to the fracture of fibers, energy used up by the numerous forms of abrasion mentioned above and finally, the energy needed to form additional cracks, like those resulting from axial tube splitting [93]. In existing studies, the amount of energy dissipated due to each process is not clear, although it is known that the numerous abrasion forces account for as much as half of the total energy dissipated due to Mode-I failure [94]. Of the three failure modes described, Mode-I was identified as the failure mode that results in the highest amount of energy being absorbed during crushing and usually also results in the most stable failure. An example of a composite tube that has undergone Mode-I failure when subjected to quasi-static axial compression can be seen in Figure 10a).

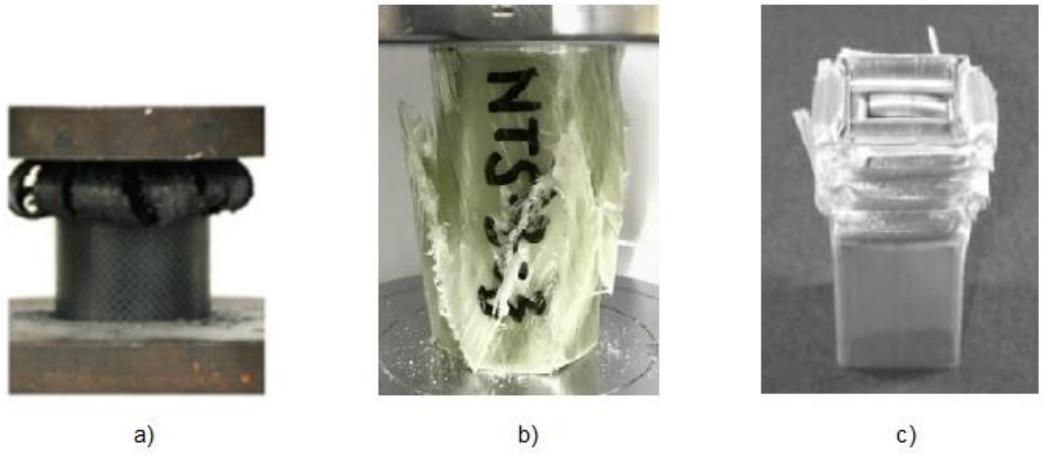

Figure 10. Examples of composite tubes that have undergone: a) Mode-I, b) Mode-II, and c) Mode-III failure [95, 96, 97]

In Mode-II, failure occurs due to brittle fracture of the composite tube. This failure mode may be initiated by either longitudinal or circumferential crack propagation. Transverse shear is also usually a contributing factor. In some cases of failure due to transverse shear, the two halves of the crushed composite sample on either side of the consequent fracture plane not wholly separate. Further loading may then result in the interpenetration of the two halves of the composite tube. This interpenetration, in turn, can give the composite tube some residual load-bearing capacity. The energy absorption occurs during the fragmentation failure Mode-Is mainly from the fracture of fibers and the matrix material. As there is an absence of fronds or other debris pieces that can slide against each other or the load plates, it has been seen that abrasion effects hardly contribute to the specific energy absorption of composite tubes that fail due to fragmentation [98]. Usually, a debris wedge does not form in the fragmentation failure mode. The broken fragments of the samples fall away from the crush zone, and after this, they do no contribute a different

part to the energy absorption. Mode-II is the failure mode associated with the least energy absorption of the three failure modes specified and generally also results in relatively unstable failure. An example of a composite tube that has undergone Mode-II failure when subjected to quasi-static axial compression is included in Figure 10b).

Finally, in Mode-III, failure occurs due to progressive folding and hinging, reminiscent of thin-walled metal and plastic tubes' compression behavior. Folding occurs when the compressive stress exerted on the composite tube is large enough that it causes the tube wall to buckle locally and form a hinge. Once the compressive stress reaches high enough once again, another hinge will form under the existing one, and the process recurs. Each hinge results in the formation of an additional fold until the entire length of the tube collapses. When tubes undergo Mode-III failure, this may cause them to have a considerable amount of interlaminar and circumferential cracks due to hinge formation [91]. One of the advantages that this failure mode has compared to fiber splaying and fragmentation is that the matrix material and fibers remain relatively undamaged. This means that the tube's fragments will not break off during crushing, which is useful for cases where energy-absorbing structures must remain fastened after a crash. Composite specimens that contain some ductile fibers demonstrate this property, and therefore, the need for this trait sometimes can lead to the use of hybrid composites [99]. When compared to Modes I and II, Mode-III exhibits a medium energy absorbing capacity. An example of a composite tube that has undergone Mode-III failure when subjected to quasi-static axial compression is shown in Figure 10c).

During the actual failure of a composite, these failure modes may occur concurrently. In general, energy is absorbed through the breakdown of the composite. Energy absorption mechanisms common to all three failure modes include delamination/ debonding, bending (during folding), fiber breakage, matrix cracking, and frictional resistance to axial movement between adjacent layers composite tube. In Mode-I, there are some additional energy absorption mechanisms due to the formation of fronds.

2.10. Existing Research on Energy Absorption of Composite Tubes

The energy absorption properties of composite tubes intended for use in structures that may experience collisions can be tailored by adjusting numerous parameters such as fiber type, matrix type, fiber orientation, the geometry of the composite, manufacturing conditions, and fiber volume fraction. This section reviews the related literature. As such, the papers reviewed are exclusively those in which composite tubes undergo quasi-static axial compression.

Sun et al. [100] carried out a study in which the composite tubes tested were made up of an inner aluminum tube overwrapped in carbon fiber reinforcement, while epoxy resin served as the composite's matrix material. These hybrid aluminum/CFRP tubes were manufactured using the filament winding method. Quasi-static axial compression tests were performed to investigate the effects of fiber orientation angle and the composite tubes' wall thickness on their crashworthiness characteristics. The hybrid tube's energy absorption results, the aluminum tube on its own, and the CFRP tubes on its own were compared to demonstrate the advantages of the hybrid tube. Twenty-five different circular tubes were

tested with four different fiber angles (25°, 50°, 75°, and 90°) and three contrasting wall thicknesses (3-ply, 6-ply, and 9-ply) being made use of, specifically consisting of 1 individual aluminum tube, 12 CFRP tubes of specific parameters and 12 aluminum/CFRP hybrid tubes of differing parameters. The quasi-static axial compression tests were carried out using a standard universal testing machine INSTRON-5985, which has a maximum load capacity of 150 kN at standard temperatures. For all the experiments conducted, the machine's upper crosshead speed was set to a constant value of 4 mm/min. The CFRP reinforced aluminum tube's effectiveness is observed by contrasting the sum of the energy absorbed by the individual components to the hybrid's energy absorbed. Both the fiber orientation angle and the composite tube wall thickness were found to significantly affect the failure modes and crushing properties of the CFRP and hybrid tubes. For specimens with equivalent laminate thickness, an increase in the winding angle of the tested composite tube was shown to decrease the specific energy absorbed (SEA), energy absorbed (EA), and the peak crushing force (PCF) for both the samples consisting of CFRP only and the hybrid tubes. For samples with the same fiber orientation angle for the CFRP tubes, an increased thickness of the CFRP tubes increased in the SEA, EA, and PCF for the samples consisting of CFRP tubes only and the hybrid tubes. The samples that had the highest overall SEA were the 9-ply CFRP tube with a winding angle of 25° and the 9-ply CFRP/aluminum hybrid tube with a winding angle of 25° (48.74 J/g and 79.05 J/g), respectively. Furthermore, it was determined that the energy absorbed by the hybrid tubes was more significant than the sum of that of the individual CFRP and aluminum tubes, which shows that the hybrid tubes had better crashworthiness characteristics than their constituents.

Mahdi et al. [101] carried out an experimental investigation to optimize the energy absorbed by composite tubes due to quasi-static axial crushing. The circular composite tubes tested were manufactured using layers of E-glass woven fabric and epoxy resin. All the composite tube walls of the samples were fabricated using eight layers of E-glass fiber/epoxy. The main objective of the study was to investigate the effect of using different fiber orientation angles, specifically 0°/90°, 15°/-75°, 30°/-60°, 45°/-45°, 60°/-30°, and 75°/-15°. The wet wrapping process was utilized when fabricating the specimens, as this method is cost-effective. Quasi-static axial compression tests were conducted to determine the primary failure mechanisms of the tested composite tubes and how much energy they absorbed. Five tests were carried out for each fiber orientation angle to demonstrate the repeatability of the results, and the average results of these tests were determined. The data acquisition system of the universal tensile testing machine used recorded the load and displacement values for the compression tests conducted, for which the upper load plate was set to move downwards with a constant crosshead speed of 15 mm/min. The results showed that the composite tubes with a fiber orientation of 15°/-75° and 75°/-15° respectively had the largest load-carrying capacity and possessed the highest initial peak force. Following this, the composite tubes with the second-largest load-carrying capacity were those with a fiber orientation of 30°/-60° and 60°/-30°, respectively. For the pre-crushing stage, the composite tube that absorbed an enormous amount of energy was the tube with a fiber orientation angle of 15°/-75°, with a value of 0.425 kJ, followed by the tube with a fiber orientation of 45°/-45°, with a value of 0.316 kJ. For the post-crushing stage, the most considerable amount of energy was absorbed by the composite tube with

fiber orientation of 15°/-75°, with a value of 7.927 kJ, followed by the tube with a fiber orientation of 30°/-60°, with a value of 6.585 kJ. Therefore, from analysis of the overall results for the tested material system, the fiber orientations 15°/-75° and 75°/-15° had the best load capacity and energy absorption performance and are recommended for use as a collapsible composite tubular energy absorber.

Chiu et al. [102] published a paper that focused on the experimental investigation of a carbon fiber/epoxy composite tube's energy absorption behavior under quasi-static and dynamic loading with varying strain rates not exceeding 100 s^{-1}. The main reason this research was conducted despite a large number of existing studies on the performance of composite structures under compressive loading is that there is still disagreement in the literature regarding the effect of changing the strain rate on the crushing behavior of composites. The energy absorption behavior of cylindrical carbon fiber/epoxy composite samples with a tulip trigger subjected to compression at increasing strain rates was inspected. The failure mechanisms were identified through post-test examinations. The tests' load-displacement response was used to determine the specific energy absorbed (SEA), peak and steady-state loads, and crush force efficiency. Analysis of the results indicated that the tested composite tubes were strain rate-independent for strain rates not exceeding 100 s^{-1}. The failure modes were found to remain unchanged with the increasing loading rate the composite tube specimens experienced. The specific energy absorbed and the steady-state crush force did not change significantly for the applied strain rates. Although there was some variation in the peak force and the samples' crushing force efficiency, this was credited to the experimental procedure used as opposed to changes in

the composite tube's behavior. It was concluded that this independence rate could be attributed to the composite having a high fiber volume fraction. For materials that have a similarly high fiber volume fraction, it is expected that the effect of the strain rate can be ignored. This assumption can potentially speed up the analysis of composite energy-absorbing structures by decreasing the required material property data necessary for input, thereby permitting the analysis to be carried out using quasi-static assumptions and utilizing time scaling in numerical models viable.

Jia et al. [103] systematically evaluated the effects of a geometric factor, fiber orientation angle, and pre-crack angle on the energy absorption behavior of filament wound CFRP circular composite tubes subjected to quasi-static axial crushing. Using a particular geometric factor, known as an end reinforcing layer (Figure 11), on the crushing behavior of CFRP cylinders was examined.

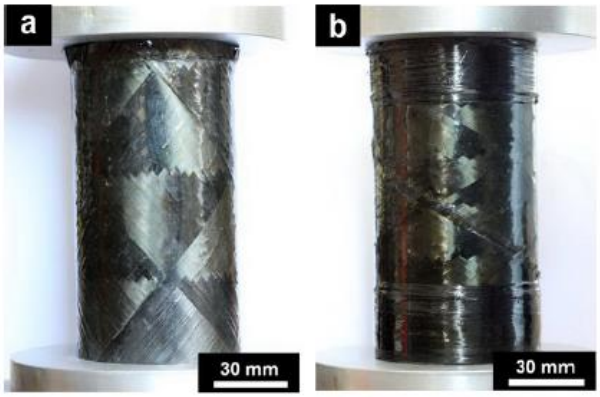

Figure 11. Images of CFRP cylinders subjected to crushing (a) without and (b) with an end reinforcing layers [103]

The change of compressive behavior of CFRP circular composite tubes with varying carbon fiber orientation angles was also assessed. For the tests carried out, the corresponding failure mechanisms and crushing force efficiency were evaluated using optical and SEM observations. In addition, the effect of the pre-crack angle on the crushing behavior of CFRP circular composite tubes was also analyzed. With the selected matrix material, epoxy resin, filament wound composite circular tube specimens with fiber orientation angles of 20°, 40°, 60°, and 90° were fabricated, with four carbon fiber layers each, using a filament winding machine. Quasi-static axial compression tests were conducted on the composite cylinder specimens using a universal tensile testing machine (Instron 1121), with the crosshead speed set to 0.5 mm/min. The load plates were parallel to one another prior to testing, and all-composite cylinders were compressed up to a predetermined displacement. The final load-displacement values used for each specimen were averaged from five tests. The CFRP composite tubes with end reinforcing layers demonstrated good compressive characteristics, and failure was observed to take place due to crack propagation in the samples' central circumference. With an increase in fiber orientation angle, the compressive strength, compressive modulus, and the length of cracks in the composite cylinder typically demonstrated a decreasing trend, while, in contrast, the crushing efficiency increased. At a low fiber orientation angle of 20°, the composite tubes exhibited brittle fracture failure mode, while composite tubes exhibited transverse shear failure mode at higher fiber orientation angles of 60° and 80°. On the other hand, the composite tubes' failure mechanisms were predominantly the local buckling failure mode at the medium angle of 40°. Finally, with increasing pre-crack angle, the compressive strength and modulus of the composite tubes initially reduced to their minimum values up

till the pre-crack angle were equivalent to the fiber orientation angle, after which the values increased.

Mahdi and Sebaey [104] carried out a study where composite tubes with four distinct transverse cross-sectional geometries underwent quasi-static axial compression testing to determine which cross-section performed the best in terms of the crushing load and energy absorption capabilities. Three of these cross-sections were nonconventional, and the composite tubes manufactured with these cross-sections were subjected to quasi-static axial compression tests with similar test conditions. The crushing behavior of these composite tubes was then compared with that of traditional circular composite tubes. One of the tubes' cross-section consisted of an arc, with a slightly larger circumference than a semicircle, joined to a flat section. The other two nonconventional tubes consisted of circular cross-sections with one and two webs inside the tubes, respectively, to improve the buckling behavior by increasing the structure’s moment of inertia (Figure 12).

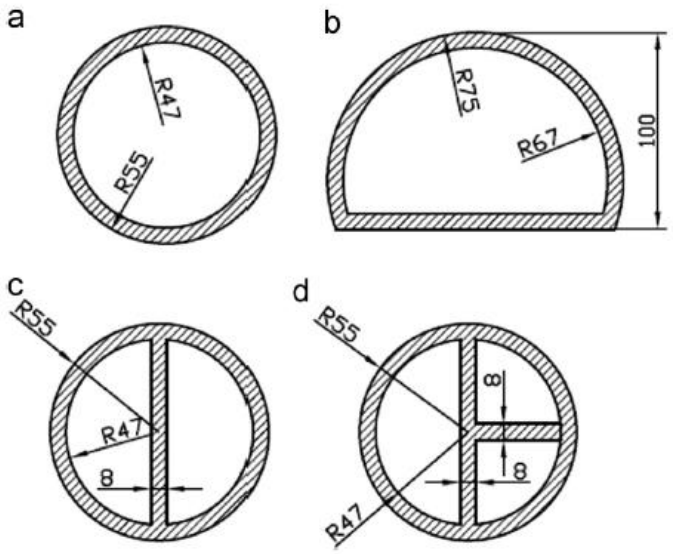

Figure 12. Illustration of the cross-sections of the examined specimens (all dimensions in mm) [104]

The E-glass woven fabric/epoxy composite tubes with eight layers were fabricated and tested to determine their basic failure mechanisms' energy absorption capability. This testing machine's data acquisition system recorded the load and displacement values for the tests, while specimens were crushed at a constant crosshead speed of 15 mm/min. The results demonstrated that the tubes with webs had the best performance in peak load, average crushing load, crush load efficiency, energy absorbed, and specific energy absorbed. In comparison with the conventional circular tube, the tube with two geometrical reinforcements, which had the overall best performance of the tested cross-sectional geometries, showed a 41% enhancement in the peak load, a 98% increase in the average crushing load, and a 38% increase in the specific energy absorbed. The tubes with a cross-section consisting of an arc, with a slightly larger circumference than a semicircle, joined to a flat section exhibited the most inadequate response when compared to that of the other tubes. The results of this show that it is possible to improve the crashworthiness

characteristics of composite tubes by reinforcing the interior of the tubes with composite webs.

Hu et al. [105] experimentally investigated the effect of fiber orientation angle on the crashworthiness properties of composite circular tubes manufactured from 759/5224 woven glass cloth/epoxy under quasi-static axial compression and impact testing. This study aimed to determine whether the performance of the composite tube allowed them to be utilized in the subfloor structure of a helicopter. 759/5224 woven glass cloth is considerably more affordable than carbon, and the manufacture of composites using this material is significantly less complicated. Composite tubes with a fiber orientation of ±15°, ±30°, ±45°, ±60°, and ±75° were fabricated and tested. During fabrication, the top end of each sample was chamfered with an external angle of 45°. The purpose of this chamfer was to act as a trigger, thus reducing the peak load and helping to make the failure more progressive. Quasi-static axial compression tests were carried out using a standard servo-hydraulic system MTS 880 with a maximum load capacity of 250 kN. The specimens were compressed up to a displacement of 100 mm at a load rate of 10 mm/min. The axial impact crushing tests were conducted with a drop hammer testing system. The drop hammer had a mass of 81.5 kg. The specimens were carefully positioned at the center of the impact testing system platform, directly underneath the center of mass of the hammer. Experimental results demonstrated that fiber orientation had a considerable influence on the composite tubes' energy absorption capabilities. For both the quasi-static compression and impact tests, the peak load initially reduced with increasing fiber orientation from 15° to 45° but subsequently increased with rising fiber orientation from 45° to 75°. Crushing

load efficiency first demonstrated a tendency to increase with rising fiber orientation from 15° to 60° but after this showed a decreasing trend with rising fiber orientation from 60° to 75° for both quasi-static compression and impact tests. On the other hand, specific energy absorbed (SEA) did not show a notable trend with increasing fiber orientation. The composite tube with a fiber orientation of 45° had the smallest SEA for both the quasi-static compression and impact tests, while the composite tubes with fiber orientation of 30° and 60° had comparatively high SEA.

Hamada et al. [106] carried out quasi-static axial compression tests on carbon fiber/epoxy and carbon fiber/PEEK tubes manufactured using unidirectional prepreg fabrics. This paper examines the matrix material's crashworthy characteristics, with particular focus on the contrast between thermosetting and thermoplastic polymers. Three fiber orientation angles were also inspected, i.e., unidirectional fibers parallel (0°) to the composite tube axis, ±30°, and ±45°. A set of composite tubes was fabricated with a 45° chamfer at the top end in order to encourage progressive crushing, while another set had conventional square ends to ascertain the compressive strength of the composite specimens. The composite tubes were manufactured using unidirectional fiber prepreg sheets from Q-112/HTA Toho Rayon Co for the carbon fiber/ epoxy and from APC-2/AS4 ICI-Fiberite Co for the carbon fiber/ PEEK samples. The fiber volume fractions of the prepregs were 55% and 61%, respectively. The specimens were subjected to quasi-static axial compression tests using a Mand 250 kN servo-hydraulic machine. In the crushing tests carried out on the chamfered specimens, the crosshead speed was a constant 1 mm/min, while for the compressive tests conducted on the square-ended specimens, the

crosshead speed was maintained at 0.01 mm/min. The most noteworthy aspect of the results was the incredibly high specific energy absorption value (180 kJ kg -1) found for the 0° carbon fiber/PEEK tubes. On the other hand, the chamfered 0° carbon fiber/epoxy tubes underwent failure at low loads, with substantial cracks forming parallel to the fibers. This demonstrates that samples using PEEK as a matrix material are much more resistant to crack formation between the fibers, meaning that these samples are more likely to exhibit progressive crushing failure. Stable, progressive crushing was observed only for the ±45° carbon fiber/epoxy tubes and the 0° carbon fiber/PEEK tubes. A limited portion of the progressive crushing was present in the load-displacement curve for the ±30° carbon fiber/PEEK tubes. For the composite tubes where progressive crushing was observed, generally a decrease in mean crush load, mean crush stress, and specific energy absorption occurred with increasing fiber orientation from 0° to ±30° to ±45°.

Elgalai et al. [107] examined the crushing behavior of composite corrugated tubes subjected to quasi-static axial compression. This study aimed at exploring the effect of geometry and material on the crashworthiness characteristics of composite corrugated tubes. The effect of geometry was examined by utilizing four corrugation angles (β =10°, 20°, 30°, and 40°) (Figure 13). On the other hand, for the effect of material, two kinds of fiber reinforcement material were tested. These were woven roving glass fiber and unidirectional carbon fiber with a fiber orientation of 90°. Epoxy resin was used as the matrix material for the fabrication of the composite corrugated tubes.

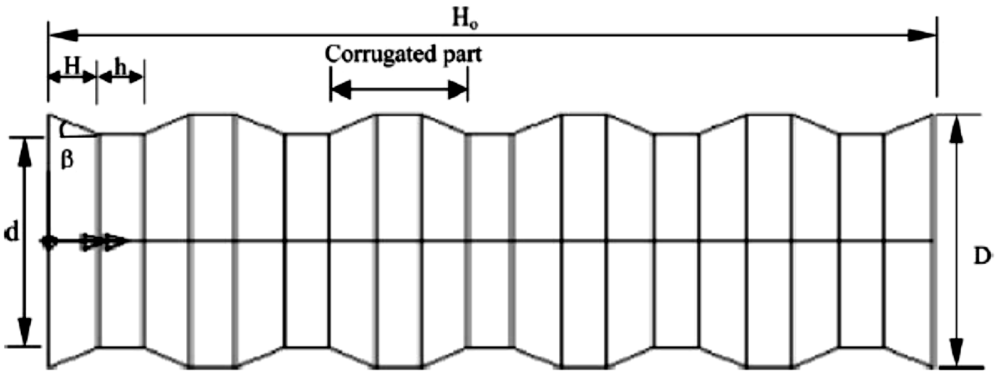

Figure 13. Sketch of typical corrugated tubes [107]

The volume fractions for the glass and carbon fibers employed were 0.55 and 0.56 respectively. The wet filament winding method was utilized to manufacture the carbon fiber/epoxy composite tubes, while the wet roving wrapping method was utilized for the production of the woven roving glass fiber/epoxy composite tubes. Quasi-static axial compression tests were conducted using an Instron 8500 digital-testing machine with a maximum load capacity of 250 kN. Testing was carried out at a constant crosshead speed of 25 mm/min. The results for this study indicated that the GFRE specimens exhibited a more stable load-carrying capacity as compared to the CFRE specimens. Although there were cases where the carbon fiber/epoxy composite corrugated tubes produced greater crush failure loads, this was accompanied by a higher chance of the CFRE specimens experiencing catastrophic failure during the post-crushing failure stage as compared to the GFRE composite corrugated tubes. The amount of specific crushing energy absorbed by the axially crushed composite corrugated tubes was found to change significantly with increasing corrugation angle. It could be seen that for the carbon fiber/epoxy composite corrugated tubes, as the corrugation angle rose, the specific energy increased. On the other hand, for the glass fiber/epoxy composite corrugated tubes, there was no clear, consistent

trend observed in the changing amount of specific energy absorbed corresponding when the corrugation angle varied.

Yan et al. [108] experimentally investigated the effect of utilizing foam filler and trigger mechanisms to improve the crashworthiness characteristics of natural fiber reinforced composite tubes. The composite tubes manufactured for this study use flax fabric as the reinforcing material and epoxy as the matrix material. All manufactured samples had a circular cross-section. Polyurethane foam with a density of 160 kg/m^3 was selected as the foam filler to be used. Composite tubes of two different inner diameters, 64 mm and 86 mm, were manufactured with the walls of the tubes consisting of 2, 4, and 6 plies of woven flax fabric/epoxy respectively, giving a total of 6 different composite tube configurations. For each of these configurations, samples of four types were produced. These were: 1) empty woven flax fabric/epoxy composite tube samples without a trigger, 2) empty woven flax fabric/epoxy composite tube samples with a 45° chamfer trigger, 3) polyurethane foam filled woven flax fabric/epoxy composite tube samples without a trigger and 4) polyurethane foam filled woven flax fabric/epoxy composite tube samples with a 45° chamfer trigger. All in all, a total of 24 different sample considerations were experimentally investigated. Quasi-static axial compression of the composite tube samples was conducted using an Instron 5567 universal testing machine with a maximum load capacity of 100 kN. Tests were carried out with a crosshead speed of 10 mm/min. From the test results, it was seen that, for a particular inner tube diameter, there was generally a higher load-bearing capacity and energy absorption capability as the number of plies increased. Also, the composite tube samples with an inner diameter of 64 mm generally

had better crashworthiness characteristics than those with an inner diameter of 86 mm. For the effect of using a chamfer trigger, it was concluded that the presence of a trigger mechanism noticeably decreased the initial peak load while also increasing the mean crushing load, thereby resulting in a remarkable increase in crush force efficiency. On the other hand, the presence of polyurethane foam significantly increased the amount of energy absorbed during crushing. The combination of a 45° chamfer and polyurethane foam was able to comprehensively increase the crashworthiness characteristics of the woven flax fabric/epoxy composite tubes tested.

CHAPTER 3. METHODOLOGY

The methodology used to perform the present study is described. To this end, the fabrication process of GFRP overwrapped PVC tubes, preparation of specimens, testing procedure, and energy absorption calculations procedure will be explained in detail.

3.1. Fabrication Process

The winding process used to prepare samples is an automated open molding process that uses a rotating mandrel as the mold. Winding process results in a high degree of fiber loading, which provides high tensile strength in the manufacture of hollow and circular tubes. Continuous reinforcement was fed through a resin bath and wound onto a rotating mandrel. For the fabrication of composite tube specimens for this thesis, glass fiber was used as the reinforcing material in the form of E glass fiber rovings, while the epoxy resin was used as the matrix material. The ratio of hardener to epoxy resin is 30 parts to 100 parts. The roving feed is run through a trolley that moves along the length of the mandrel. The reinforcement was laid down according to a preprogrammed geometric pattern that provides maximum strength in the requisite directions. Once sufficient layers had been applied, the laminate was allowed cured on the mandrel. The wrapped PVC tube was then removed from the mandrel. This process was used to wrap long PVC pipes with glass fiber/epoxy at winding angles of 45°, 55°, 65°, and 90°, where the reference axis 0° corresponds to the longitudinal axis of the tubes. The specific engineering properties of GFRP are shown in Table 3. For each angle, a total of 8 layers was applied before curing. Table 4 summarizes the values selected for the winding process. Figure 14 shows the five-

axis machine and the ongoing fabrication of overwrapped PVC plastic pipe. On the other hand, Figure 15 shows the glass fiber/epoxy overwrapped pipes before cutting.

Table 3. Typical Engineering Properties of GFRP

Properties	GFRP
E_{11}(GPa)	40.0
E_{22}(GPa)	11.9
E_{33}(GPa)	11.9
G_{12}(GPa)	3.52
G_{13}(GPa)	3.52
G_{23}(GPa)	3.28
ν_{12}	0.28
ν_{13}	0.66
ν_{23}	0.28

Table 4. Summary of the Winding Values in the Fabrication Process

Winding angle (degree)	Fiber speed (m/min)	Feed (m/min)	Spindle speed (RPM)
90	7.8	9.56	27
65	25	9.92	27
55	25	10.2	27
45	25	10.6	27

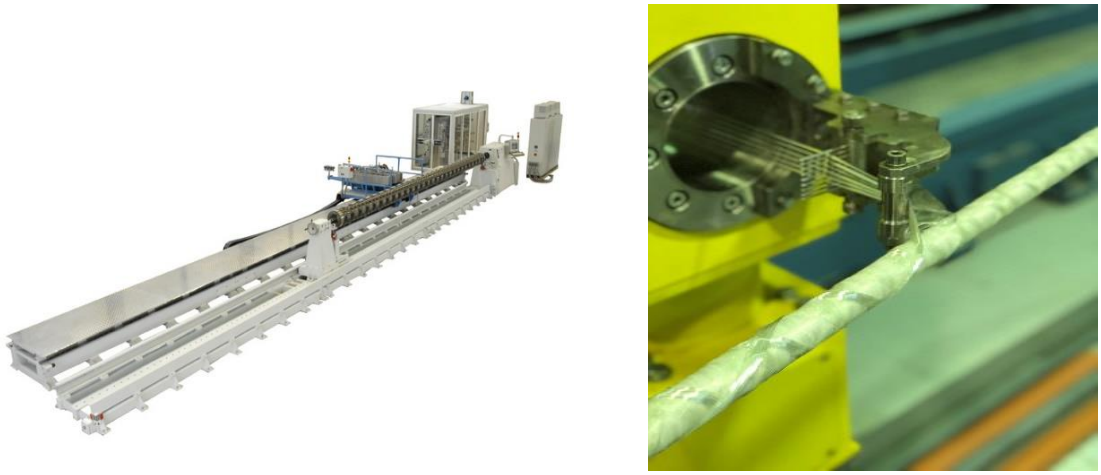

a) b)

Figure 14. a) 5-axis filament winding machine, b) Ongoing fabrication of GFRP composite overwrapped PVC pipe

Figure 15. Glass fiber/epoxy overwrapped PVC pipes before cutting

3.2. Loading Conditions

One loading condition was applied to all the circular composite tubes. The loading condition was quasi-static axial crushing, as shown in Figure 16.

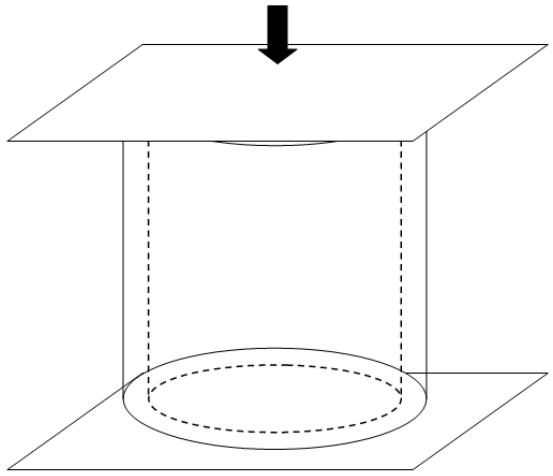

Figure 16. Schematic representation of the loading condition

Quasi-static crushing was carried out using the INSTRON material testing machine. Before testing started, the upper and lower plates were positioned to contact the upper and lower surfaces of the tested sample, respectively. The lower plate of the testing machine was kept static/stationary while the upper plate moved downwards at a constant speed. All specimens were crushed at a 500 mm/min speed up to a displacement of 75 mm. The PVC pipe specimens (unwrapped) were an exception to this as it was found that they experienced material densification at a displacement of over 75 mm. Therefore, for the PVC pipe specimens, the tests were stopped once a 180 kN load was reached instead. The maximum capacity of the machine used was 250kN. The machine computerized data acquisition system automatically recorded Load-displacement curves. Videos of the

crushing process for all specimens under compressive loading were taken to provide the crushing process's history and allow the crushing mechanisms to be observed.

3.3. Experimental Procedure

Specimens of approximately 100 m were cut from the overwrapped PVC pipes using a pipe cutter. These specimens were then flattened on either side using a turning machine to ensure that the circular faces of each side of the specimen were perpendicular to each other, as necessary for compressive testing (Figure 17).

Figure 17. The sample being faced using a turning machine

The final samples prepared for compressive testing had a length of 94 mm. The PVC tube itself had an outer diameter of 50 mm and a thickness of 2 mm. In addition, the thickness of the overwrapped glass fiber/epoxy was an average value of approximately 3 mm (Figure 18). The thickness of the samples was different, although eight layers were applied for each fiber orientation angle. It was noted that the thickness for the 45° samples

was closer to 2.5 mm, with the thickness increasing for increasing fiber orientation angle until approximately 3.5 mm for the 90° samples. This was also reflected when weighing the samples' mass as it was found that the 45° samples weighed the least while the 90° samples weighed the most. ALL samples were weighed before carrying out the compressive tests as the samples' masses were needed for specific energy absorption calculations.

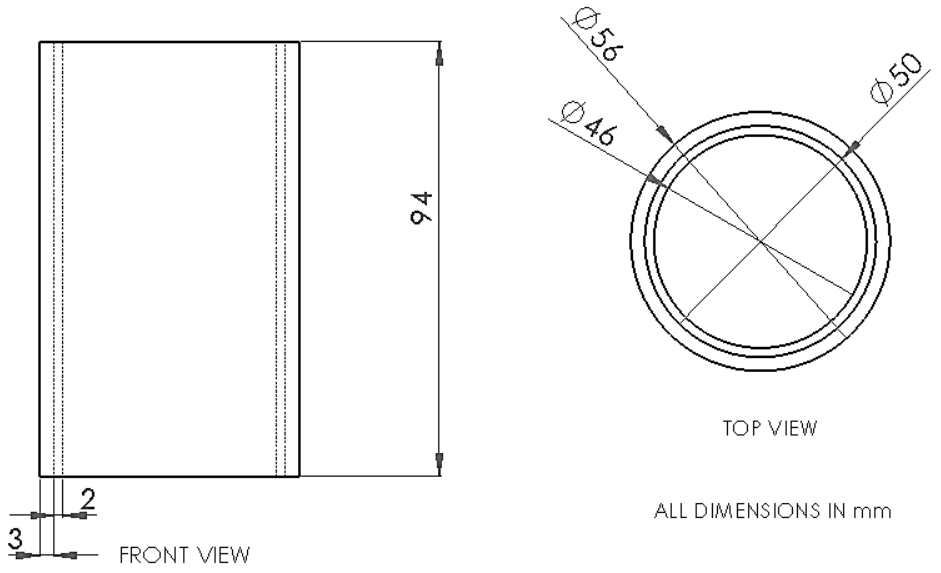

Figure 18. Front and top view for overwrapped circular tube samples

It should also be remembered that the surface of the overwrapped samples was uneven, meaning that the glass fiber/epoxy thickness fluctuated along the surface of the samples (Figure 19).

Figure 19. Completed sample with an uneven surface

The completed samples were then placed between square plates for the compression tests (Figure 20), which were carried out using an Instron Universal Testing Machine.

Figure 20. Sample positioned between compressive plates before the test

As a standard, a total of 3 tests were carried out for each of the four wrapping angles, respectively, in order to verify the results obtained. Three tests were also carried out on PVC pipe samples of the same size without any wrapping to show the effectiveness

of the glass fiber/epoxy reinforcement. After this, samples were prepared for each wrapping angle by completely removing 3.5 mm of the fiberglass/epoxy wrapping from the top of the reinforced PVC pipes (Figure 21). This slight change of the samples' design compared to the conventional circular tube geometry was introduced based on the results for the PVC tube samples. Further explanation of this change's reasoning in the design of the geometry will be given in section 4. Orthographic front and top views for composite tubes with this design change implemented are illustrated below:

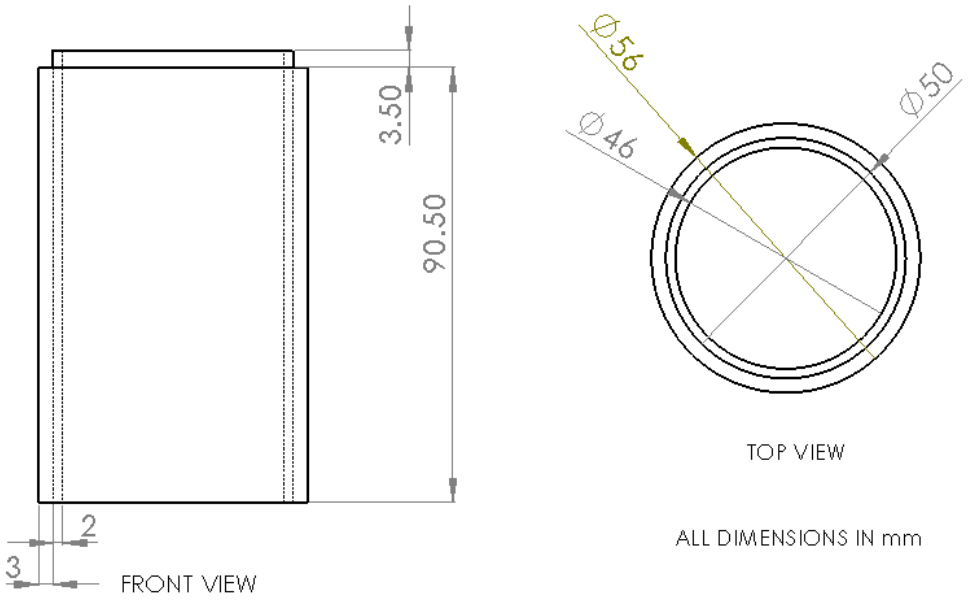

Figure 21. Front and top view for overwrapped samples with 3.5 mm fiberglass removed

A total of 3 tests were carried out for this design for each of the four wrapping angles, respectively, to verify the results obtained. Following the analysis of the results obtained for these tests, a further change was introduced into the circular tubes' design. Fiberglass/epoxy wrapping was first wholly removed from the top 3.5 mm section of the reinforced PVC pipes, as was done previously. After this, a 1 mm thickness of the glass

fiber/epoxy wrapping was removed from the 10 mm section of the tube directly below this 3.5 mm section. The orthographic front and top views for this second design tested are shown in Figure 22.

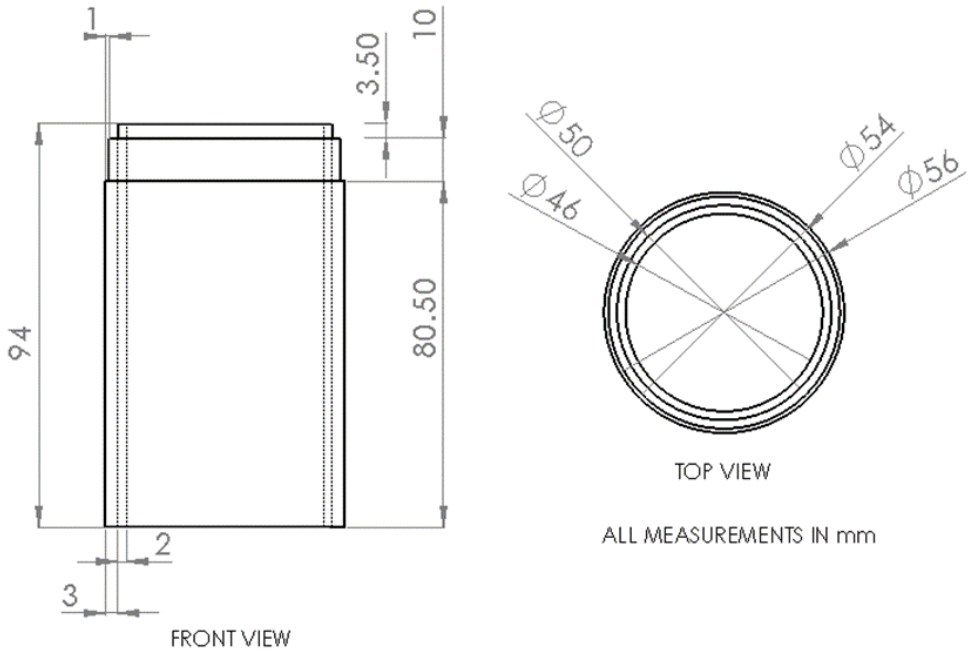

Figure 22. Front and top view for overwrapped samples with 3.5 mm fiberglass removed and a further 1 mm of glass fiber/epoxy removed for the following 10 mm length of the tube

As for the previous geometrical designs, a total of 3 tests were carried out for each of the four wrapping angles, respectively, in order to verify the results obtained.

From all the crushing tests up to this point, the above design, with 3.5 mm of glass fiber/epoxy wholly removed from the top section of the samples followed by 1 mm of glass fiber/epoxy being removed from the subsequent 10 mm section of the tubes, was shown to be effective. In particular, the specimens with a fiber orientation of 45°, and these changes

implemented were shown to have the best performance of all the preceding tested samples. As it was seen that the effect of the implementation of these changes was very similar to that of a trigger mechanism, samples with a fiber orientation of 45° and chamfer triggers (Figure 23) were prepared to serve as a direct comparison.

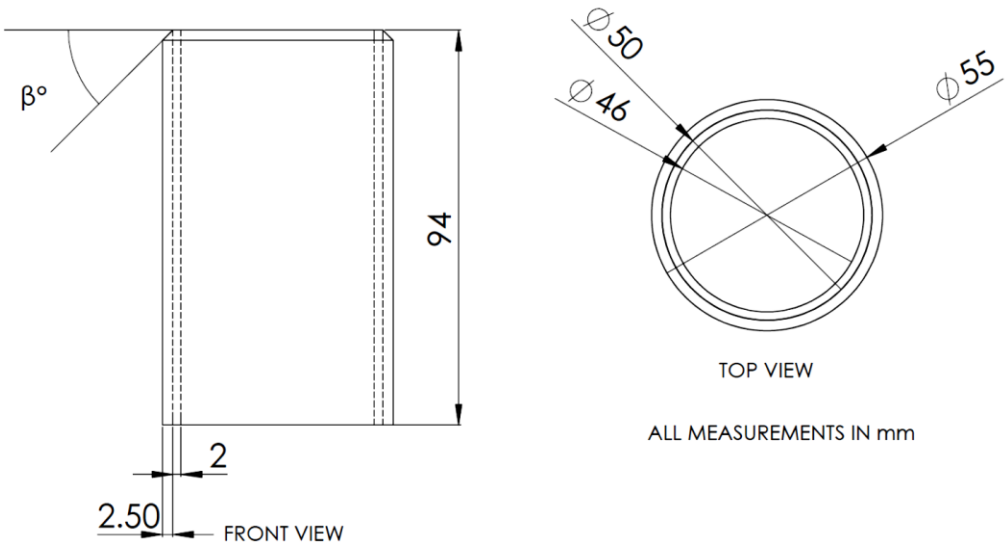

Figure 23. Front and top view for overwrapped samples with chamfer trigger

For a more comprehensive comparison, samples with a fiber orientation of 45° and chamfer trigger angles of β = 30°, 45°, and 60° respectively were prepared. A total of 3 tests were carried out for each chamfer trigger angle to verify the results obtained.

Finally, composite tube samples with a fiber orientation of 45° and 3.5 mm of glass fiber/epoxy wholly removed from the top section of the samples, followed by 1 mm of glass fiber/epoxy being removed from the subsequent 10 mm section of the tubes, were

filled with foam cores in an attempt to enhance their performance further. For the final tested samples, foam cores were machined using a CNC (Figure 24) machine and inserted into the center of the composite tube samples. Foam cores of four different geometries were machined from a sheet of low-density rigid polyurethane foam, which had a density of approximately 10 kg/m^3.

Figure 24. CNC machine used for machining foam cores

All the machined foam cores had a height of 94 mm, which was the same as that for the composite tubes, and an outer diameter of about 46.5 mm, which was slightly larger than the inner diameter of the PVC tubes used as the frame for the composite tubes. This allowed an interference fit to form between the composite tubes and foam cores so that adhesive did not have to be applied before testing. The design specifications for the four different geometries of the foam cores used are shown in Figure 25.

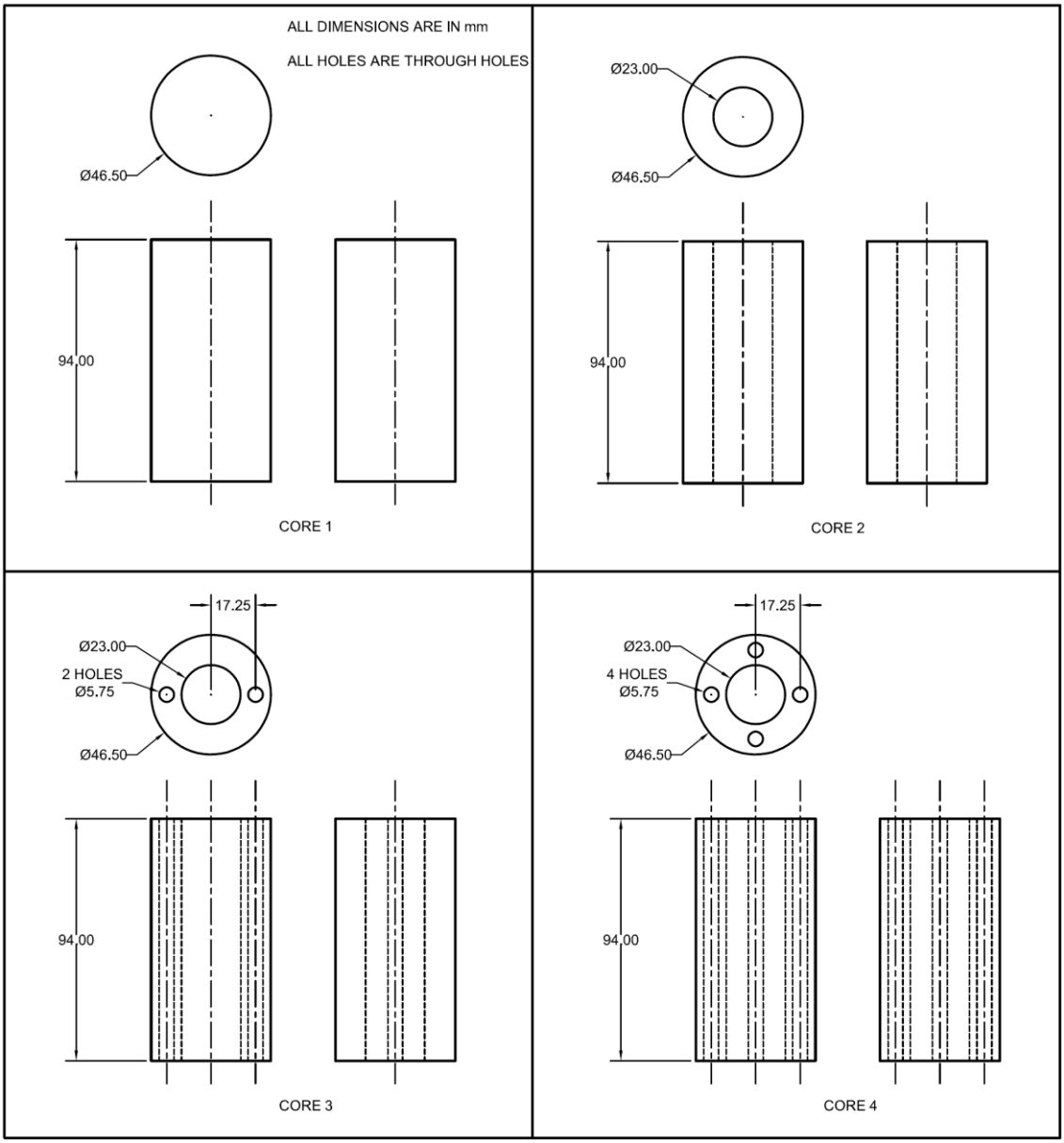

Figure 25. Front, top, and right orthographic views for Core 1, Core 2, Core 3, and Core 4

A SOLIDWORKS 3D view of the four foam core geometries is shown in Figure 26. The CNC machine employed the 3D step files for the foam core geometries for fabrication purposes.

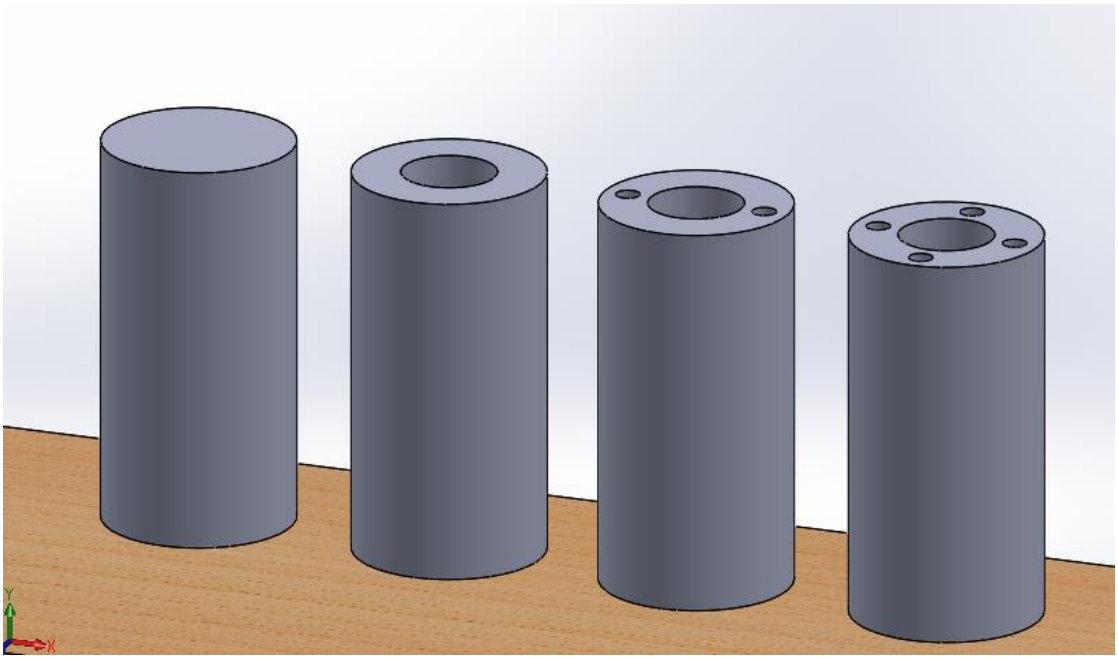

Figure 26. SOLIDWORKS 3D view of core geometries Core 1, Core 2, Core 3, and Core 4 (from left to right)

A total of 3 tests were carried out using each of the four core geometries respectively in combination with the composite tube sample configuration with the best performance, as specified previously, to verify the results obtained.

For the energy absorption calculations wolframalpha.com, an online computational search engine, was used to calculate the area under the load-displacement curves for the compressive tests. The load-displacement curves were first to split into the pre-crushing stage, post-crushing stage, and material densification stage (Figure 27).

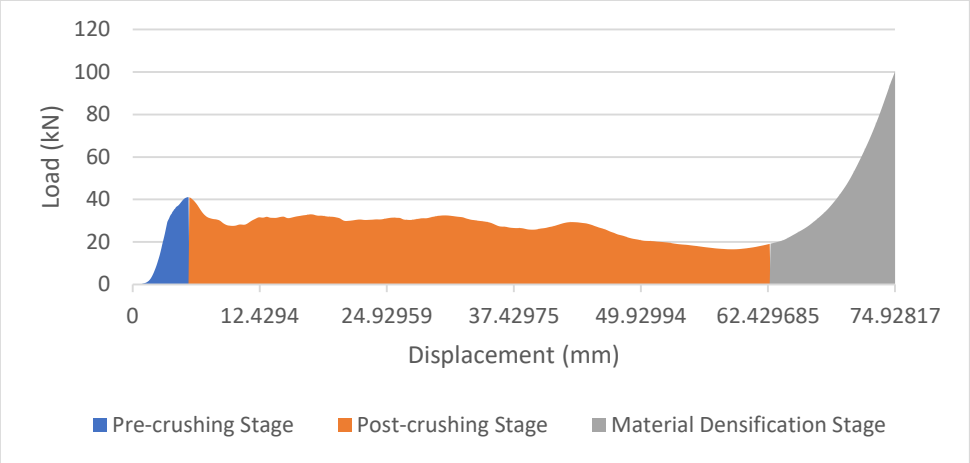

Figure 27. Pre-crush, post-crushing and material densification stages for 45° sample

Once the load-displacement graph was separated into three separate graphs, Excel was used to find the trendlines for each of these graphs (e.g., the graph of the pre-crushing stage for 45° sample in Figure 28), and the corresponding trendline equations were then utilized, along with the respective displacement values, to find the area under the curves using integration on wolfram alpha.

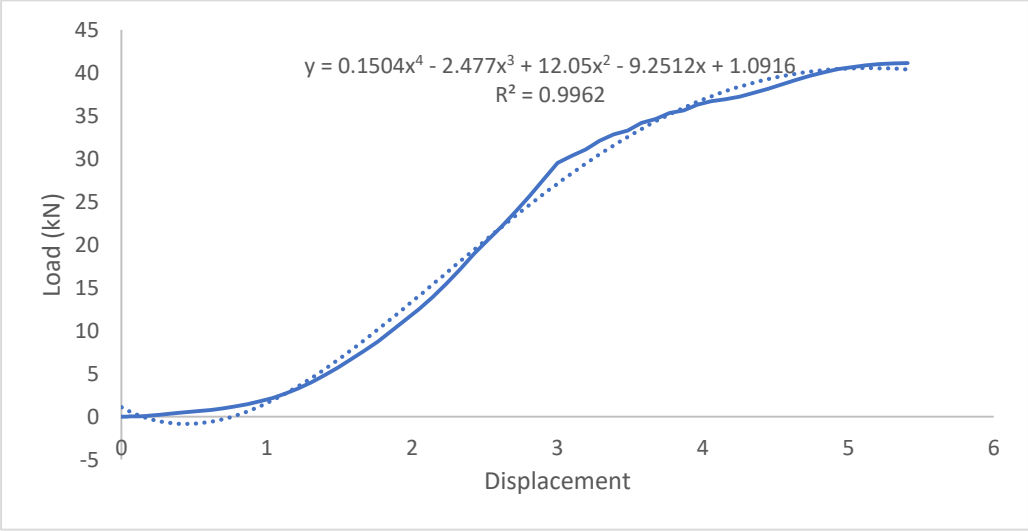

Figure 28. Graph, trendline, and trendline equation for the pre-crushing stage for 45° sample

As can be seen from the graph, the R^2 for the graph is relatively high, which shows that the trendline is a good fit for the data. The R^2 values for most of the trendlines were above 0.9. It should be noted that the energy absorption calculations were carried out using curves produced from the average load-displacement values from the three tests carried out for each respective sample.

Finally, a single sample of each of the GFRP/PVC composite tubes of different fiber orientations with standard circular tube geometry, after crushing, was given to the Central Laboratory Unit (CLU) to take zoomed-in images of the structure of the samples using a scanning electron microscope (SEM). The SEM uses the feedback of the interactions of a focused beam of electrons with the samples' surface topography to produce zoomed-in images of the samples. These zoomed-in images allow one to examine the microstructure changes of the samples that have been crushed. So, through the use of videos taken during the quasi-static crushing, one can examine the macroscopic mechanisms of failure, while the microscopic images taken by the SEM allow one to examine the changes in the microstructure of the composites that result due to these mechanisms of failure

CHAPTER 4. RESULTS AND DISCUSSION

In this chapter, the results of quasi-static axial compression tests carried out on the various composite tubes are categorized, presented, and discussed. The effect of many factors on the load-bearing behavior, crush force efficiency, and energy absorption capability is examined in detail. First, the effect of reinforcing PVC pipes using GFRP wrapping is demonstrated. Next, the effect of changing the fiber orientation of the GFRP wrapping is examined. Following this, the effect of making slight changes to the design of a conventional circular composite tube is shown. The reasons for the specific changes made to the design are also explained. After implementing the two suggested design changes, the sample configuration with the overall best performance from all the previously tested samples is selected. Finally, the selected composite tube was tested in combination with four different polyurethane foam cores to compare the performance of core and core-less composite tubes. For all quasi-static axial compression tests conducted, videos were taken and some images corresponding to the tested composite tubes' load-displacement behavior to assist in identifying the failure modes that the samples experienced.

4.1. Effect of Reinforcing PVC Pipes Using GFRP Wrapping

4.1.1. Effect on Load Bearing Behavior

In order to distinguish the effect of using GFRP wrapping to reinforce the PVC tubes used as the frame for the composite tubes, it was necessary to first observe the load behavior of a PVC tube on its own, with the PVC tube having dimensions identical to those used in the composite tubes for the crushing tests. Figure 29 shows the load-displacement curve for the PVC tube and the corresponding images.

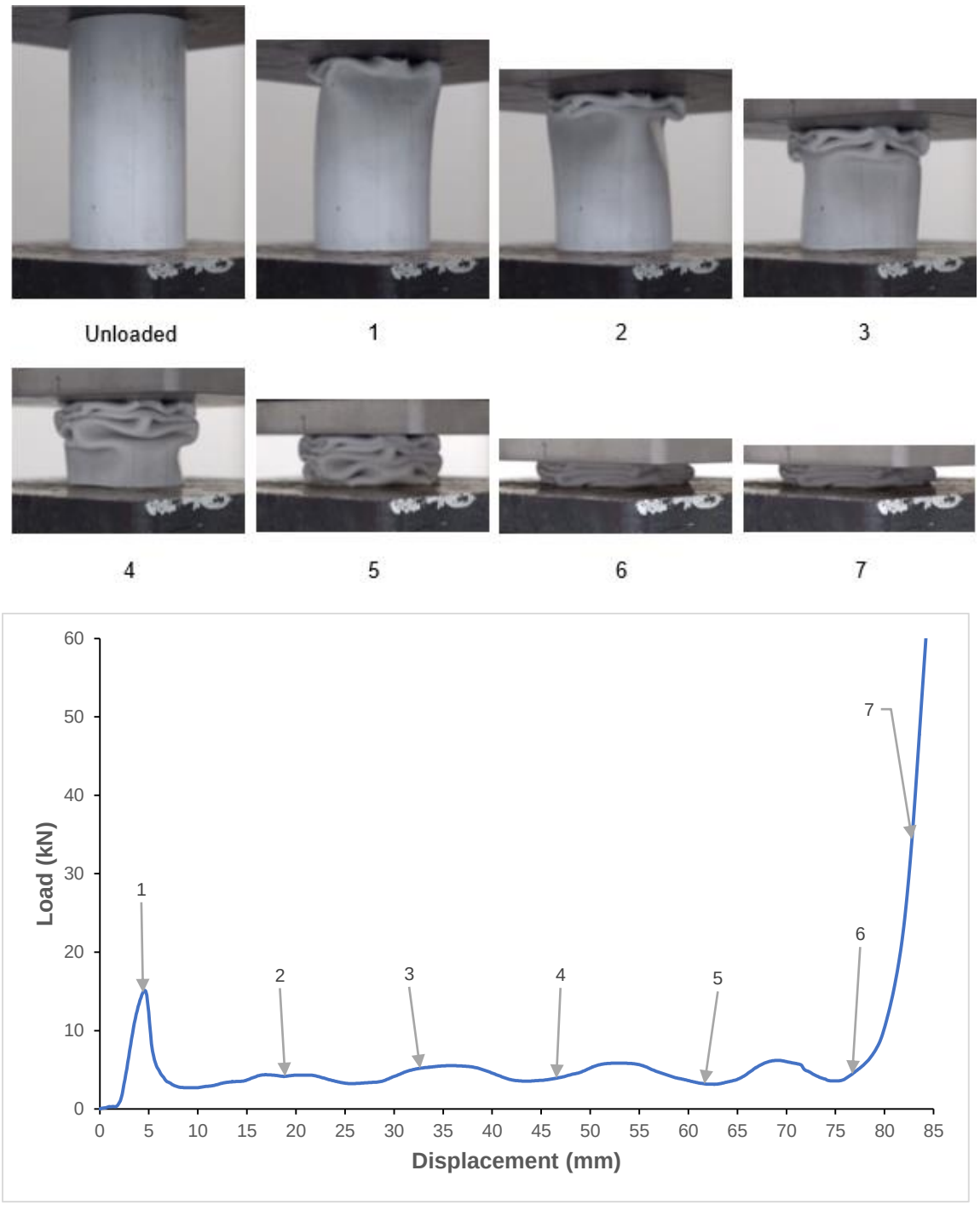

Figure 29. Load displacement curve for axial compression test of PVC pipe and corresponding images

It can be seen from Figure 29 that initially, the graph has a straight-line region, where load increases in direct proportion to the displacement of the composite tube. This region is referred to as the elastic region. For composite testing, the pre-crushing stage includes the elastic region and ends at the displacement corresponding with the first turning point of the graph, at which the specimen experiences its first drop in load-bearing capability. The maximum load reached before this drop is the initial peak force. For the PVC tube, the initial peak force had a value of approximately 15.14 kN and occurred at a displacement of about 4.599 mm. From the images in Figure 27, it can be seen that the failure mechanism for the PVC tube was progressive folding. This was expected as plastic tubes usually undergo progressive folding under compression, as is characteristic of Mode-III failure. The compressive stress exerted on the PVC tube increased until it was large enough that it caused the tube wall to buckle locally and form a hinge. It was observed that the formation of the first hinge in the PVC tube happened simultaneously as the initial peak force was reached. After this, for the first fold, quite a considerable drop in load-bearing capability occurred, indicative of catastrophic failure, as it dropped from 15.14 kN down to about 2.732 kN. Following this, folds continued to form, and for each fold, stresses built up in the tube wall, forming a hinge, followed by a subsequent drop in the load-bearing capacity as folding occurred. However, for the second fold onwards, the load's rise and fall were not as high, and the failure was more stable as a result. The region starting from the displacement where the initial peak force occurred, 4.599 mm, up to the displacement at which densification began for the PVC tube, 77.56 mm, is commonly referred to as the post-crushing stage. For the post-crushing stage of the PVC tube, the average load was approximately 4.397 kN. After the displacement value of 77.56 mm, the load value

increases drastically. This is the densification stage. The rapid rise of the load value is because the length of the PVC tube was already consumed, and the mass of the tube is subsequently being compressed.

The load-displacement curves for all the conventional circular composite tubes with different fiber orientation angles were plotted on the same graph as the load-displacement curve for the PVC tube (Figure 30).

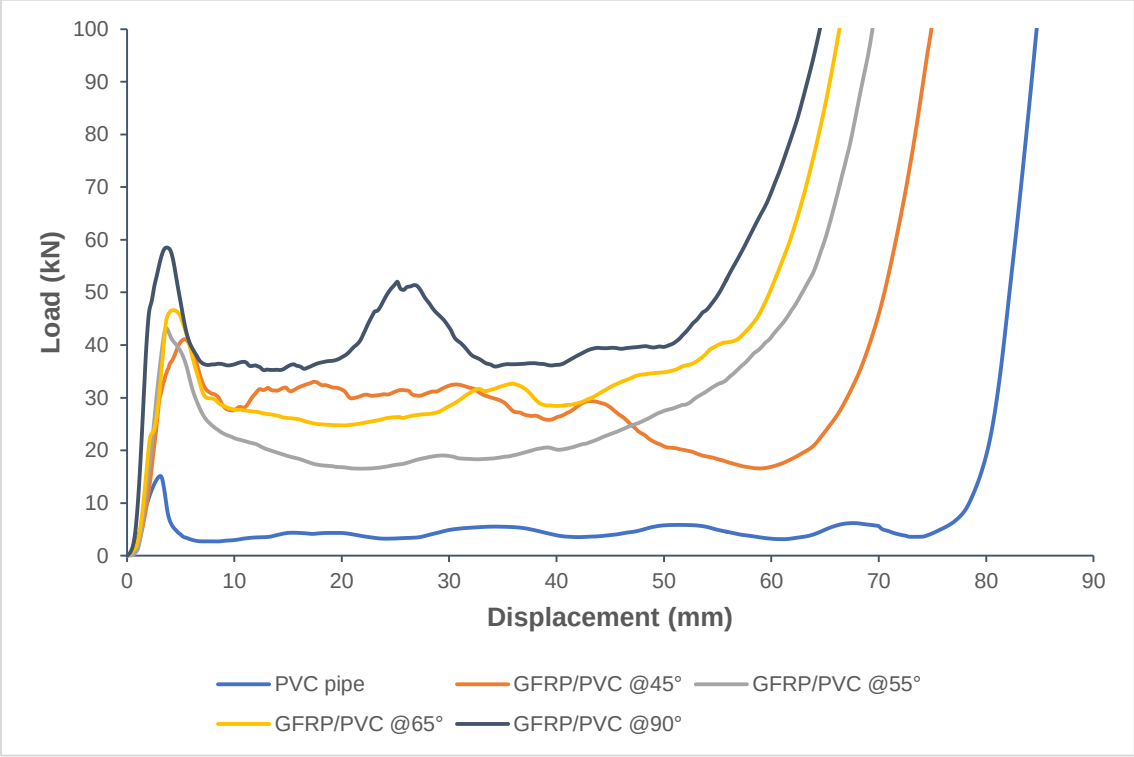

Figure 30. Load displacement curve for axial compression test of all GFRP overwrapped samples vs. PVC pipe

From the load-displacement curves in Figure 30, it can be easily seen that all of the GFRP overwrapped specimens had a considerably higher load-bearing ability than the PVC

tube on its own. For a more quantifiable comparison, the PVC tube can be compared to the GFRP/PVC tube with a fiber orientation of 45°, which has the lowest minimum load in the post-crushing region besides the PVC tube for the displayed curves. The PVC tube's initial peak force was 15.14 kN, while the initial peak force for GFRP/PVC 45° composite tube was approximately 41.11 kN, more than double that of the PVC tube. Also, if we compare the average loads for the post-crushing stages for both the specimens, the PVC tube had an average load of 4.397 kN, while the GFRP/PVC 45° composite tube had an average load of about 27.16 kN, which is over six times that of the PVC tube.

4.1.2. Effect on Crush Force Efficiency

Table 5. CFE and %iCFE within 0.1 from Ideal for GFRP/PVC Tubes and the PVC Tube

Sample configuration	Overall CFE	% iCFE ±0.1 from Ideal
PVC	0.2903	28.21
GFRP/PVC @45°	0.6607	31.27
GFRP/PVC @55°	0.5017	29.12
GFRP/PVC @65°	0.6569	39.53
GFRP/PVC @90°	0.6838	57.07

From Table 5, it can be seen that the crush force efficiency for all the GFRP overwrapped PVC tubes was noticeably more extensive than that of the PVC tube. The GFRP/PVC 55°, the sample with the lowest CFE from the overwrapped samples, had a crush force efficiency of 0.5017, which was a significant 72.82% higher than the CFE value of 0.2903 for the PVC tube. Although the percentage instantaneous crush force efficiency

within 0.1 of the excellent value was also higher for the overwrapped samples than the PVC tube, there was not as much of a difference. The GFRP/PVC 55°, the sample with the lowest % iCFE within 0.1 of the ideal from the overwrapped samples, had a 29.12% value, which was only 0.91% larger than the 28.21% value for the PVC tube.

4.1.3. Effect on Energy Absorption Capability

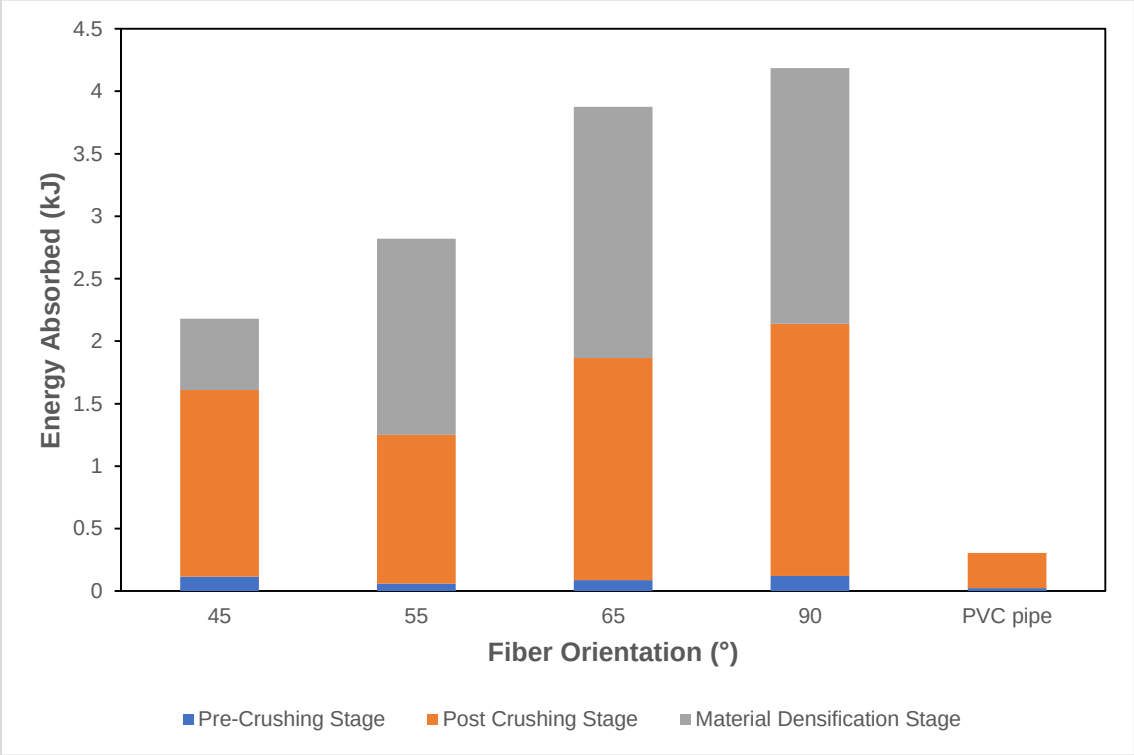

Figure 31. Energy absorbed by the GFRP overwrapped PVC tubes and the PVC tube on its own

To determine the energy absorbed by the different composite tubes, the area under the load-displacement curves was calculated up to a 75 mm displacement for all the tubes. Therefore, although the PVC tube experienced densification since this occurred after a 75

mm displacement, the energy absorbed during the material densification stage was not considered. From Figure 31, for both the pre-crushing and post-crushing stages; however, it could be seen that the energy absorbed by the PVC tube was considerably less than that absorbed by the GFRP overwrapped PVC tubes. Since the energy absorbed that is considered useful during collision is from the pre-crushing and post-crushing stages, this is a significant result. The energy absorbed by the PVC tube can be compared to the energy absorbed by the GFRP/PVC 55° specimen, which had the lowest pre-crushing and post-crushing absorbed energies from the tested overwrapped samples. For the pre-crushing stage, the PVC tube absorbed about 0.0233 kJ of energy while the GFRP/PVC 55° tube absorbed approximately 0.0593 kJ of energy, which was more than double that of the PVC tube. For the post-crushing stage, the PVC tube absorbed about 0.2820 kJ of energy while the GFRP/PVC 55° tube absorbed approximately 1.190 kJ of energy, which was over four times that of the PVC tube. However, it is essential to note that the considerably lighter weight of the PVC tubes was not taken into account for these calculations. Therefore, it is more significant to calculate the specific energy absorbed, so the masses of all samples were measured before carrying out compression tests. The specific energy absorbed by the tested samples was calculated (Figure 32).

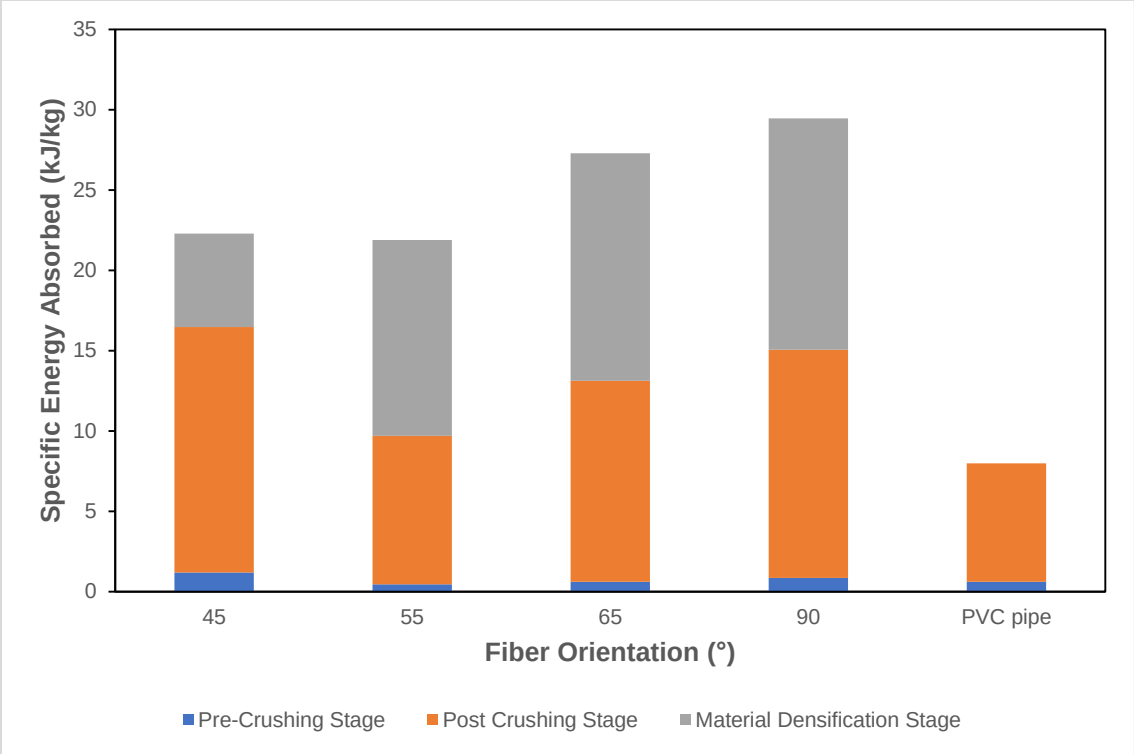

Figure 32. Specific energy absorbed by the GFRP overwrapped PVC tubes and the PVC tube on its own

The specific energy absorption results in Figure 32 show that taking the mass into account when considering the energy absorbed can make a considerable difference. For the pre-crushing stage, the specific energy absorbed by the PVC tube was comparable to that of the GFRP overwrapped PVC tubes, while for the post-crushing stage, specific energy absorbed was only slightly less than the worst-performing GFRP/PVC specimen. The specific energy absorbed by the PVC tube can be compared to the specific energy absorbed by the GFRP/PVC 55° specimen, which had the lowest pre-crushing and post-crushing specific absorbed energies from the tested overwrapped samples. For the pre-crushing stage, the PVC tube's specific energy absorption value was about 0.6090 kJ/kg, while the specific energy absorption value for the GFRP/PVC 55° tube was approximately 0.4603

kJ/kg, which was noticeably 24.41% less than that of the PVC tube. For the post-crushing stage, the PVC tube's specific energy absorption value was about 7.370 kJ/kg, while the specific energy absorption value for the GFRP/PVC 55° tube was approximately 9.234 kJ/kg, which was just 25.29% more than that of the PVC tube. For the post crush stage, this difference is much less than when energy absorbed, in kilojoules, is compared.

4.2. Effect of Different Fiber Orientations of GFRP Wrapping

4.2.1. Effect on Load Bearing Behavior

Specimens were prepared by wrapping PVC in GFRP at four different fiber orientations, respectively. The selected fiber orientation angles for investigation were 45°, 55°, 65°, and 90°. It was noted that the thickness of the samples was different, although eight layers of GFRP were applied for each fiber orientation angle. The thickness for the 45° samples was closer to 2.5 mm, while there was an increase in thickness for increasing fiber orientation angle until approximately 3.5 mm for the 90° samples. The 45° samples weighed the least while the 90° samples weighed the most.

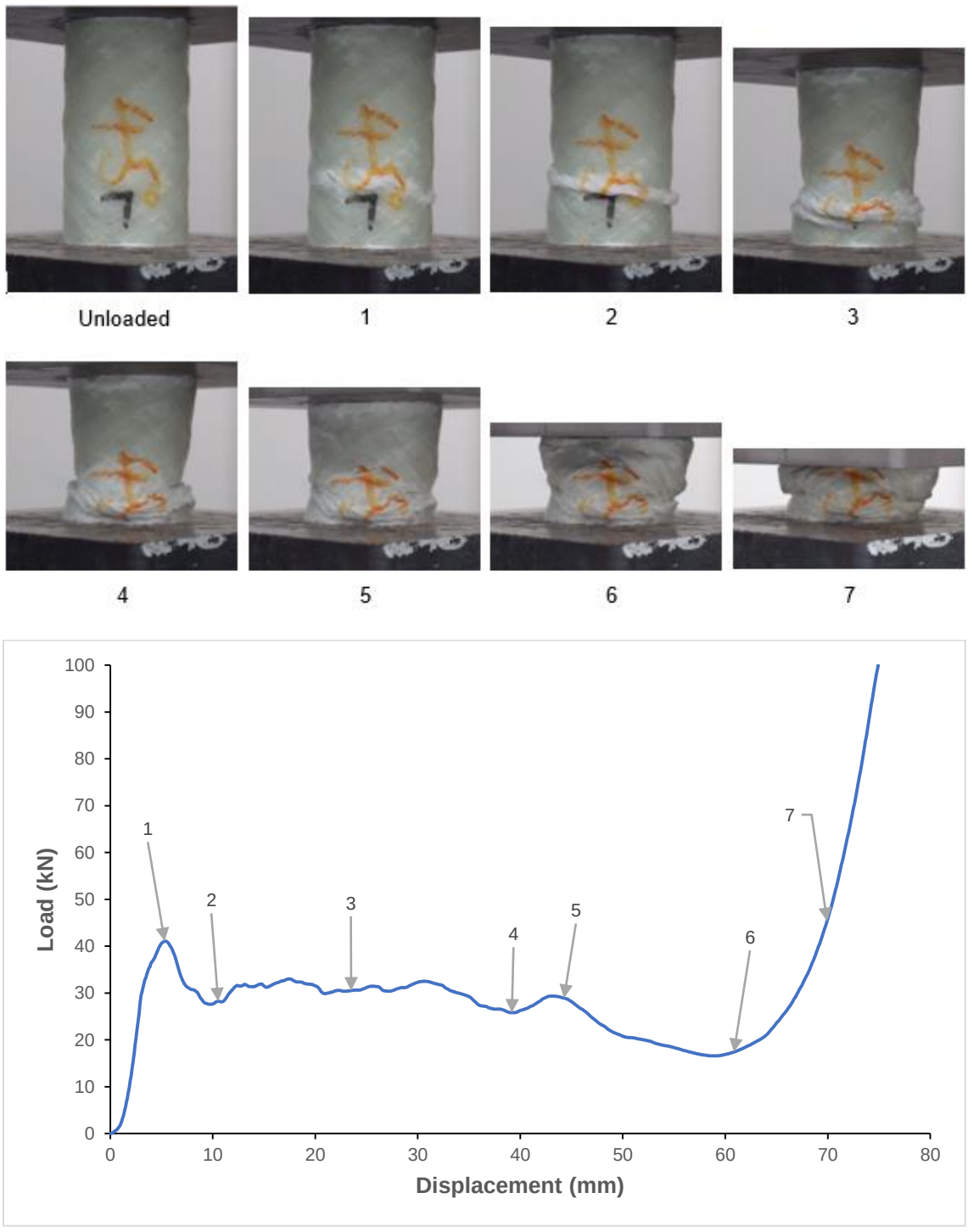

Figure 33. Load displacement curve for axial compression test of GFRP/PVC 45° sample and corresponding images

Figure 33 shows the load-displacement graph for the GFRP/PVC 45° composite tube when subjected to quasi-static axial crushing and the images corresponding to the graph's labeled points. It can be seen that the failure mode first exhibited by this sample was Mode-III failure as the initial failure of the tube occurred due to local buckling, with a hinge forming at the initial peak force of about 41.11 kN, at a displacement of 5.409 mm. Once this fold formed fully, the load reached a local minimum of approximately 27.60 kN, while the displacement at this point was about 10.93 mm. After this, until a displacement of approximately 44.09 mm, the GFRP/PVC 45° composite tube continued to display Mode-III failure as the load fluctuated about a mean value of 27.16 kN and a second fold formed in the composite tube. Subsequently, however, the top of the tube collapsed into itself, resulting in a noticeable drop in load-bearing capacity to a new overall minimum of 16.59 kN at a displacement of approximately 59.01 mm and severe matrix cracking. This drop-in load-bearing capacity bore a closer resemblance to the kind of behavior that would be expected of Mode-II brittle failure. Thus, it can be observed that the GFRP/PVC 45° composite sample exhibited Mode-III failure until a displacement of about 44.09 mm. After this, the failure mode changed to Mode-II failure until the composite tube load rose steeply as the composite tube was compacted in the densification stage. Although the damage to the GFRP/PVC 45° composite tube due to buckling, matrix cracking, and the final collapse of the sample was considerable, it was seen that the adhesion between the GFRP overwrapping and the PVC inner tube remained as the two components of the composite tube did not separate. Also, debonding during failure was negligible as even after densification, there were no noticeable hanging loose bunches of the GFRP wrapping. This was confirmed by examining a part of the sample, after crushing, that was not significantly

affected by buckling and matrix cracking using an SEM. From the SEM image of a section of the GFRP/PVC 45° composite tube after crushing, Figure 34a), it can be seen that although matrix cracking occurred, the GFRP/PVC 45° was not as damaged as the other samples. The width of the matrix crack observed was relatively smaller.

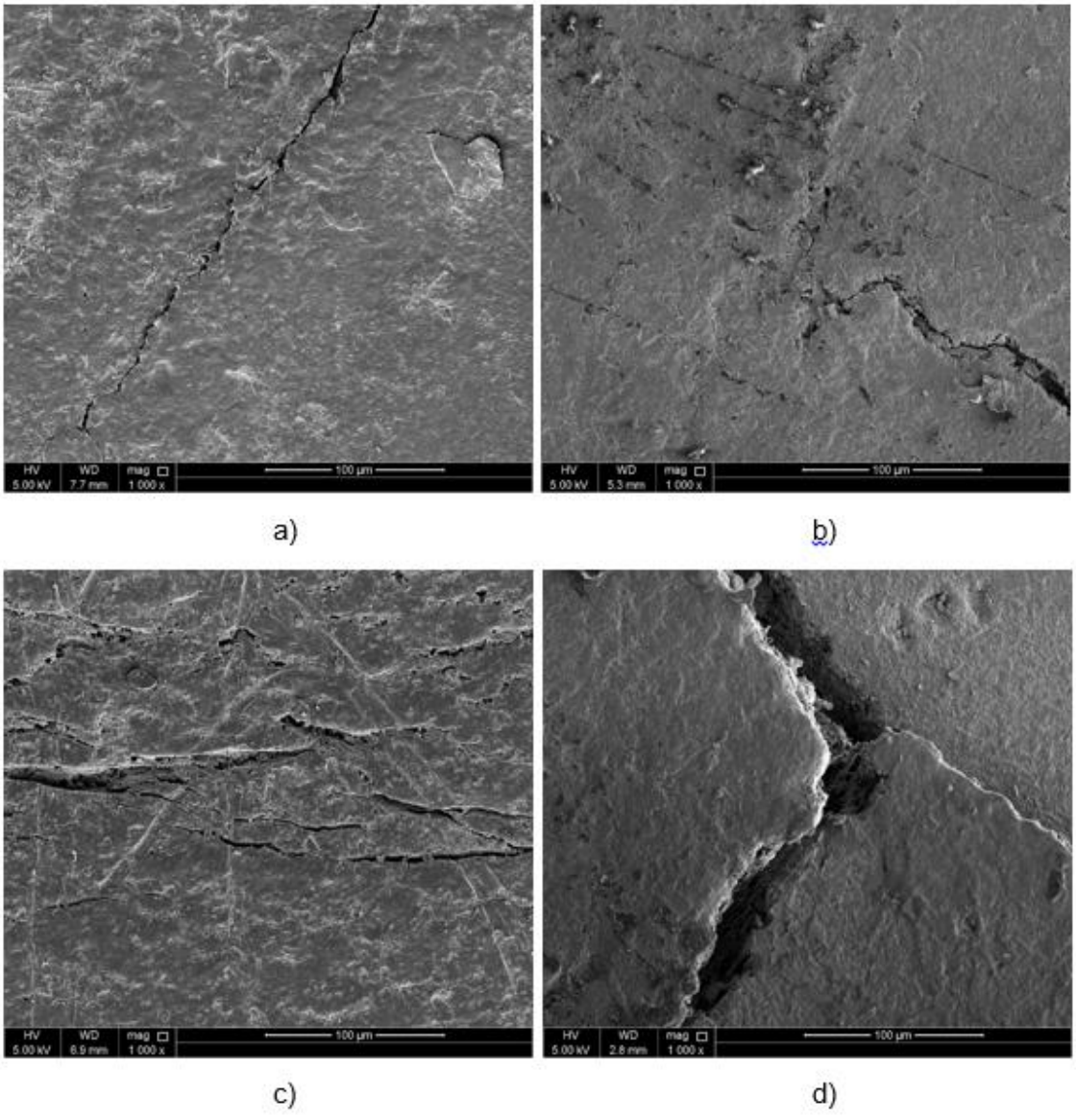

Figure 34. SEM images of side surfaces of GFRP/PVC composite tubes with fiber orientation angles of a) 45°, b) 55°, c) 65°, and d) 90° after crushing (1000 x magnification)

Figure 35 shows the load-displacement graph for the GFRP/PVC 55° composite tube when subjected to quasi-static axial crushing and the images corresponding to the points labeled in the graph.

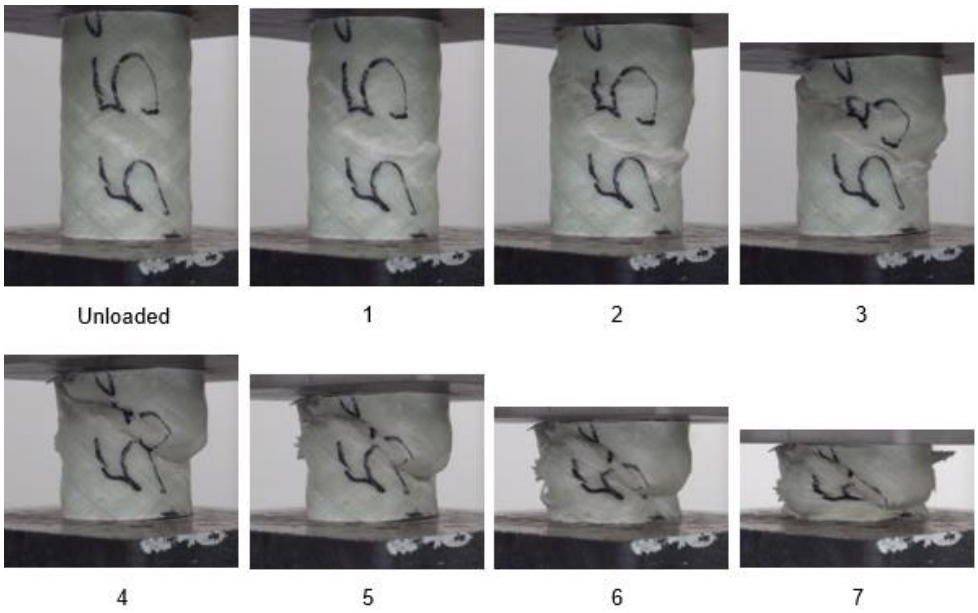

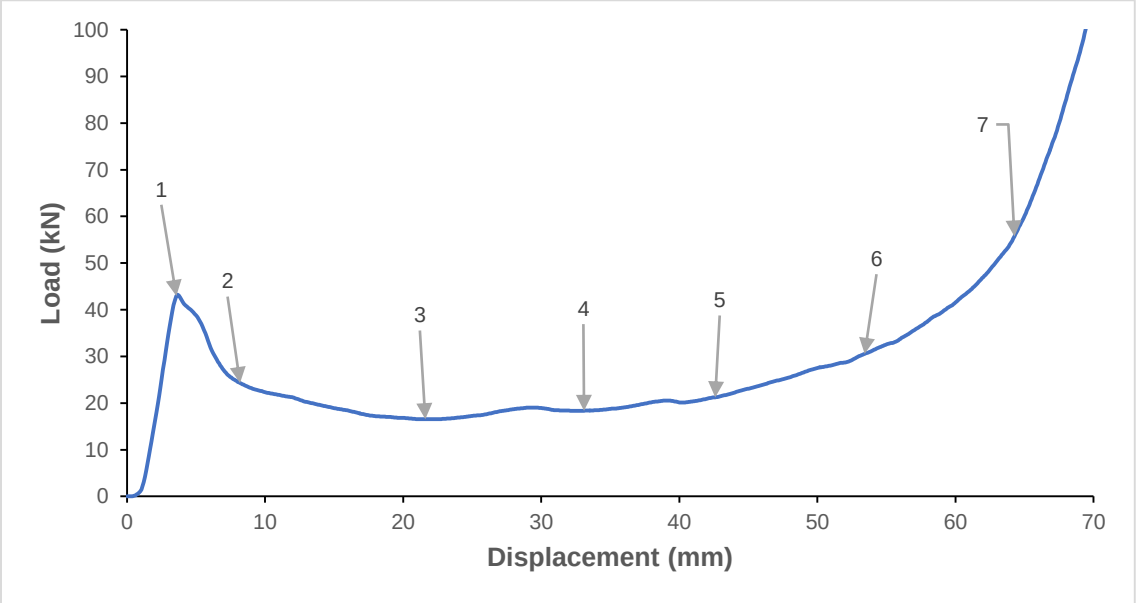

Figure 35. Load displacement curve for axial compression test of GFRP/PVC 55° sample and corresponding images

During the pre-crushing stage, the top section of the tube first shifted noticeably towards one side due to transverse shear failure. During this transverse shear failure, longitudinal cracking was almost negligible and the cracks formed were predominantly along the angle of fiber orientation. The transverse shear was not sufficient to cause complete separation across the fracture plane, and eventually, the interpenetration of the two halves of the tube on either side of the fracture plane occurred at the initial peak force of 43.21 kN and a displacement of 3.666 mm. The two halves of the tube then continued to interpenetrate through one another, causing a considerable drop in load-bearing capacity and significant matrix cracking. This type of catastrophic failure is characteristic of Mode-II failure. The bearing capacity reached a minimum of about 16.56 kN at a displacement of approximately 22.43 mm due to this. After this, the fold due to interpenetration enlarged, resulting in the matrix cracks lengthening noticeably. While the fold was enlarged, loading was relatively stable until a displacement of about 40.10 mm. Then the interpenetration fold collapsed, and the two halves of the specimen began compacting together accompanied by a rise in load. Finally, the compaction of the composite tube continued throughout the densification stage. The compaction at the end of the composite tube failure caused noticeable debonding. From the SEM image of a section of the GFRP/PVC 55° composite tube after crushing, Figure 34b), the matrix cracking that occurred can be seen.

Figure 36 shows the load-displacement graph for the GFRP/PVC 65° composite tube when subjected to quasi-static axial compression and the images corresponding to the points labelled in the graph. At first, due to the build-up of transverse shear stress, the top

third of the composite tube specimen shifted slightly to the side, and a fracture plane was formed due to circumferential cracking. The fracture plane fully formed at the initial peak load of 46.62 kN, which occurs at a displacement of about 4.245 mm.

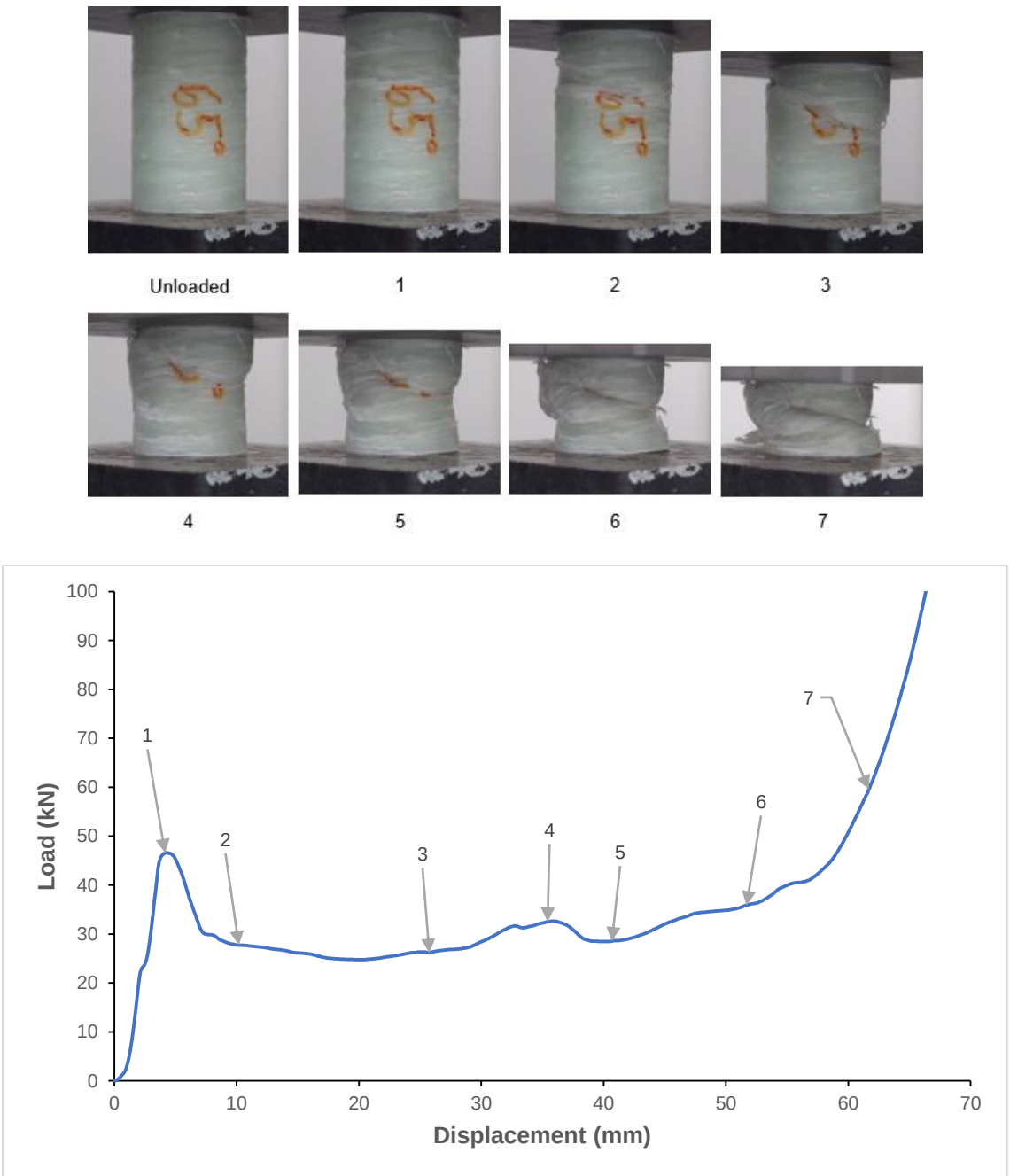

Figure 36. Load displacement curve for axial compression test of GFRP/PVC 65° sample and corresponding images

The two sections of the tube then continued to interpenetrate through one another, while the matrix cracks caused by the split also lengthened, resulting in the tube's load-bearing capacity decreasing as a result. Following this, the load dropped quite steeply until it reached a value of about 29.90 kN at a displacement of 7.625 mm. This type of catastrophic drop in load-bearing capacity is characteristic of Mode-II failure. After this, the rate at which the specimen's load-bearing capacity was dropping decreased until the load reached a local minimum of approximately 24.77 kN, at a displacement of 19.76 mm. Then, another small split due to circumferential cracking formed in the bottom third of the composite tube. As the split formed, the specimen's load-bearing capacity also increased until a fracture plane fully formed at a local maximum load of about 32.61, which occurred at a displacement of 36.10 mm. Again, the two newly formed sections on either side of the fracture plane interpenetrated one another, causing a slight drop in load-bearing capacity, up to a local minimum of 28.45 kN, which corresponded to a displacement of 40.01 mm. After this drop, the folding failure mode is observed due to this fracture, and the three sections of the tube began to compact together, giving rise to an increase in load. This compaction continued up to the densification stage, and the rate at which the load-bearing capacity was rising increased as compaction progressed. Along with the progression of compaction in the densification stage, a noticeable amount of debonding also occurred. From the SEM image of a section of the GFRP/PVC 65° composite tube after crushing, Figure 34c), the matrix cracking that occurred can be seen. In particular, it can be seen that the cracking observed was more severe than for the GFRP/PVC 45° and GFRP/PVC 55° samples.

The load-displacement behavior for the GFRP/PVC 90° composite tube when subjected to quasi-static axial compression is shown in Figure 37, along with the images corresponding to the points labeled in the graph.

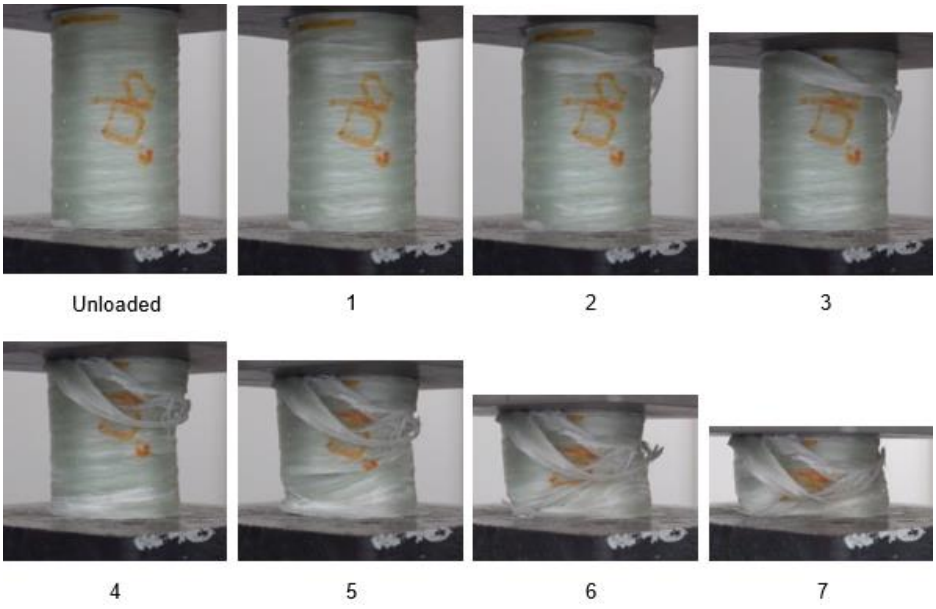

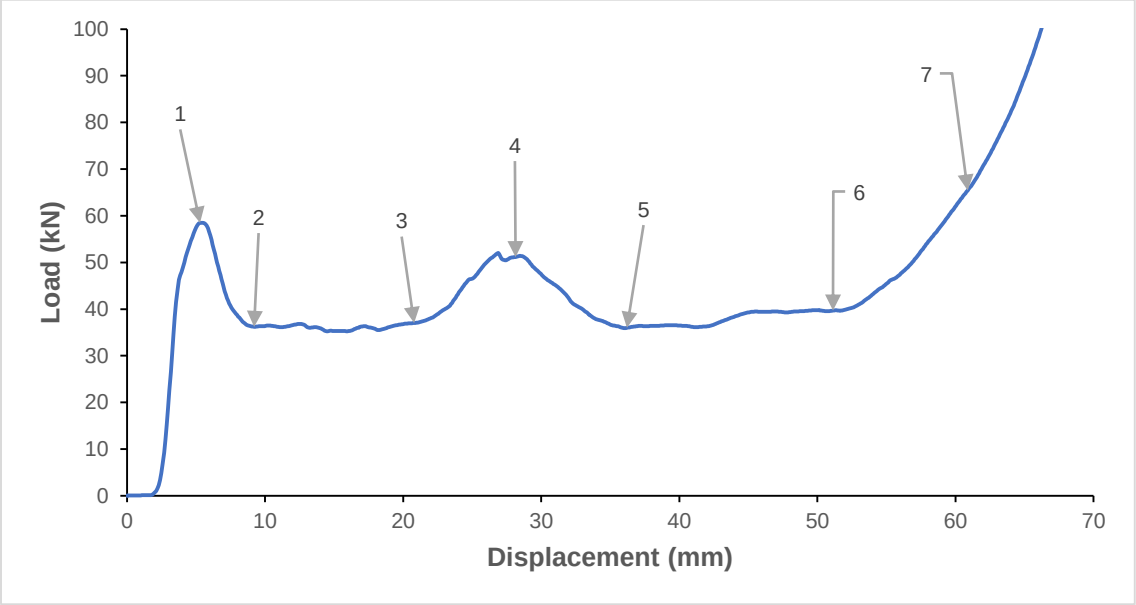

Figure 37. Load displacement curve for axial compression test of GFRP/PVC 90° sample and corresponding images

As the compression test for this composite tube progressed, due to the build-up of buckling stresses in the composite tube, circumferential cracks formed a quarter of the way down from the tube's top end. These cracks caused a fracture plane to form, resulting in the occurrence of interpenetration failure. This was accompanied by some transverse shear, which resulted in the top section of the composite tube shifting slightly to one side as interpenetration took place. This fracture plane fully formed at the initial peak load for the specimen, which was about 58.51 kN and occurred at a displacement of approximately 5.400 mm. After this peak, there was a significant drop in load as the two sections of the tube continued to compact together. A decrease followed this in the load-bearing capacity yo the load is measured to be 36.22 kN, at a displacement of 9.299 mm. This drop-in load was accompanied by significant debonding at the fold formed due to interpenetration failure, such that part of the GFRP wrapping could be seen hanging loose from the composite tube. From this, it could be seen that the GFRP/PVC 90° composite tube specimen underwent debonding much more quickly than the other GFRP/PVC specimens, as all the other specimens only exhibited debonding in the densification stage. Although the interpenetration and consequent drop in failure that occurred were reminiscent of Mode-II failure, the GFRP/PVC 90° composite tube's load-bearing capacity remained noticeably higher than that of even the GFRP/PVC 45° composite tube, which underwent Mode-III failure. This can be attributed mostly to the fiber orientation of the GFRP/PVC 90° composite tube. As the loading direction was perpendicular to the fiber orientation, the fibers provided a higher resistance to loading as compared to the other samples, and therefore a higher load was required to overcome this resistance. However, as a direct

consequence, the GFRP/PVC 90° composite tube exhibited the most severe debonding of the tested samples. Following this, the two sections of the tube were compacted together while debonding continued to occur. The compaction of the composite tube would typically have resulted in a rise in load while debonding weakens composite tubes and usually causes a drop in load. However, compaction and debonding co-occurred, and for a time, they balanced each other out, resulting in a relatively stable failure until the displacement reached about 21.22 mm. Eventually, the rise in load due to compaction became more pronounced while, at the same time, local buckling occurred at the bottom end of the tube, resulting in a rise in load up to a local maximum of approximately 50.38 kN, at a displacement of 29.05 mm. After a hinge formed due to the local buckling at the tube's bottom end, there was a subsequent drop in load as the tube folded inwards at the hinge. After this, the two opposing failure mechanisms, compaction and debonding, continued with a relatively stable load being maintained as a result until a displacement of about 52.05 mm. Finally, in the densification stage, the amount of weakening due to debonding could not keep up with the increasing load due to compaction, and the rate at which the load-bearing capacity rose increased as the compaction progressed. After the compression tests were carried out from the state of the specimens, the GFRP/PVC 90° specimen had a noticeably higher number of loose bunches of GFRP hanging from the specimen as compared to the other specimens. The comparatively more severe matrix cracking that occurred can also be seen from the SEM image of a section of the GFRP/PVC 90° composite tube after crushing, Figure 34d).

The load-bearing behavior for all the tested GFRP/PVC composite tubes is shown in Figure 38 in order to allow for easier comparison. For all the GFRP overwrapped PVC tubes, it was previously seen that local buckling and interpenetration failure were the causes of the initial failure in the tubes, and as a result, all the tubes exhibited a noticeable drop in load-bearing capacity after the initial peak load was reached. It was observed that as the fiber orientation angle of the tested samples increased, the initial peak load also increased. The GFRP/PVC 90° sample had the highest initial peak load of approximately 58.51 kN, while the GFRP/PVC 45° sample had the lowest initial peak load of about 41.11 kN. There was an irregularity in this trend for the mean crushing force of the samples during the post-crash stage.

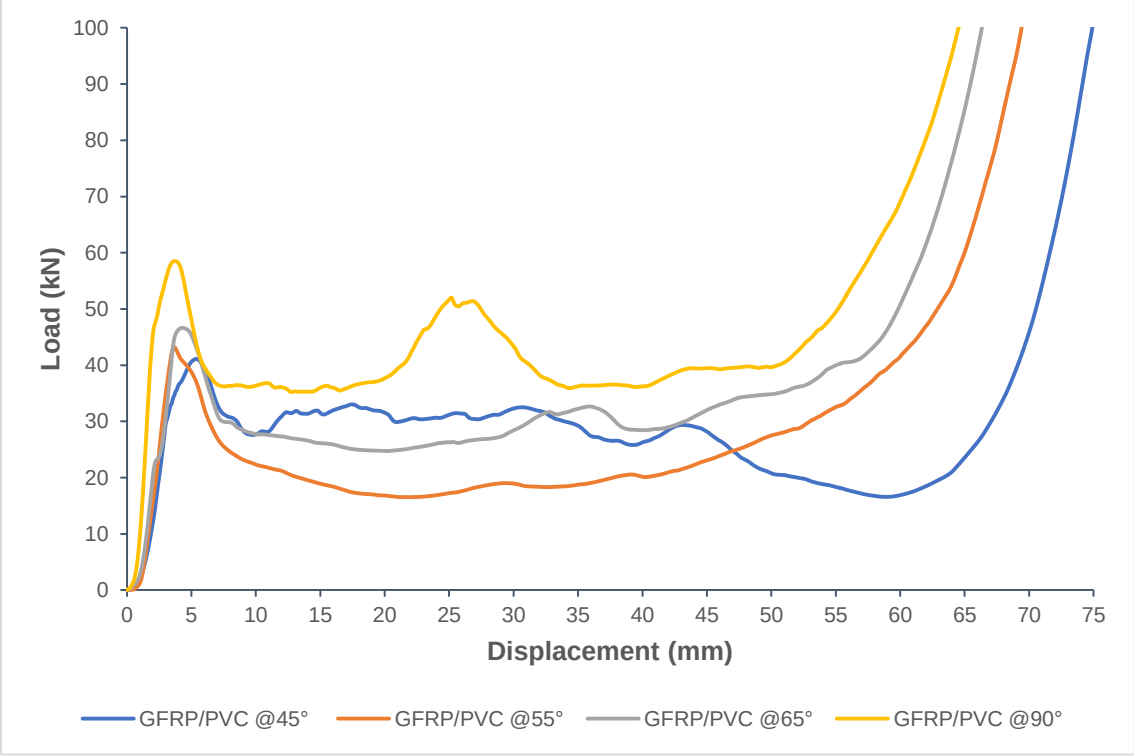

Figure 38. Load displacement curves for axial compression test of all GFRP overwrapped PVC tubes

The mean crushing force of the GFRP/PVC 55° sample was determined to have the lowest value during the post-crushing stage of 21.68 kN. For the rest of the samples, as the samples' orientation angle increased, the mean crushing load also increased. The GFRP/PVC 45° composite tube had a mean crushing force of 27.16 kN for the course of the post-crushing stage, followed by the GFRP/PVC 65° sample with a mean crushing load of 30.68 kN and finally, the GFRP/PVC 90° composite tube had the highest mean crushing load of 40.01 kN. Therefore, in terms of overall load-bearing capability, the GFRP/PVC 90° composite tube performed the best. This can be attributed to the fiber orientation of the GFRP/PVC 90° composite tube. As the loading direction was perpendicular to the fiber orientation, the fibers provided a higher resistance to loading. This load-bearing behavior suggests that the tested composite tubes had a reasonably high fiber volume fraction as only with a high fiber volume fraction would the spacing between the fibers in the GFRP/PVC 90° sample be small enough to allow for the fibers to bundle together and support each other effectively when subjected to compressive loading. The irregularity in the mean crushing force of the GFRP/PVC 45° specimen can be attributed to the fact that this sample exhibited Mode-III failure while all the other tested GFRP/PVC composite tubes exhibited Mode-II failure.

It can also be observed that the GFRP/PVC 55°, GFRP/PVC 65°, and GFRP/PVC 90° composite tube samples experienced transverse shear failure to different degrees. The load-bearing behavior of these samples indicated that with a decrease in the degree of transverse shear failure, there was a corresponding increase in load-bearing capacity.

Additionally, the matrix cracks that formed the transverse fracture planes for each of these samples respectively mostly formed along the direction of fiber orientation. This implies that crack propagation perpendicular to the fiber direction was inhibited effectively by the fibers. Another notable observation made was that no Mode-I failure, which is the most desired failure mode due to its high energy absorption, occurred during the conducted crushing experiments. This seems to be due to the PVC inner tubes' presence in the samples and the strong adhesion between the GFRP overwrapping and these inner tubes. These two factors prevent the formation of fronds while seemingly promoting the occurrence of Mode-III failure. On the other hand, the PVC inner tubes' presence also seems to reduce the severity of brittle fracture when Mode-II failure occurs. Additionally, compared to composite tubes that undergo Mode-I failure, the crushed samples' fragmentation was not as severe.

4.2.2. Effect on Crush Force Efficiency

Table 6. CFE and %iCFE within 0.1 from Ideal for GFRP/PVC Tubes

Sample configuration	Overall CFE	% iCFE ±0.1 from Ideal
GFRP/PVC @45°	0.6607	31.27
GFRP/PVC @55°	0.5017	29.12
GFRP/PVC @65°	0.6569	39.53
GFRP/PVC @90°	0.6838	57.07

From the overall CFE and % iCFE within 0.1 of ideal values in Table 6, it can be seen that, in addition to having the best load-bearing performance, the GFRP/PVC 90° composite tube also has the most stable failure for the tested fiber orientations. From the overall CFE, it can also be seen that the GFRP/PVC 45° sample performs slightly better than the GFRP/PVC 65° sample in terms of overall failure during the post-crushing stage. However, the fact that the GFRP/PVC 65° composite tube has a higher value for the % iCFE within 0.1 of the ideal value shows that the load-bearing capacity of the GFRP/PVC 45° sample has a higher degree of deviation from the mean crushing load. Finally, it was seen that the GFRP/PVC 55° sample exhibited the lowest performance in terms of crush force efficiency.

4.2.3. Effect on Energy Absorption Capability

For the energy absorption capability of composite structures, it is essential to remember that the sum of the energies absorbed in the pre-crushing and post-crushing stages is the energy that is considered useful for crashworthiness applications. It is also more important to consider the specific energy absorbed as the relatively lightweight of composites is one of the main reasons for the increasing use of composites in crashworthiness applications.

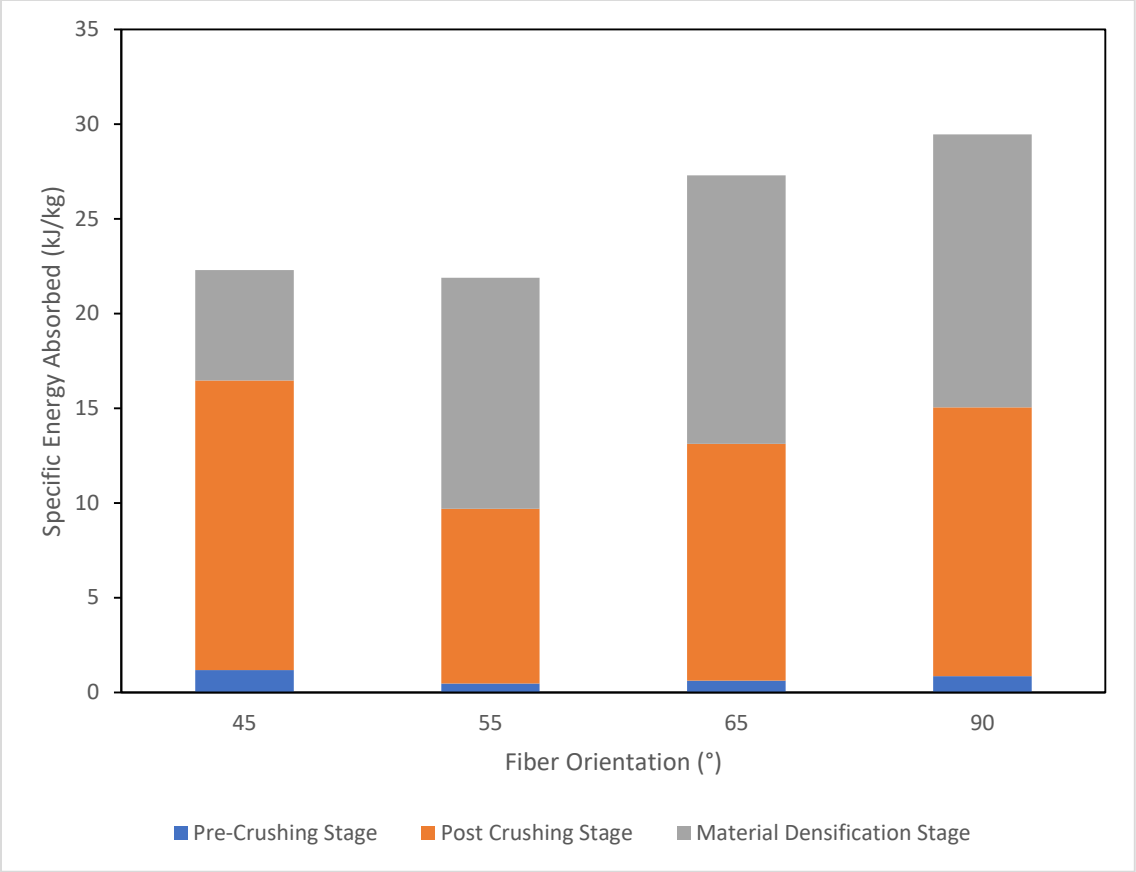

Figure 39. Specific energy absorbed by the GFRP overwrapped PVC tubes of different fiber orientation

For the total specific energy absorbed by the tested composite tubes (Figure 39), it was seen that the GFRP/PVC 45° composite tube performed the best, with pre-crushing and post-crushing specific energy absorbed adding up to approximately 16.47 kJ/kg. Thus, it was seen that although the load-bearing capability of the GFRP/PVC 45° sample did not stand out, due to its comparatively lower mass, it was able to perform well in terms of energy absorption capability. The GFRP/PVC 90° sample exhibited the next best performance with total specific energy absorbed of 15.05 kJ/kg. The energy absorption of the GFRP/PVC 55° composite tube proved to be the most lacking, at total specific energy absorbed of 9.695 kJ/kg.

4.3. Effect of Changes in Design of Conventional Circular Composite Tube

Although a considerable amount of work has been done concerning using different geometries of composite tubes, there is little work done that looks into further improving the performance of existing conventionally used geometries by making slight changes to the standard design of the geometry. The conventional geometry selected for this study was the circular composite tube, as this geometry has proven to be useful in past research work conducted on composites and can be easily incorporated in crashworthiness applications. The changes proposed to the conventional circular tube geometry in this section aim to reduce the amount of material present in a circular composite tube, thereby reducing its mass while at the same time maintaining its load-bearing capacity and crushing force efficiency. This will, in turn, result in an increase in specific energy absorption for the composite tube. Composite structures themselves are favored due to their high strength to weight ratios, and the aim of further reducing the composite samples' weight while maintaining their performance ability is to aim further to enhance one of a composite's most vital points.

4.3.1. First Design Change

When quasi-static axial compression tests were conducted for the PVC tube on its own, it was found that the initial peak load of the PVC tube was 15.14 kN and occurred at a displacement of 4.599 mm. Before this point, the behavior of the PVC tube was elastic. From this, it was expected that if the GFRP wrapping was removed entirely from the top section of a GFRP overwrapped PVC tube sample, and the height of removed material was

less than 4.599 mm. Also, the section of exposed PVC tube at the top of the sample would be able to support quasi-static axial compression until the GFRP overwrapped portion of the tube was reached without experiencing a drop in load-bearing capacity. Therefore, for the first design change, it was proposed that a portion of the GFRP wrapping at the top section of the circular composite tube samples should be removed entirely. The suggested height of removed material was set to 3.5 mm to leave a slight safety buffer and avoid a premature drop in load-bearing capacity. Therefore, specimens were prepared by removing the top 3.5 mm section of GFRP from GFRP overwrapped PVC tubes of the four previously tested fiber orientations, i.e., 45°, 55°, 65°, and 90°. A total of 3 tests were carried out for this design for each of the four wrapping angles, respectively, to verify the results obtained. From this point onwards, the samples with the top 3.5 mm section of GFRP wrapping removed are referred to by using 'R' after the fiber orientation angle, for ease of identification, e.g., GFRP/PVC 45°R sample will refer to a PVC tube that has been overwrapped with GFRP at 45° and then had the top 3.5 mm section of GFRP wholly removed.

4.3.1.1. Effect on Load Bearing Behavior

The load-displacement curves for before and after the design change for each fiber orientation angle will be compared to examine the effect of the first proposed design change on the composite tube samples' load-bearing behavior.

Figure 40 shows the load-displacement curves for the compression test of both the GFRP/PVC 45° and GFRP/PVC 45°R samples. It was observed that the GFRP/PVC 45°R

sample had a higher initial peak load of about 47.15 kN than the GFRP/PVC 45° sample, which had an initial peak load of 41.11 kN. However, it was also seen that the minimum load of the GFRP/PVC 45°R sample, which was 13.21 kN, was slightly lower than that for the GFRP/PVC 45° sample. Comparing the mean crushing loads for the two samples during the post-crushing stage, the GFRP/PVC 45°R sample had a mean load of 24.54 KN, only 9.65% less than the mean load of the GFRP/PVC 45° sample, which was 27.16 kN.

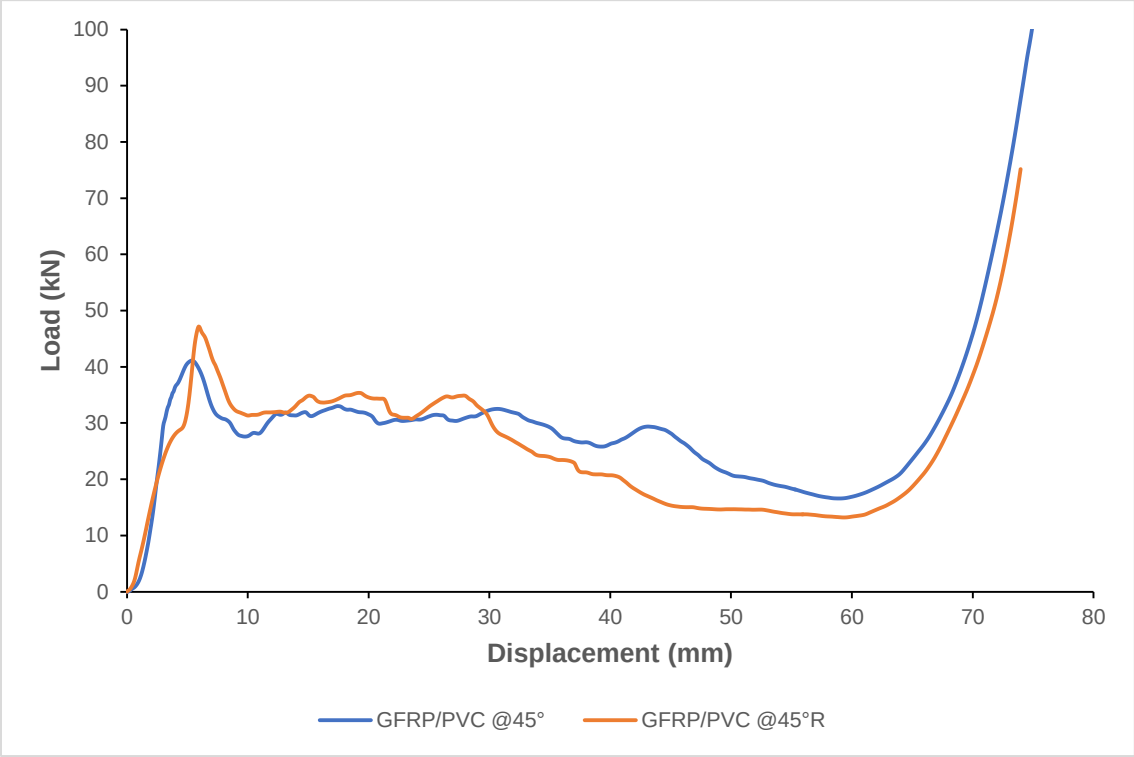

Figure 40. Load displacement curves for compression test of samples GFRP/PVC 45° and GFRP/PVC 45°R

Overall, it was seen that the load-bearing behavior of the two samples was reasonably similar. Therefore, it was shown that completely removing the top 3.5 mm

section of GFRP wrapping from the GFRP/PVC 45° sample did not significantly deteriorate the load-bearing capacity of the composite tube.

Figure 41 shows the load-displacement curves for the compression test of both the GFRP/PVC 55° and GFRP/PVC 55°R samples. Upon initial observation, it can be seen that completely removing the top 3.5 mm section of GFRP wrapping from the GFRP/PVC 55° sample seems to have increased the load-bearing capacity of the composite tube. It was observed that the GFRP/PVC 55°R sample had a higher initial peak load of about 48.47 kN than the GFRP/PVC 55° sample, which had an initial peak load of 43.21 kN. Comparing the mean crushing loads for the two samples during the post-crushing stage, the GFRP/PVC 55°R sample had a mean load of 34.94 kN, a considerable 61.16% higher than the 21.68 kN mean load of the GFRP/PVC 55° sample.

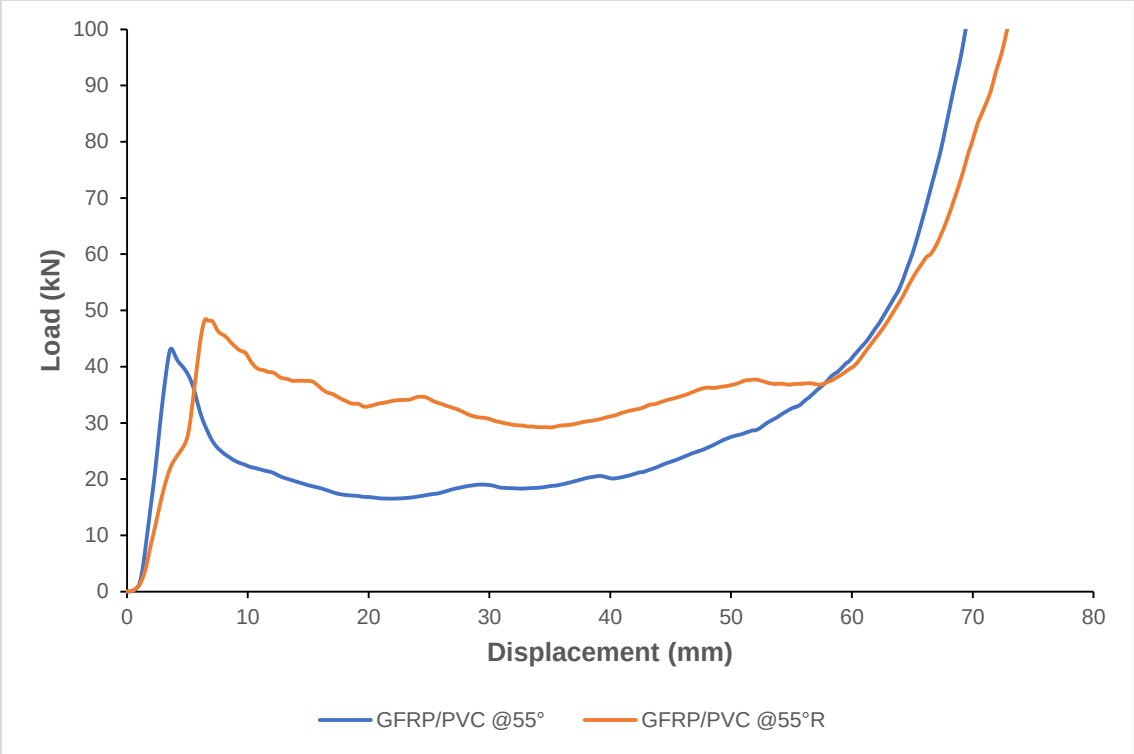

Figure 41. Load displacement curves for compression test of samples GFRP/PVC 55° and GFRP/PVC 55°R

The load-displacement curves for the compression test of both the GFRP/PVC 65° and GFRP/PVC 65°R samples are shown in Figure 42. At first glance, it can be observed that the load-bearing behavior for the two samples is very similar. It was seen that the GFRP/PVC 65°R sample had an initial peak load of about 47.48 kN, only slightly higher than the initial peak load of the GFRP/PVC 65° sample, which was 46.62 kN. Comparing the mean crushing loads for the two samples during the post-crushing stage, the GFRP/PVC 65°R sample had a mean load of 30.85 kN, almost equivalent to the mean load of the GFRP/PVC 65° sample, which was approximately 30.63 kN. Therefore, it can be seen that completely removing the top 3.5 mm section of GFRP wrapping from the GFRP/PVC 65° sample did not adversely affect its load-bearing capabilities.

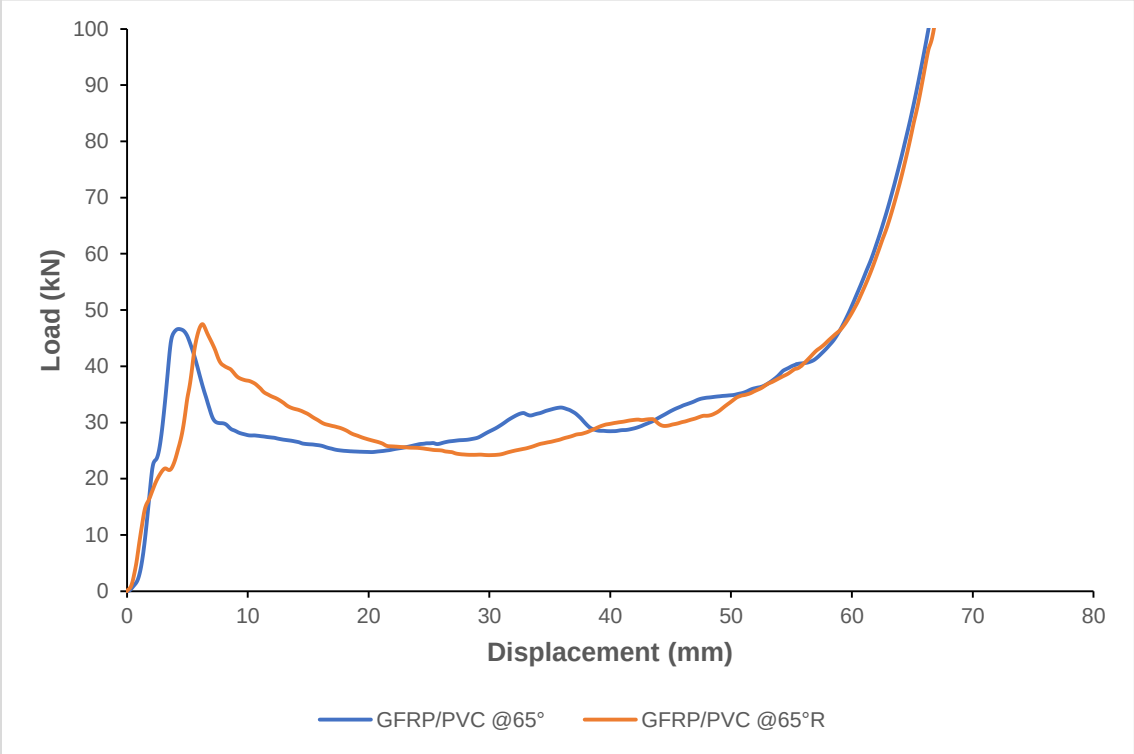

Figure 42. Load displacement curves for compression test of samples GFRP/PVC 65° and GFRP/PVC 65°R

Figure 43 below shows the load-displacement curves for the compression test of both the GFRP/PVC 90° and GFRP/PVC 90°R samples. For these two samples as well, the load-bearing behavior seems to be comparable. The GFRP/PVC 90°R sample had an initial peak load of about 59.81 kN, only slightly higher than the initial peak load of the GFRP/PVC 90° sample 58.51 kN. The mean crushing loads of the pre-crushing stages for the GFRP/PVC 90°R and the GFRP/PVC 90° samples was 41.35 kN and 40.01 kN, respectively, which were very close in value. This shows that for the GFRP/PVC 90° sample, completely removing the top 3.5 mm section of GFRP wrapping from the sample did not adversely affect its load-bearing capabilities.

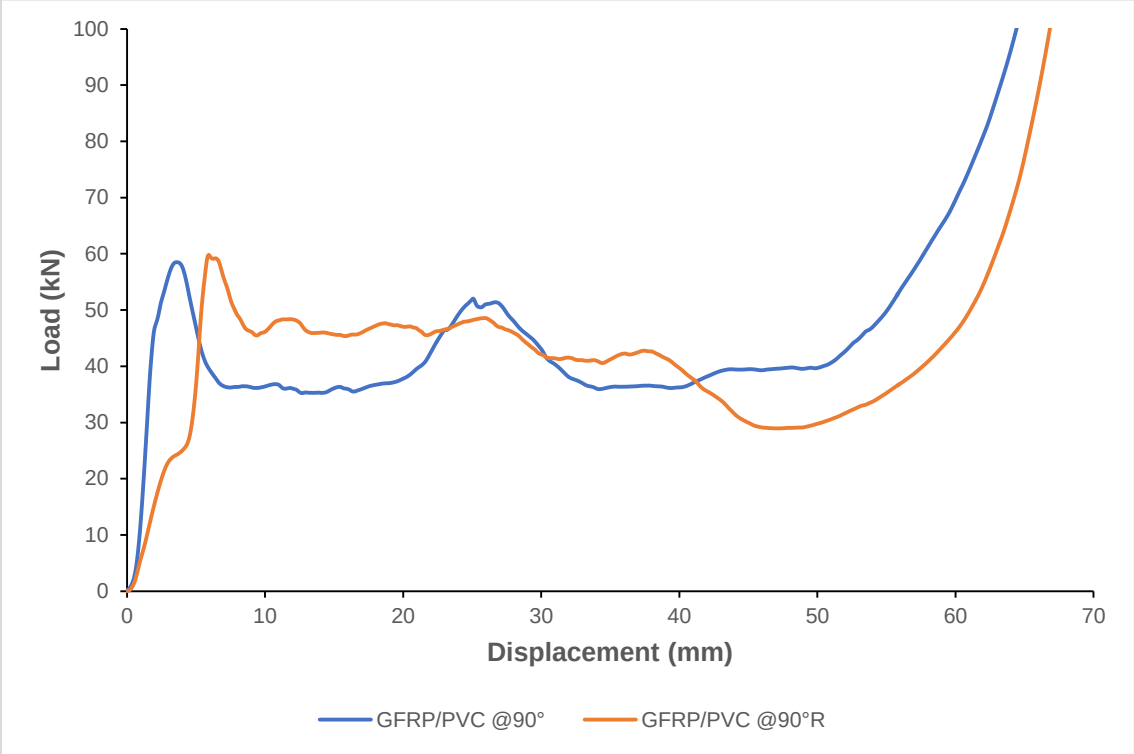

Figure 43. Load displacement curves for compression test of samples GFRP/PVC 90° and GFRP/PVC 90°R

In summary, it was shown that the load-bearing capabilities of the samples for all tested fiber orientations were acceptably maintained when the first proposed design change was implemented.

4.3.1.2. Effect on Crush Force Efficiency

From Table 7, containing the CFE and % iCFE within 0.1 of the ideal, it can be seen that there are some notable changes to the value of these two parameters due to implementing the proposed design change. There is a significant 21.20% drop in the CFE value of the GFRP/PVC 45°R sample and a noticeable 21.50% drop in its % iCFE within

0.1 of the excellent value, as compared to the GFRP/PVC 45° sample. This shows that the GFRP/PVC 45°R sample exhibits a more considerable amount of fluctuation around the mean and has a more considerable difference between its mean and initial peak load values. In contrast, the two parameters increased significantly for the GFRP/PVC 55°R, as compared to the GFRP/PVC 55° sample. For the GFRP/PVC 55°R sample, the composite load's failure is comparatively more stable after the proposed design change, and the mean and initial peak load values are close together. Only the CFE for the GFRP/PVC 65°R and GFRP/PVC 90°R samples remained almost unchanged after implementing the proposed design change.

Table 7. CFE and %iCFE within 0.1 from Ideal for GFRP/PVC Tubes and GFRP/PVC R Tubes

Sample configuration	Overall CFE	% iCFE ±0.1 from Ideal
GFRP/PVC @45°	0.6607	31.27
GFRP/PVC @55°	0.5017	29.12
GFRP/PVC @65°	0.6569	39.53
GFRP/PVC @90°	0.6838	57.07
GFRP/PVC°@45°R	0.5206	9.77
GFRP/PVC @55°R	0.7208	63.59
GFRP/PVC @65°R	0.6498	36.62
GFRP/PVC @90°R	0.6914	39.53

However, there was a slight drop in % iCFE within 0.1 of the ideal values for the GFRP/PVC 65°R sample and GFRP/PVC 90°R sample, as compared to the GFRP/PVC 65° sample and the GFRP/PVC 90° sample. This shows that the failure of the GFRP/PVC

65°R and GFRP/PVC 90°R samples due to axial compression shows more deviation from the mean than their counterparts. Overall, the GFRP/PVC 55°R is an outlier in this case, and the spike in the initial peak load of the tested samples after the design change lower the crush force efficiency of the samples.

4.3.1.3. Effect on Energy Absorption Capability

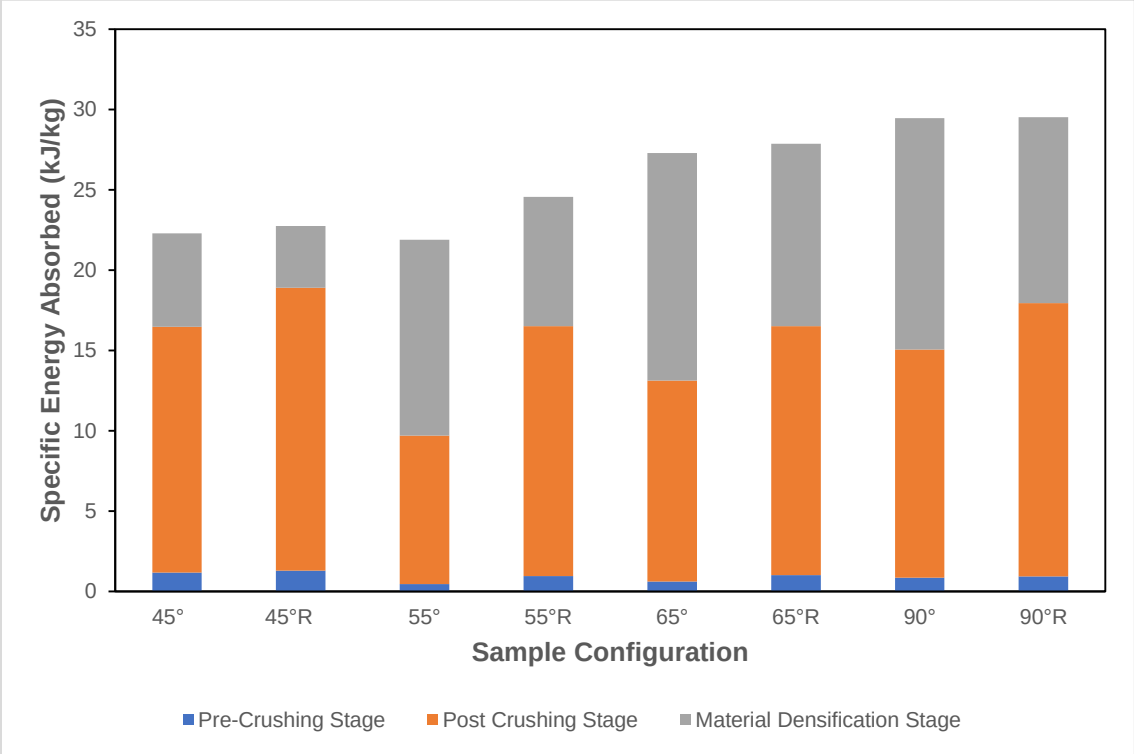

Figure 44. Specific energy absorbed by the GFRP/PVC tubes and GFRP/PVC R tubes

From an earlier section of the report, it was seen that the load-bearing capabilities of the samples for all tested fiber orientations were acceptably maintained when the proposed design change was implemented. At the same time, it should be remembered that the design change entailed removing GFRP wrapping, which would also lead to a decrease

in the mass of the samples. Therefore, one would expect that the GFRP/PVC R tubes' specific energy absorbed values would be noticeably higher than those for the GFRP/PVC tubes. This is reflected in the results shown in Figure 44.

As was mentioned previously, the sum of the energies absorbed in the pre-crushing and post-crushing stages is the energy that is considered useful for crashworthiness applications. The specific energy absorbed by the GFRP/PVC 45°R tube was approximately 18.91 kJ/kg, a significant 14.81% higher than the 16.47 kJ/kg value for the GFRP/PVC 45° sample. It should also be noted that the GFRP/PVC 45°R sample was the sample with the best performance in terms of use specific energy absorbed. The composite tubes with fiber orientations of 65° and 90° also experienced a significant increase in the specific energy absorbed due to the proposed design change. The useful energy absorbed value for the 65° sample increased from 13.12 kJ/kg to 16.51 kJ/kg, while that for the 90° sample rose from 15.05 kJ/kg to 17.95 kJ/kg. However, the most pronounced increase was experienced by the composite tube sample with a fiber orientation of 55°. The useful energy absorbed value for the 55° sample rose by a steep 70.19%, from 9.695 kJ/kg to 16.50 kJ/kg, after the first design change was implemented.

4.3.2. Second Design Change

After the first proposed design change to the conventional circular tube, geometry was implemented, it was observed that although the load-bearing capabilities of the samples were maintained and their specific energy absorption values increased, the spike in initial peak load of the tested samples after the design change lower the crush force

efficiency of the samples. However, if the transition from the top 3.5 mm section of the composite tube samples, for which the GFRP wrapping was removed entirely, and the overwrapped portion of the tubes directly below was more gradual, this could potentially deter the spike in initial peak load that occurs and, by so doing, increase the crush force efficiency of the samples. Whether or not the advantages of maintained load-bearing capacity and increased specific energy absorption would be retained as well remains to be seen. Therefore, for the second proposed design change, the GFRP wrapping was first wholly removed from the top 3.5 mm section of the GFRP/PVC tubes, as was done for the first design change. After this, a 1 mm thickness of the GFRP wrapping was removed from the 10 mm section of the tube directly below this 3.5 mm section, essentially forming a small step. Orthographic views for this second proposed design change can be seen in Chapter 3. A total of 3 tests were carried out for this design for each of the four wrapping angles, respectively, to verify the results obtained. From this point onwards, the samples with the second proposed design change will be referred to by using 'RS' after the fiber orientation angle, where 'R' signifies the repetition of the first proposed design change and 'S' signifies the small step added to act as a transition. e.g., GFRP/PVC 45°RS sample will refer to a PVC tube that has been overwrapped with GFRP at 45° and then had the top 3.5 mm section of GFRP wholly removed, followed by the removal of a 1 mm thickness of the GFRP wrapping from the 10 mm section of wrapping directly below this 3.5 mm section.

4.3.2.1. Effect on Load Bearing Behavior

Previously, it was determined that the load-bearing capabilities for the composite tubes tested after implementation of the first proposed design change were comparable to

those of the composite tubes with a conventional circular geometry tested before the first design change was applied. One of the main reasons for the suggestion of the second design change was to deter the spike in the initial peak force that occurred as a result of the first design change. Therefore, to examine the effectiveness of the second proposed design change, the load-displacement curves for composite tubes that have undergone the first design change and composite tubes that have experienced the second design change will be compared.

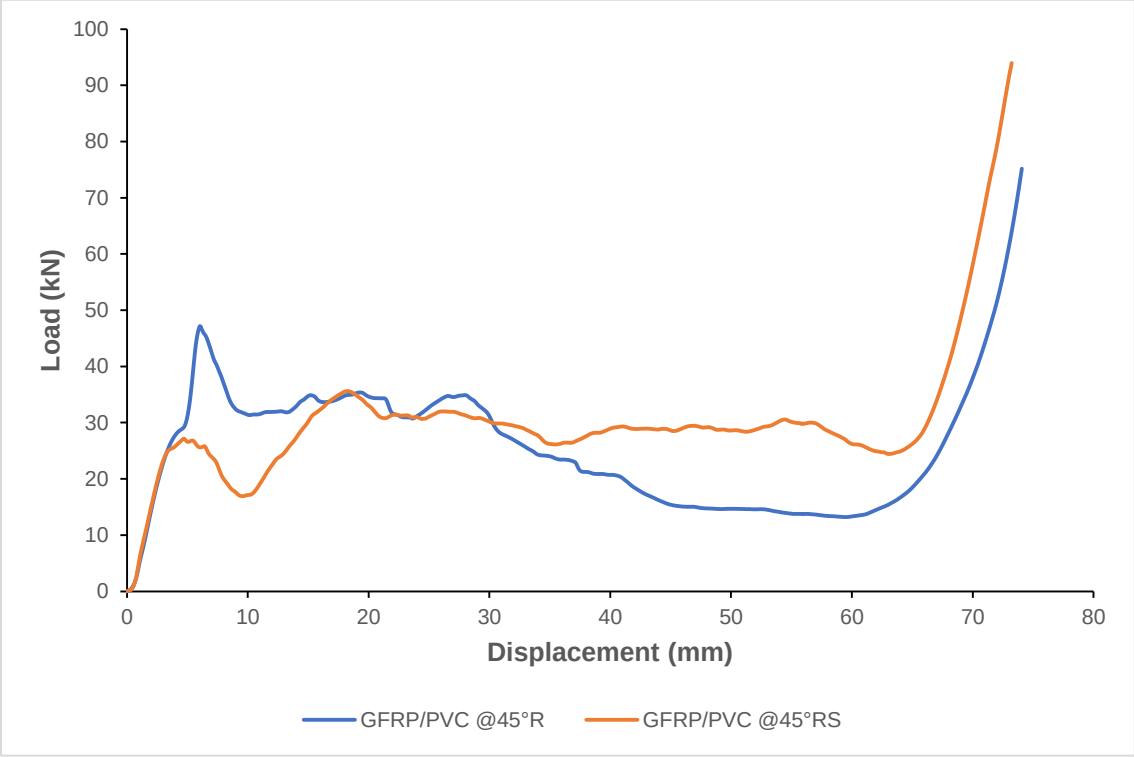

Figure 45. Load displacement curves for compression test of samples GFRP/PVC 45°R and GFRP/PVC 45°RS

Figure 45 shows the load-displacement curves for the compression test of both the GFRP/PVC 45°R and GFRP/PVC 45°RS samples. After implementing the second design

change, it was seen that the GFRP/PVC 45°RS sample had a considerably lower initial peak load of 27.15 kN than the GFRP/PVC 45°R sample, which had an initial peak load of about 47.15 kN. Thus, when implementing the second proposed design change, the spike in the initial peak load resulting from the first design change was deterred, as desired. Comparing the mean crushing loads for the two samples during the post-crushing stage, the GFRP/PVC 45°RS sample had a mean load of 28.23 KN, slightly higher than the mean load of the GFRP/PVC 45°R sample, which was 24.54 kN. Therefore, it can be concluded that the load-bearing capacity of the composite tube was maintained after applying the second design change.

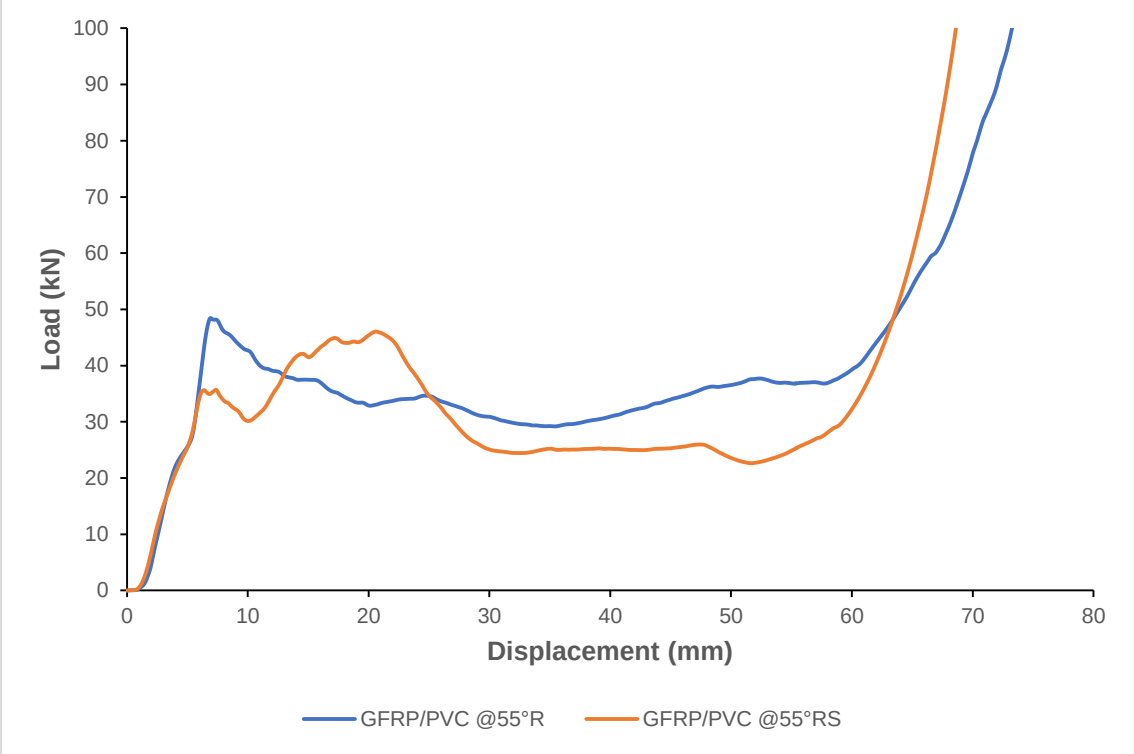

Figure 46. Load displacement curves for compression test of samples GFRP/PVC 55°R and GFRP/PVC 55°RS

The load-displacement curves for the compression test of both the GFRP/PVC 55°R and GFRP/PVC 55°RS samples are shown in Figure 46. After applying the second design change, it was seen that the GFRP/PVC 55°RS sample had a significantly lower initial peak load of about 35.67 kN than the GFRP/PVC 55°R sample, which had an initial peak load of 48.47 kN. Thus, the aim of reducing the initial peak load was achieved. Comparing the mean crushing loads for the two samples during the post-crushinging stage, the GFRP/PVC 55°RS sample had a mean load of 30.36 kN, only slightly lower than the mean load of the GFRP/PVC 55°R sample, which was approximately 34.94 kN. Therefore, it can be determined that implementing the second proposed design change did not significantly deteriorate the load-bearing capacity of the composite tube.

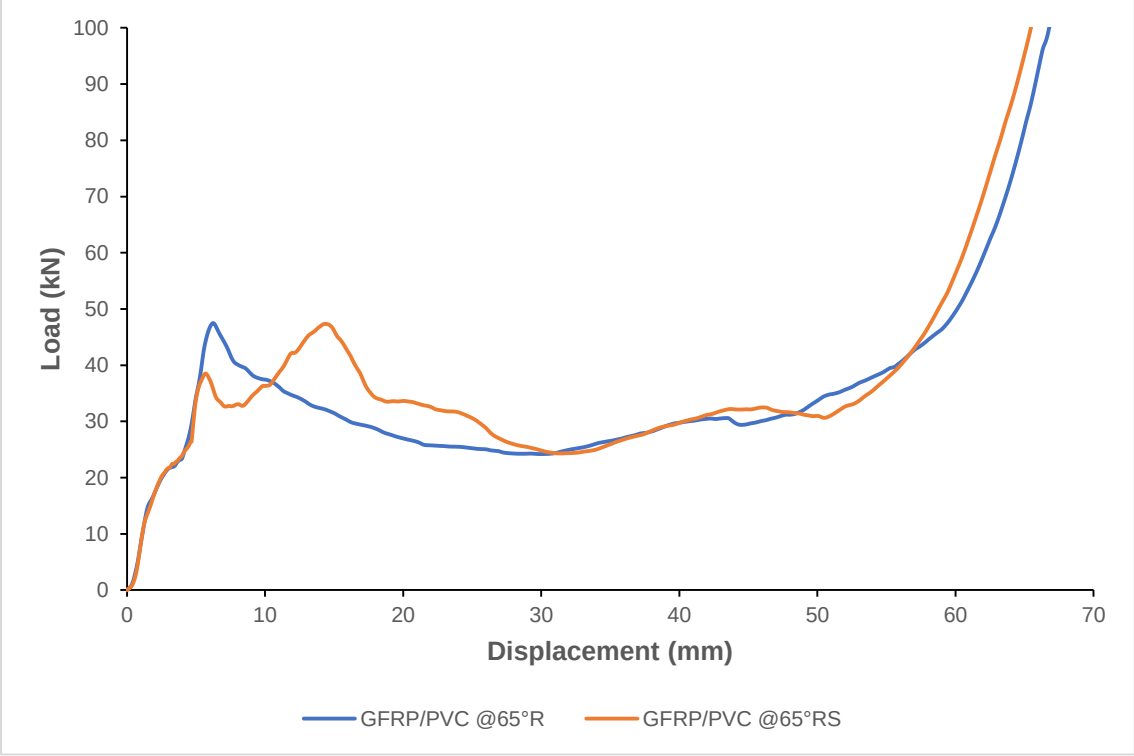

Figure 47. Load displacement curves for compression test of samples GFRP/PVC 65°R and GFRP/PVC 65°RS

Figure 47 shows the load-displacement curves for the compression test of both the GFRP/PVC 65°R and GFRP/PVC 65°RS samples. After implementing the second design change, it was seen that the GFRP/PVC 65°RS sample had a lower initial peak load of about 38.51 kN than the GFRP/PVC 65°R sample, which had an initial peak load of 47.48 kN. Thus, when implementing the second proposed design change, the spike in the initial peak load resulting from the first design change was deterred, as desired. Comparing the mean crushing loads for the two samples during the post-crushinging stage, the GFRP/PVC 65°RS sample had a mean load of 31.355 kN, slightly higher than the mean load of the GFRP/PVC 65°R sample, which was approximately 30.85 kN. Therefore, it can be concluded that the load-bearing capabilities of the composite tube were maintained after applying the second design change.

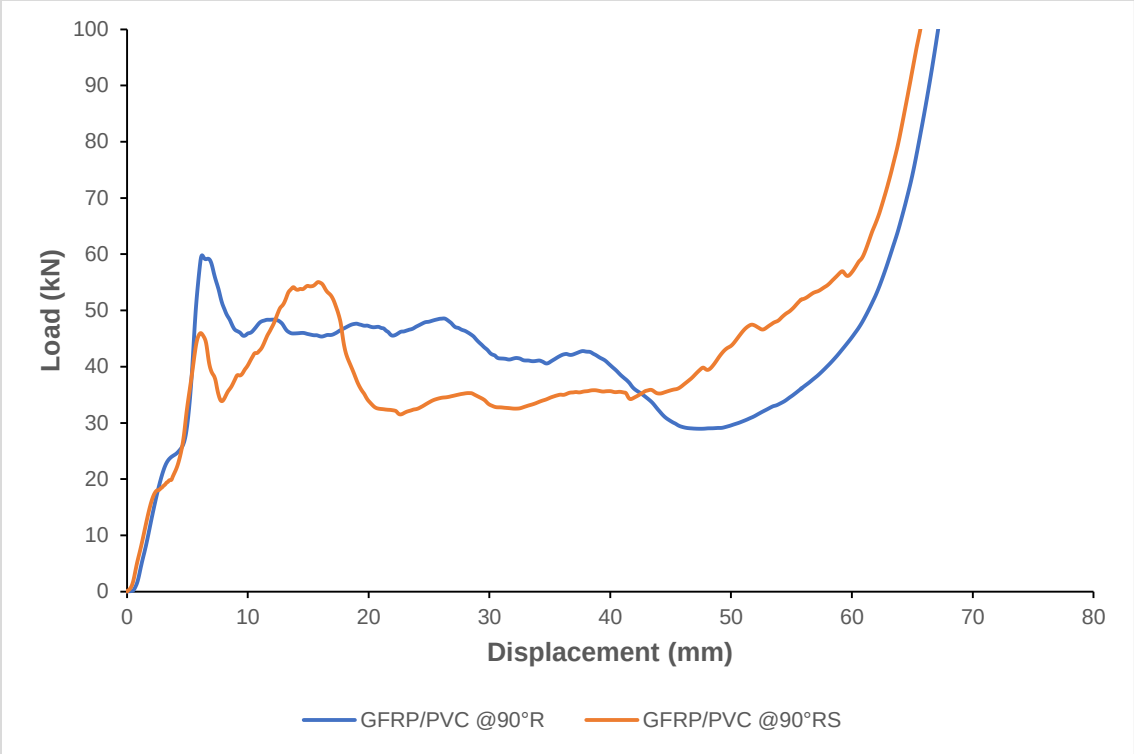

Figure 48. Load displacement curves for compression test of samples GFRP/PVC 90°R and GFRP/PVC 90°RS

The load-displacement curves for the compression test of both the GFRP/PVC 90°R and GFRP/PVC 90°RS samples are shown in Figure 48. After applying the second design change, it was seen that the GFRP/PVC 90°RS sample had a noticeably lower initial peak load of about 45.97 kN than the GFRP/PVC 90°R sample, which had an initial peak load of 59.81 kN. Thus, the aim of reducing the initial peak load was achieved. Comparing the mean crushing loads for the two samples during the post-crushing stage, the GFRP/PVC 90°RS sample had a mean load of 40.71 kN, only slightly lower than the mean load of the GFRP/PVC 90°R sample, which was approximately 41.35 kN. Therefore, it can be determined that implementing the second proposed design change did not significantly deteriorate the load-bearing capacity of the composite tube.

In summary, it was shown that the load-bearing capabilities of the samples for all tested fiber orientations were acceptably maintained when the second design change was implemented.

4.3.2.2. Effect on Crush Force Efficiency

Table 8. CFE and %iCFE within 0.1 from Ideal for GFRP/PVC R Tubes and GFRP/PVC RS Tubes

Sample configuration	Overall CFE	% iCFE ±0.1 from Ideal
GFRP/PVC @45°R	0.5206	9.77
GFRP/PVC @55°R	0.7208	63.59
GFRP/PVC @65°R	0.6498	36.62
GFRP/PVC @90°R	0.6914	39.53
GFRP/PVC°@45°RS	1.0396	69.87
GFRP/PVC @55°RS	0.8521	15.13
GFRP/PVC @65°RS	0.8401	52.59
GFRP/PVC @90°RS	0.8854	18.17

The overall CFE values for the GFRP/PVC RS tubes in Table 8 indicate that the second proposed design change's implementation increased the crush force efficiency of the composite tubes considerably. On average, the overall CFE values for the different samples increased by 43.82%, compared to those after the first design change was applied. However, it can be seen that although the CFE values rose significantly for the 55° and 90° samples after applying the second design change, their % iCFE within 0.1 from ideal values also noticeably decreased. This shows that for these two fiber orientations, although the

samples' mean crushing load became closer to their initial peak load due to the second design change, the amount of deviation from the mean that they experienced during their failure also increased. On the other hand, the 45° and 65° samples experienced a rise in both overall CFE and % iCFE within 0.1 from ideal values after applying the second design change, which demonstrates that for these two fiber orientations, their mean crushing load became closer to their initial peak load while their failure also became more stable. This was especially true for the GFRP/PVC 45° RS tube, which demonstrated the most sizeable increase in overall CFE and % iCFE within 0.1 from ideal values due to the second design change implementation. Of particular note was that the overall CFE value for the GFRP/PVC 45° RS samples was very close to 1, showing that it had been close to ideal failure.

4.3.2.3. Effect on Energy Absorption Capability

When the specific energy absorbed during the pre-crushing and post-crushing stages is added together, this gives the specific energy absorbed that is considered useful for crashworthiness applications. As was previously shown, implementing the first design change resulted in a significant increase in the specific energy absorbed for the composite tubes of all the different tested fiber orientations. Therefore, when applying the second proposed design change, the main aim of energy absorption capabilities was to maintain the higher specific energy absorption that resulted in the composite tubes tested after the first design implementation.

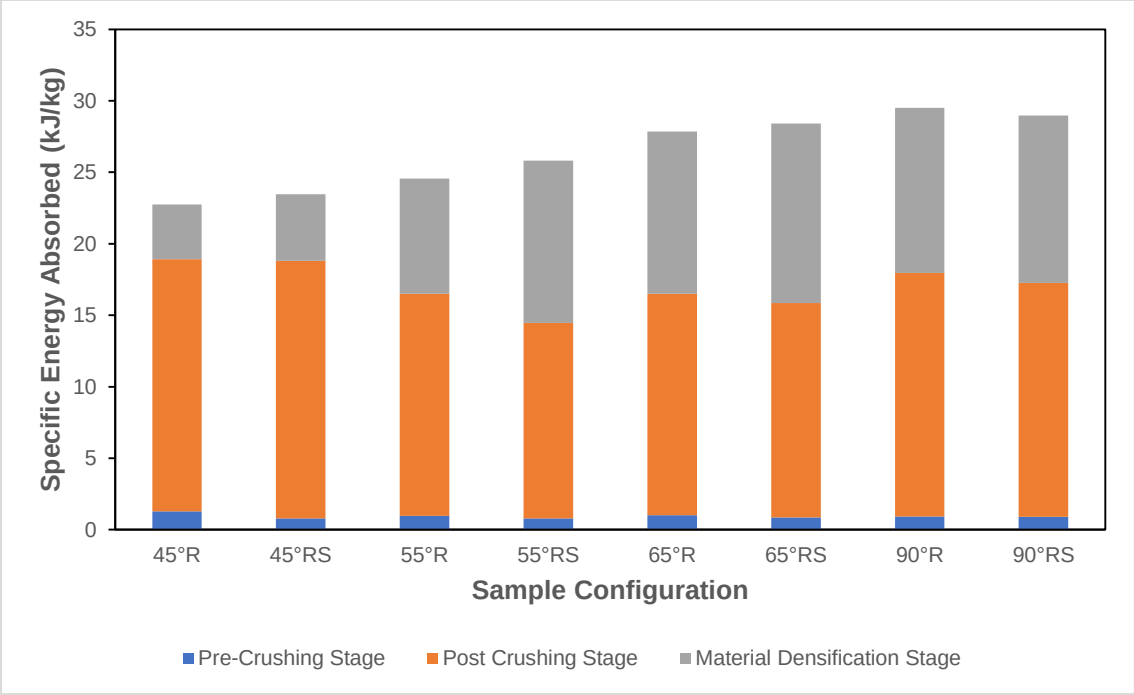

Figure 49. Specific energy absorbed by the GFRP/PVC R tubes and GFRP/PVC RS tubes

From the bar graph's values shown in Figure 49, it can be seen that this aim was achieved. Since the second design change had the effect of reducing the initial peak force, there was a reduction in the specific energy absorbed as compared to the tested samples after the first design change. However, the specific energy absorbed by the samples for each fiber orientation was still higher than for the tested initially samples with conventional circular tube geometry. For the samples with a fiber orientation of 45°, there was only a very slight 0.53% decrease in specific energy absorbed after the second design change was applied, from 18.91 kJ/kg to 18.81 kJ/kg. For the samples with a fiber orientation of 65° and 90°, there was a noticeable reduction in specific energy absorbed after the second design change was applied, from 16.51 kJ/kg to 15.86 kJ/kg and from 17.95 kJ/kg to 17.27 kJ/kg. On the other hand, the 55° samples exhibited a considerable 12.24% reduction in

specific energy absorbed, from 16.50 kJ/kg to 14.48 kJ/kg, after the second design change was implemented.

Therefore, it was demonstrated that by applying the second proposed design change, the advantage of increased specific energy absorption was retained, while at the same time, there was a sizeable increase in crush force efficiency. At the same time, the load-bearing capacity of the samples was maintained.

4.4. Selection of Composite Tube with Best Performance

In this section, the composite tube with the best performance from all the samples tested in this study is selected. A weighted scoring system is used to score the composite tubes' performance in terms of their crashworthiness characteristics. Table 9 shows the values of the parameters used for scoring, the composites' ranking for each parameter, and the total scores for all the tested composite tubes. The weight attributed to each parameter is shown next to the table's parameter in square brackets. The formula used to find the score for each parameter is also shown below. From the weighting, it can be seen that the crush force efficiency was given the most importance. This was followed by the specific energy absorbed and, lastly, the load-bearing capacity. The cost was also taken into account and was considered directly proportional to the composite tubes' mass. Cost and initial peak force are the only parameters in the table for which a lower value is awarded a higher ranking. This is because a reduced cost is advantageous while a lower initial peak force helps to reduce the size of reaction forces experienced by a passenger when an energy

absorber is utilized. On the other hand, for all the other parameters in the table, a larger value is desirable and is accordingly given a higher ranking.

$$Score\ for\ category = Points\ allocated\ to\ category - [Points\ allocated\ to\ category \times \left(\frac{rank - 1}{13 - 1}\right)]$$

Table 9. Weighted Scoring Table to Select Composite with Best Performance

Sample configuration	Cost [/1]		Load at 1st Failure [/1]		Pre-crushing Energy [/2]		Post-crushing Energy [/4]		Densification Energy [/1]		Overall CFE [/6]		% iCFE ±0.1 from Ideal [/10]		Total Score [/25]
	Rank	mass (kg)	Rank	(kN)	Rank	SE (kJ/kg)	Rank	SE (kJ/kg)	Rank	SE (kJ/kg)	Rank	(Unitless)	Rank	%	
PVC	1	0.0382	13	15.1431	12	0.6090	13	7.3707	13	0	13	0.2903	10	28.21	3.67
GFRP/PVC@45	4	0.0977	9	41.1104	2	1.1810	7	15.2859	10	5.8274	8	0.6607	8	31.27	11.83
GFRP/PVC@55	7	0.1289	8	43.2145	13	0.4603	12	9.2343	4	12.1891	12	0.5017	9	29.12	5.83
GFRP/PVC@65	12	0.1420	6	46.6240	11	0.6151	11	12.5037	2	14.1643	9	0.6569	5	39.53	11.25
GFRP/PVC@90	13	0.1421	2	58.5122	7	0.8516	9	14.1960	1	14.4039	7	0.6838	3	57.07	15.58
GFRP/PVC@45°R	3	0.0968	5	47.1451	1	1.2882	2	17.6230	12	3.8379	11	0.5206	13	9.77	8.25
GFRP/PVC@55°R	6	0.1281	3	48.4683	4	0.9628	5	15.5415	9	8.0646	5	0.7208	2	63.59	19.08
GFRP/PVC@65°R	10	0.1378	4	47.4769	3	1.0187	6	15.4911	7	11.3499	10	0.6498	7	36.62	12.00
GFRP/PVC@90°R	11	0.1383	1	59.8086	5	0.9355	3	17.0187	6	11.5555	6	0.6914	5	39.53	16.58
GFRP/PVC@45°RS	2	0.0947	12	27.1524	9	0.7896	1	18.0182	11	4.6505	1	1.0396	1	69.87	21.83
GFRP/PVC@55°RS	5	0.1248	11	35.6743	10	0.7848	10	13.6916	8	11.3361	3	0.8521	12	15.13	8.58
GFRP/PVC@65°RS	9	0.1342	10	38.5153	8	0.8475	8	15.0098	3	12.5511	4	0.8401	4	52.59	15.92
GFRP/PVC@90°RS	8	0.1336	7	45.9743	6	0.9046	4	16.3667	5	11.7072	2	0.8854	11	18.17	12.92

The GFRP/PVC 45° RS tube was selected as the composite tube with the best performance. Comparing the individual parameter scores for the GFRP/PVC 45° and GFRP/PVC 45° R samples to that of the GFRP/PVC 45° RS sample, its effectiveness of the two proposed design changes can be clearly seen. Implementing the first designed change is significantly increased the specific energy absorbed, while there was also a corresponding decrease in crush force efficiency. Applying the second change resulted in a slight drop in the specific energy absorbed. However, the specific energy absorbed was still higher than that of the original GFRP/PVC 45° sample. On the other hand, executing the second design change resulted in a considerable increase in crush force efficiency. The crush force efficiency of 1.0396 and % iCFE within 0.1 from the ideal value of 69.87 for the GFRP/PVC 45° RS sample was the highest of all the tested samples.

4.5. Comparison with Effect of Trigger Mechanisms

It is often the case that when composite tubes undergo crushing failure, they experience a catastrophic drop in load-bearing capacity after reaching their initial peak crushing force. This change indicates unstable failure and can also have a negative influence on the amount of energy absorbed by composite tubes. Trigger mechanisms are regularly used to solve this issue as they generally can reduce the initial peak crushing force of composite tubes, thereby noticeably increasing the stability of their failure. Combining the two proposed design changes to the conventional geometry of composite tubes in the previous sections has effects similar to that of a trigger mechanism. This combination of design can be considered a novel step trigger that can be applied to composite tubes with an inner tube. From all of the tested samples up to this section, the GFRP/PVC 45°RS

sample was performed the best. To compare the combined effect of the proposed design changes with that of a conventional trigger mechanism, composite tubes with a fiber orientation of 45° and chamfers of 30°, 45°, and 60°, respectively, were prepared. These samples are referred to as GFRP/PVC 45°C30, GFRP/PVC 45°C45, and GFRP/PVC 45°C60 from this point onwards for ease of identification.

4.5.1. Effect on Load Bearing Behavior

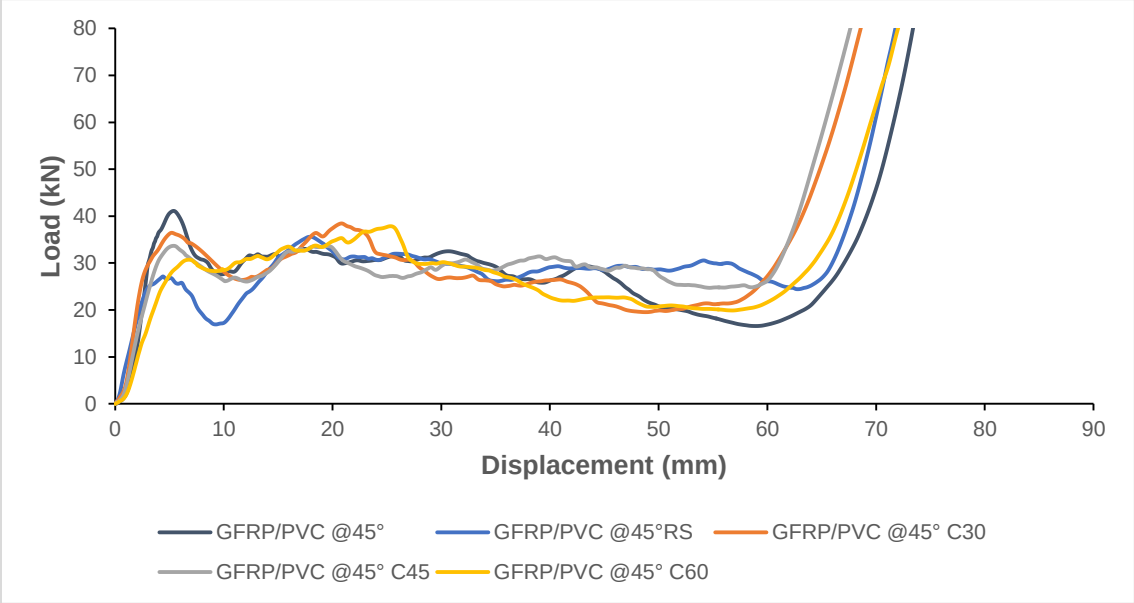

Figure 50. Load displacement curves for axial compression test of GFRP/PVC 45°, GFRP/PVC 45°RS, and all chamfer trigger samples

From Figure 50, it can be seen that the initial peak crushing force for all the chamfer trigger specimens was lower than that of the GFRP/PVC 45°, showing the effectiveness of this conventional trigger. Also, for the chamfer triggers, it is apparent that as the angle of the chamfer triggers increased, the initial peak force correspondingly decreased. The initial

peak loads achieved by the samples were 36.45 kN, 33.67 kN, and 30.72 kN for a chamfer angle of 30°, 45°, and 60°, respectively. For the GFRP/PVC 45°C60 sample, in particular, the trigger was able to reduce the initial peak force by 25.27%. However, the GFRP/PVC 45°RS was able to outperform all the chamfer triggers in this respect, with an initial peak force of 27.15, 33.96 % lower than that of the GFRP/PVC 45° sample. On the other hand, there was no clear trend for the effect of the various triggers on the mean crushing force. The mean crushing force for the GFRP/PVC 45° sample was approximately 27.16 kN. For the chamfer trigger samples, there was only a slight increase in this value. The mean crushing force for the GFRP/PVC 45°C30, GFRP/PVC 45°C45, and GFRP/PVC 45°C60 samples was 27.27 kN, 28.70 kN, and 27.21 kN, respectively. Similarly, the GFRP/PVC 45°RS sample had a mean crushing force of 28.23 kN, which was only 3.94% higher than that of the GFRP/PVC 45° sample.

4.5.2. Effect on Crush Force Efficiency

Table 10. CFE and %iCFE within 0.1 from Ideal for GFRP/PVC 45°, GFRP/PVC 45°RS, and all chamfer trigger samples

Sample configuration	Overall CFE	% iCFE ±0.1 from Ideal
GFRP/PVC°@45°	0.6607	31.27
GFRP/PVC°@45°RS	1.0396	69.87
GFRP/PVC°@45°C30	0.7481	40.56
GFRP/PVC @45°C45	0.8524	73.20
GFRP/PVC @45°C60	0.8856	28.36

Both the combined effect of the proposed design changes and the chamfer triggers significantly increased the overall crush force efficiency of the composite tubes with 45° fiber orientation. From the overall CFE values in Table 10, it can be concluded that the overall stability of failure increased with increasing chamfer angle for the chamfer trigger samples. On the other hand, the GFRP/PVC 45°RS sample had an overall CFE value closer to the ideal CFE of 1 than that of the chamfer trigger sample with the most stable overall failure. For the GFRP/PVC 45°RS sample, the overall CFE was only 3.96% greater than 1, while for the GFRP/PVC 45°C60 sample, the overall CFE was 11.44 % less than 1. Thus, the proposed design changes' combined effect resulted in a more stable overall failure than any of the chamfer triggers tested. The value of %iCFE withing 0.1 of ideal did not show a clear trend for the various samples. However, the value of %iCFE withing 0.1 of the ideal of 28.36 % for the GFRP/PVC 45°C60 sample indicates that although this sample had the largest overall CFE from chamfer triggers, it also had the highest amount of deviation from the mean. As this deviation was evenly spread around the mean, the sample's overall CFE remained relatively high. This is an example of how consideration of only the overall CFE value when looking at failure's stability can sometimes be misleading.

4.5.3. Effect on Energy Absorption Capability

When the specific energy absorbed during the pre-crushing and post-crushing stages is added together, this gives the specific energy absorbed that is considered useful for crashworthiness applications. From Figure 51, it can be seen that the specific energy absorbed by both GFRP/PVC 45°C30 sample and the GFRP/PVC 45°C45 sample was very close in value to that of the GFRP/PVC 45° sample. The GFRP/PVC 45°C60 sample

outperformed both of its chamfer trigger counterparts with a specific energy absorbed value of 17.72 kJ/kg, 7.59% greater than that of the GFRP/PVC 45° sample. In contrast, the GFRP/PVC 45°RS sample had a specific energy absorbed value of 18.81 kJ/kg, 14.21% higher than that of the GFRP/PVC 45° sample.

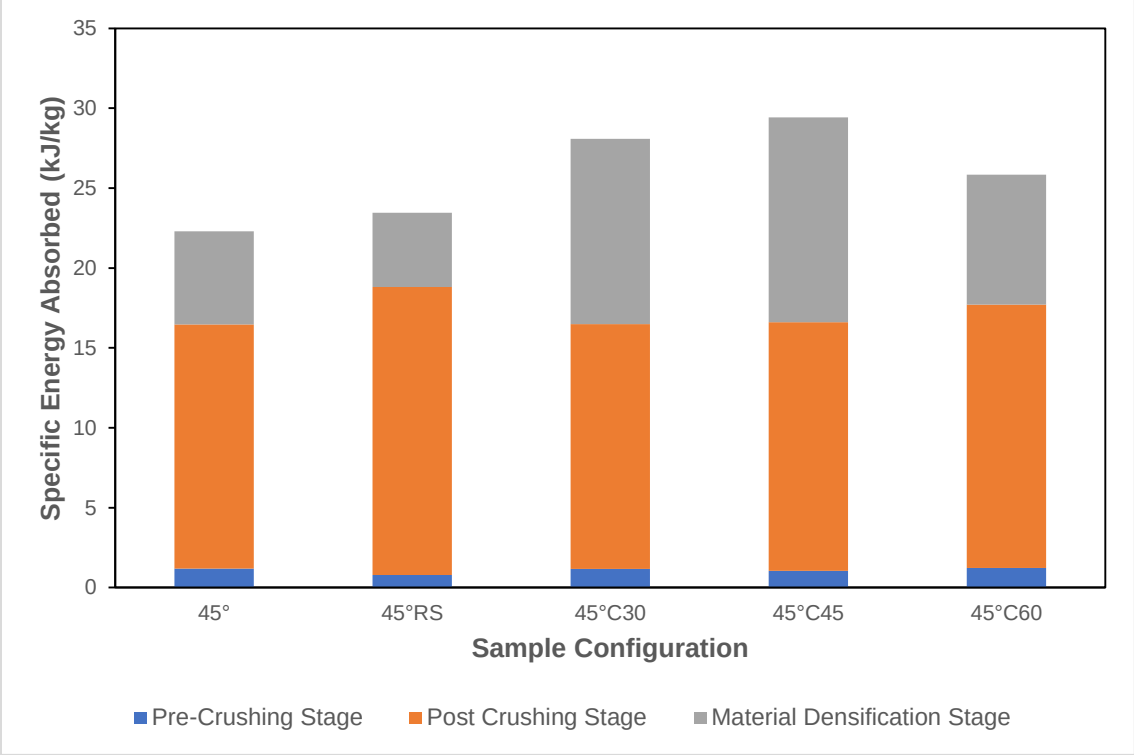

Figure 51. Specific energy absorbed by GFRP/PVC 45°, GFRP/PVC 45°RS, and all chamfer trigger samples

Overall, the GFRP/PVC 45°RS sample outperformed all the chamfer trigger specimens to suppress the initial peak force, failure stability, and energy absorption capability. Thus, the combination of the two proposed design changes was comprehensively more effective in enhancing the crashworthiness characteristics of the

composite tubes with a 45° fiber orientation compared to the conventional triggers considered.

4.6. Effect of Filling Composite Tube with Foam Core

As was stated previously, engineering theory is known that the flexural stiffness of a structure is proportional to the cube of its thickness. Intuitively, it would also be expected that filling a composite tube with a core would increase its load-bearing capability, as the load the composite tube is subjected to will be spread over a larger contact surface area. The core material selected for this study was low-density rigid polyurethane foam, as this material was expected to allow for a significant increase in stiffness while minimizing the additional weight of the composite. Thus, by using foam cores fabricated from this material, the specific energy absorbed by core composite tubes was expected to be significantly larger than for core-less composite tubes. However, what remains to be seen is the effect that introducing the foam cores will have on the stability of failure. A total of four different core geometries, designated as Core 1, Core 2, Core 3, and Core 4, were used in combination with the GFRP/PVC 45°RS sample configuration. The design for these core geometries can be seen in Chapter 3. The samples formed by filling this composite tube configuration with the different foam cores are referred to as GFRP/PVC 45°RSFC1, GFRP/PVC 45°RSFC2, GFRP/PVC 45°RSFC3, and GFRP/PVC 45°RSFC4, respectively from this point onwards for ease of identification.

4.6.1. Effect on Load Bearing Behavior

As was expected, it can be seen from Figure 52 that the introduction of foam cores was able to noticeably increase the load-bearing capability of the GFRP/PVC 45°RS sample. To compare the GFRP/PVC 45°RS core-less sample's initial peak load with the lowest initial peak load achieved by the four GFRP/PVC 45°RS core samples, a 29.13% increase in value was seen, from about 27.15 kN to 35.06 kN. For the mean crushing load, the difference was not as pronounced, with the mean load of the GFRP/PVC 45°RS core-less sample, which was approximately 28.23 kN, being only 8.18% lower than that of the smallest mean load achieved by the GFRP/PVC 45°RS core samples, with a value of 30.54 kN.

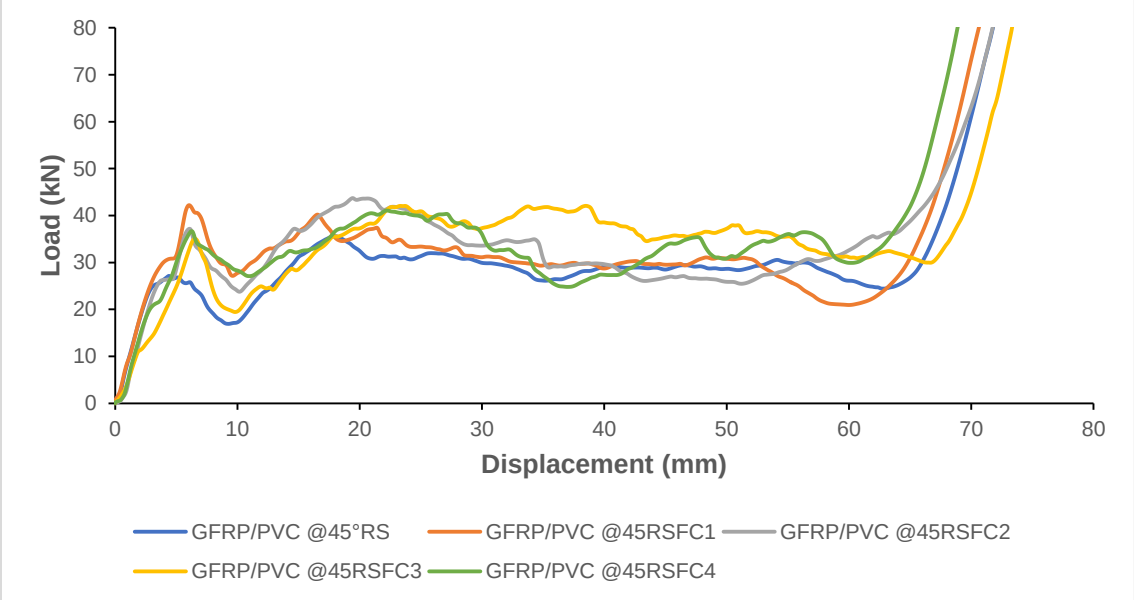

Figure 52. Load displacement curves for axial compression test of all GFRP/PVC 45°RS samples with foam cores vs. GFRP/PVC 45°RS core-less sample

The initial peak loads achieved by the GFRP/PVC 45° RS core samples were 42.20 kN, 37.19 kN, 35.06 kN, and 36.69 kN for Core 1, Core 2, Core 3, and Core 4, respectively. So, it can be seen that as the volume of material for the foam cores decreased, there was a corresponding decrease in initial peak load, up to the GFRP/PVC 45°RSFC3 sample. However, the initial peak load for the GFRP/PVC 45°RSFC4 sample was higher than that for the GFRP/PVC 45°RSFC3 sample. However, for the mean crushing load, this trend was reversed. The mean crushing loads achieved by the GFRP/PVC 45°RS foam core samples was 30.54 kN, 32.41 kN, 34.83 kN, and 33.05 kN for Core 1, Core 2, Core 3, and Core 4, respectively. Therefore, it can be seen that as the volume of material for the foam cores decreased, there was a corresponding increase in mean crushing load up to the GFRP/PVC 45°RSFC3 sample. The GFRP/PVC 45°RSFC4 sample was once again the exception to the general trend, as it is average crushing load was lower than that for the GFRP/PVC 45°RSFC3 sample.

4.6.2. Effect on Crush Force Efficiency

Table 11. CFE and %iCFE within 0.1 from Ideal for GFRP/PVC 45°RS Tube and GFRP/PVC RSFC Tubes

Sample configuration	Overall CFE	% iCFE ±0.1 from Ideal
GFRP/PVC°@45°RS	1.0396	69.87
GFRP/PVC°@45°RSFC1	0.7237	61.71
GFRP/PVC @45°RSFC2	0.8716	38.48
GFRP/PVC @45°RSFC3	0.9935	52.22
GFRP/PVC @45°RSFC4	0.9008	55.55

Looking at the values of overall CFE and % iCFE within 0.1 of the ideal in Table 11, it can be seen that when the foam cores Core 1, Core 2, and Core 4 are used in combination with the GFRP/PVC 45°RS, the stability of failure is adversely affected. For these three cores, it can be seen that as the volume of material in the foam core decreases, the value of overall CFE becomes closer to its ideal value of 1. The value of %iCFE withing 0.1 of ideal, however, does not show a clear trend, with the GFRP/PVC 45°RSFC2 sample having the lowest value, indicating that the GFRP/PVC 45°RSFC2 sample shows the largest deviation of the load from the mean during the post-crushing stage. However, the sample that shows the most significant results is the GFRP/PVC 45°RSFC3 sample. For this sample, the overall CFE value is lower than that for the GFRP/PVC 45°RS core-less sample. Nevertheless, it should be mentioned that for the overall CFE value, what is important is how far the value is from the ideal value of 1. For the GFRP/PVC 45°RSFC3 sample, the overall CFE value was only 0.65 % less than the ideal value, while for the GFRP/PVC 45°RS core-less sample, the overall CFE was 3.96% greater than ideal. Thus, it can be determined that in terms of the overall CFE, the failure of the GFRP/PVC 45°RSFC3 sample was more stable than for the GFRP/PVC 45°RS core-less sample. However, from the %iCFE within 0.1 from ideal, the GFRP/PVC 45°RSFC3 sample had a 17.65 % lower value than for the GFRP/PVC 45°RS core-less sample. This shows that the GFRP/PVC 45°RSFC3 sample's load exhibited comparatively more deviation from the mean crushing load during the post-crushing stage.

4.6.3. Effect on Energy Absorption Capability

Low-density rigid polyurethane foam was chosen as the material to fabricate the foam cores used in combination with the GFRP/PVC 45°RS composite tubes. This material was expected to allow for a significant increase in stiffness while minimizing the composite's additional weight. As can be seen from the increased specific energy absorbed by core composite tubes compared to the core-less samples (Figure 53), the use of cores proved to be effective in raising the energy absorption capabilities of the GFRP/PVC 45°RS composite tubes. It was found that the foam cores used had an average mass of only 0.0050 kg, as compared to the GFRP/PVC 45°RS composite tubes, which had an average mass of 0.0944 kg. The additional energy absorbed due to the use of foam cores more than made up for the very slight increase in the samples' mass due to their inclusion. It is known that when the specific energy absorbed during the pre-crushing and post-crushing stages is added together, this gives the specific energy absorbed that is considered useful for crashworthiness applications.

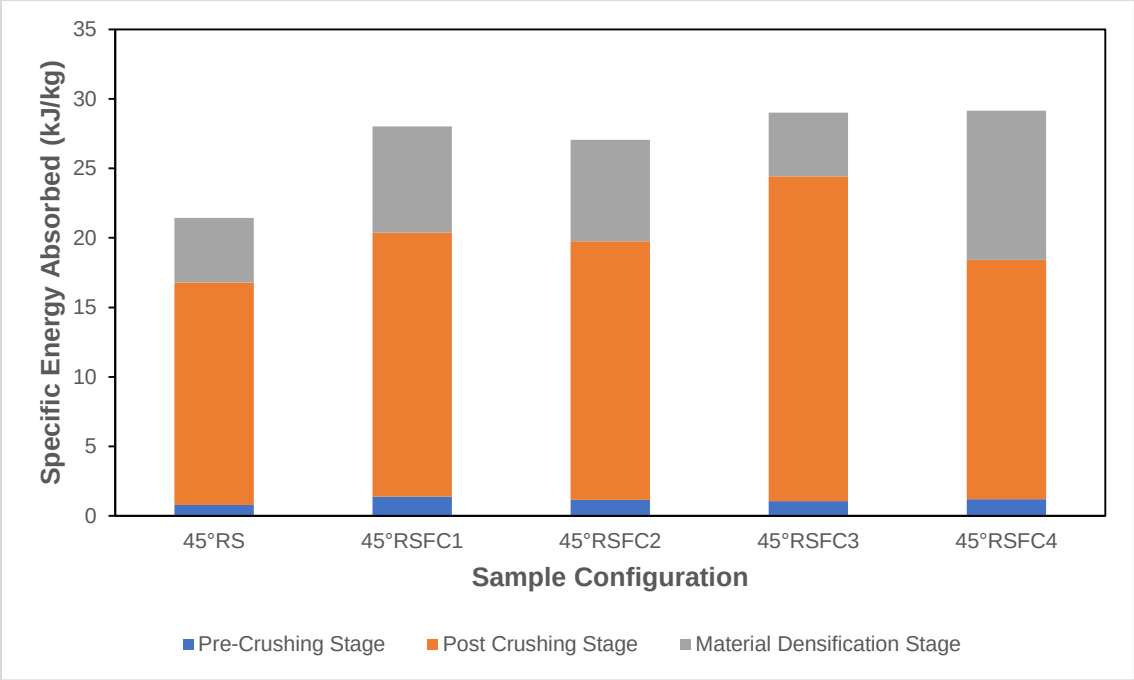

Figure 53. Specific energy absorbed by the GFRP/PVC 45°RS tube and GFRP/PVC RSFC tubes

Even for the core composite tube sample with the lowest specific energy absorption value, the GFRP/PVC 45°RSFC4 composite tube, the specific energy absorbed of 18.41 kJ/kg was about 9.649 % greater than that of the GFRP/PVC 45°RS core-less composite tube, which was approximately 16.79 kJ/kg. The specific energy absorbed values for the core composite tubes with core geometries Core 1, Core 2, and Core 4 were 20.38 kJ/kg, 19.76 kJ/kg, and 18.41 kJ/kg. So it was observed that, for these three core geometries, as the foam core volume decreased, there was a corresponding fall in the specific energy absorbed. The GFRP/PVC 45°RSFC3 sample was the exception to this rule and had the highest specific energy absorbed value of approximately 24.44 kJ/kg. This was a considerable 45.56 % higher than the specific energy absorbed by the GFRP/PVC 45°RS core-less sample.

In summary, the introduction of foam cores was able to noticeably increase both the load-bearing capability and the specific energy absorption of the GFRP/PVC 45°RS composite tubes. Simultaneously, though, the failure of the composite tubes with cores was not as stable. In particular, the GFRP/PVC 45°RSFC3 sample absorbed approximately 45.56% more specific energy than the GFRP/PVC 45°RS core-less sample. Also, the GFRP/PVC 45°RS3 sample's crush force efficiency was not as adversely affected as the rest of the core composite tubes. It was determined that in terms of the overall CFE, the GFRP/PVC 45°RSFC3 sample's failure was more stable than for the GFRP/PVC 45°RS core-less sample. However, from the %iCFE within 0.1 from ideal values, it was seen that the load for the GFRP/PVC 45°RSFC3 sample for the post crushing stage showed a higher degree of fluctuation from the mean that the GFRP/PVC 45°RS core-less sample. Thus, although the 45°RSFC3 sample had a mean crushing load that was closer to its initial peak value, as compared to its core-less counterpart, its failure exhibited a more considerable amount of fluctuation from the mean and therefore was not as stable. However, the 45°RSFC3 sample's advantages in its increased load-bearing capacity and energy absorption abilities are apparent. Choosing between the 45°RSFC3 sample and the 45°RS core-less sample would depend on the most important for the intended application.

CHAPTER 5. CONCLUSION AND RECOMMENDATIONS

In this study, PVC tubes overwrapped in GFRP at four different fiber orientations were subjected to quasi-static axial compression tests to determine the effect of fiber orientation on their crashworthiness properties. Furthermore, slight changes were made to the design of conventionally used circular composite tubes to improve the crashworthy characteristics of the GFRP overwrapped PVC pipes tested for all of the four different fiber orientations. The proposed design changes aimed to reduce the composite samples' weight while maintaining their load-bearing capabilities and crush force efficiency during failure. The combined effect of the proposed design changes was very similar to that of trigger mechanisms. Crushing tests were carried out on composite tubes with chamfer triggers of three different angles, which had the same fiber orientation as the best performance composite tube. Following this, a direct comparison was made between the effect of the proposed design changes and conventional chamfer triggers. Finally, foam cores of four different geometries were used in combination with the composite tube sample configuration with the best performance. Low-density rigid polyurethane foam was used to fabricate the foam cores, as this material was expected to allow for a significant increase in stiffness while minimizing the additional weight of the composite.

5.1. Conclusion

Based on the experimental results, the following conclusions were drawn:

i. The composite formed by wrapping PVC tube with GFRP has a significantly higher load-bearing capacity, crush force efficiency, and energy absorption capability during failure due to compression than the PVC tube on its own.

ii. The failure mechanisms commonly exhibited by the GFRP/PVC composite tubes used when crushed were local bucking, transverse shear, interpenetration, debonding, and matrix cracking.

iii. For the GFRP/PVC samples of different fiber orientations with standard circular tube geometry, load-bearing capacity and crush force efficiency generally improved with increasing fiber orientation. The GFRP/PVC 55° sample was an exception to this rule, as it exhibited the worst crashworthiness characteristics of the tested samples.

iv. For the GFRP/PVC samples of different fiber orientation with standard circular tube geometry, energy absorption capability generally improved with increasing fiber orientation. The GFRP/PVC 45° sample was an exception to this rule as, due to its comparatively lower mass and the fact that it underwent Mode-III failure, it had the highest value for the specific energy absorbed.

v. The first proposed design change to the conventional circular composite tube geometry increased specific energy absorbed, while load-bearing capacity was also maintained. However, it also resulted in a noticeable decrease in crush force efficiency during failure. The GFRP/PVC 55°R sample was an exception to this rule, as it exhibited an increase in crush force efficiency.

vi. In the second proposed design change to the conventional circular composite tube geometry, the advantages of maintained load-bearing capacity and increased specific energy absorption, seen for the first design change, were retained. At the same time, a sizeable increase in crush force efficiency was also observed. The

GFRP/PVC 55°RS sample was an exception to this rule, as it exhibited a decrease in crush force efficiency.

vii. The GFRP/PVC 45°RS sample was the composite tube that exhibited the best performance when using the weighted scoring system proposed to score the tested sample configurations in terms of their crashworthiness characteristics.

viii. The GFRP/PVC 45°RS sample outperformed all the tested chamfer trigger specimens to suppress the initial peak force, failure stability, and energy absorption capability.

ix. The introduction of foam cores was able to noticeably increase both the load-bearing capability and the specific energy absorption of the GFRP/PVC 45°RS composite tubes. Simultaneously, though, the failure of the composite tubes with cores was not as stable. In particular, the GFRP/PVC 45°RSFC3 sample absorbed approximately 45.56% more specific energy than the GFRP/PVC 45°RS core-less sample.

5.2. Recommendations for Future Work

It is recommended that non-linear finite element analysis be utilized to find the best design for an energy absorber fabricated from the composite material used in this study. Although experimental work is essential, finite element analysis has the edge in terms of cost-effectiveness and flexibility. Factors that have not been investigated in this study that could be examined in the future include:

i. The use of an inner tube of a different material. Aluminium is an alternative inner tube material that has been investigated extensively.

ii. Foam cores of various densities can be considered, as well as foam cores of different materials.

iii. The number of layers of GFRP can be changed and layers of different fiber orientation can be combined for each sample.

iv. Different loading conditions can be considered, such as quasi-static oblique loading and axial impact loading.

v. Alternative reinforcing and matrix materials can also be considered.

REFERENCES

1. Xu, P., Yang, C., Peng, Y., Yao, S., Xing, J., & Li, B. (2016). Cut-out grooves optimization to improve the crashworthiness of a gradual energy-absorbing structure for subway vehicles. *Materials & Design*, *103*, 132-143.
2. Yan, L., & Chouw, N. (2013). Crashworthiness characteristics of flax fiber-reinforced epoxy tubes for energy absorption application. *Materials & Design*, *51*, 629-640.
3. Jacob, G. C., Fellers, J. F., Simunovic, S., & Starbuck, J. M. (2002). Energy absorption in polymer composites for automotive crashworthiness. *Journal of composite materials*, *36*(7), 813-850.
4. Campbell, F. C. (2010). *Structural composite materials*. Russell Township, OH: ASM international.
5. Almurib, H. A., Al-Qrimli, H. F., & Kumar, N. (2012). Experimental tensile study on the behavior of Composite material with roving waviness. *Applied Mechanics and Materials*, *117*, 975-979.
6. Mamalis, A. G., Manolakos, D. E., Demosthenous, G. A., & Ioannidis, M. B. (1998). *Crashworthiness of composite thin-walled structures*. Boca Raton, FL: CRC Press.
7. Hu, D. Y., Luo, M., & Yang, J. L. (2010). Experimental study on crushing characteristics of brittle fiber/epoxy hybrid composite tubes. *International journal of crashworthiness*, *15*(4), 401-412.
8. Abosbaia, A. S., Mahdi, E., Hamouda, A. M. S., Sahari, B. B., & Mokhtar, A. S. (2005). Energy absorption capability of laterally loaded segmented composite tubes. *Composite structures*, *70*(3), 356-373.

9. Geier, B., Meyer-Piening, H. R., & Zimmermann, R. (2002). On the influence of laminate stacking on buckling of composite cylindrical shells subjected to axial compression. *Composite structures*, *55*(4), 467-474.
10. Will, M. A., Franz, T., & Nurick, G. N. (2002). The effect of laminate stacking sequence of CFRP filament-wound tubes subjected to projectile impact. *Composite structures*, *58*(2), 259-270.
11. Mamalis, A. G., Manolakos, D. E., Demosthenous, G. A., & Ioannidis, M. B. (1996). Energy absorption capability of fiberglass composite square frusta subjected to static and dynamic axial collapse. *Thin-Walled Structures*, *25*(4), 269-295.
12. Alkateb, M., Sapuan, S. M., Leman, Z., Ishak, M. R., & Jawaid, M. (2018). Vertex angles effects in the energy absorption of axially crushed kenaf fibre-epoxy reinforced elliptical composite cones. *Defence Technology*, *14*(4), 327-335.
13. Palanivelu, S., Van Paepegem, W., Degrieck, J., Vantomme, J., Kakogiannis, D., Van Ackeren, J., Van Hemelrijck, D., & Wastiels, J. (2011). Crushing and energy absorption performance of different geometrical shapes of small-scale glass/polyester composite tubes under quasi-static loading conditions. *Composite structures*, *93*(2), 992-1007.
14. Mallick, P.K. (2007). *Fiber-reinforced composites: materials, manufacturing, and design*. Boca Raton, FL: CRC Press.
15. Crouch, I. G., Sandlin, J., & Thomas, S. (2017). *The Science of Armour Materials*. Sawston, CB: Woodhead Publishing.

16. GangaRao, H. (2017). Infrastructure applications of fiber-reinforced polymer composites. In *Applied Plastics Engineering Handbook* (pp. 675-695). Norwich, NY: William Andrew Publishing.
17. Sauer, M., Kuhnel, M., Witten, E., & Mathes, V. (2018). *Composites Market Report 2018 - Market developments, trends, outlook, and challenges*. AVK Industrievereinigung Verstarkte Kunststoffe, e.V. Frankfurt, Germany.
18. Siromani, D., Henderson, G., Mikita, D., Mirarchi, K., Park, R., Smolko, J., Awerbuch, J. & Tan, T. M. (2014). An experimental study on the effect of failure trigger mechanisms on the energy absorption capability of CFRP tubes under axial compression. *Composites Part A: applied science and manufacturing*, *64*, 25-35.
19. Yan, L., Chouw, N., & Jayaraman, K. (2014). Effect of triggering and polyurethane foam-filler on axial crushing of natural flax/epoxy composite tubes. *Materials & Design (1980-2015)*, *56*, 528-541.
20. Pervaiz, M., Panthapulakkal, S., Sain, M., & Tjong, J. (2016). Emerging trends in automotive light-weighting through novel composite materials. *Materials sciences and Applications*, *7*(01), 26-38.
21. Grant, C. (2006). Automated processes for composite aircraft structure. *Industrial Robot: An International Journal*, *33*(2), 117-121.
22. Choi, C. H., Hahm, Y. H., & Kang, H. M. (2012). *U.S. Patent Application No. 13/039,806*.
23. Chrysler, F. (2004). Carmakers increase their use of composites. *Reinforced Plastics*, *48*(2), 26-32.

24. Mouritz, A. P. (2012). *Introduction to aerospace materials*. Sawston, CB: Woodhead Publishing.
25. Marsh, G. (2013). Composites poised to transform airline economics. *Reinforced Plastics*, *57*(3), 18-24.
26. Elmarakbi, A. (2015). Novel composite materials for automotive applications: concepts and challenges for energy-efficient and safe vehicles. *10th International Conference on Composites Science and Technology*, Lisbon, Portugal.
27. Jones, R. M. (2014). *Mechanics of composite materials*. Boca Raton, FL: CRC Press.
28. Mallick, P. K. (Ed.). (1997). *Composites engineering handbook*. Boca Raton, FL: CRC Press.
29. Cech, V., Palesch, E., & Lukes, J. (2013). The glass fiber–polymer matrix interface/interphase is characterized by nanoscale imaging techniques. *Composites Science and Technology, 83, 22-26.*
30. Daniel, I. M., & Ishai, O. (2006). *Engineering Mechanics of Composite Materials*. Oxford, ON Oxford University Press.
31. Rastgoftar, H., Eghtesad, M., & Khayatian, A. (2008). Boundary control of vibration of an asymmetric composite laminated plate. *IFAC Proceedings Volumes*, *41*(2), 11847-11852.
32. Greer, J. R. (2013). Nanotwinned metals: It's all about imperfections. *Nature Materials*, *12*(8), 689-690.
33. Zweben, C., & Rosen, B. W. (1970). A statistical theory of material strength with application to composite materials. *Journal of the Mechanics and Physics of Solids*, *18*(3), 189-206.

34. Verma, D., Gope, P. C., Maheshwari, M. K., & Sharma, R. K. (2012). Bagasse fiber composites-A review. *Journal of Materials and Environmental Science*, *3*(6), 1079-1092.

35. Liu, Y., & Hu, H. (2010). A review on auxetic structures and polymeric materials. *Scientific Research and Essays*, *5*(10), 1052-1063.

36. Agarwal, B. D., Broutman, L. J., & Chandrashekhara, K. (2017). *Analysis and performance of fiber composites*. Hoboken, NJ: John Wiley & Sons.

37. Kurkjian, C. R., Gupta, P. K., Brow, R. K., & Lower, N. (2003). The intrinsic strength and fatigue of oxide glasses. *Journal of Non-Crystalline Solids*, *316*(1), 114-124.

38. Hearle, J. W. (Ed.). (2001). *High-performance fibers*. Boca Raton, FL: CRC Press.

39. Komanduri, R. (1997). Machining of fiber-reinforced composites. *Machining science and technology*, *1*(1), 113-152.

40. Chung, D. D. L. (2016). A review of exfoliated graphite. *Journal of materials science*, *51*(1), 554-568.

41. Hausrath, R. L., & Longobardo, A. V. (2010). High-strength glass fibers and markets. In *Fiberglass and glass technology* (pp. 197-225). Bostan, MA: Springer.

42. Shokoohi, S., Arefazar, A., & Khosrokhavar, R. (2008). Silane coupling agents in polymer-based reinforced composites: a review. *Journal of Reinforced Plastics and Composites*, *27*(5), 473-485.

43. Mohammed, O. A. (2013). Vibration analysis of hybrid laminated composite beam-eng. *Al- Rafidain Engineering Journal*, *21*(4), 1-13.

44. Hartwig, G., Hübner, R., Knaak, S., & Pannkoke, C. (1998). Fatigue behavior of composites. *Cryogenics*, *38*(1), 75-78.

45. *Standard Specification for Glass Fiber Strands*, D 578-98, Annual Book of ASTM Standards, ASTM
46. Wallenberger, F. T., MacChesney, J. B., Naslain, R., & Ackler, H. D. (2011). *Advanced inorganic fibers: processes-structure-properties-applications*. Norwell, MA: Kluwer Academic Publishers.
47. Wallenberger, F. T. (2010). Commercial and experimental glass fibers. In *Fiberglass and glass technology* (pp. 3-90). Boston, MA: Springer.
48. Hausrath, R. L., & Longobardo, A. V. (2010). High-strength glass fibers and markets. In *Fiberglass and glass technology* (pp. 197-225). Boston, MA: Springer.
49. Wallenberger, F. T. (2000). Structural silicate and silica glass fibers. In *Advanced Inorganic Fibers* (pp. 129-168). Boston, MA: Springer.
50. Plummer, C. J. G., Bourban, P. E., & Manson, J. A. E. (2008). Polymer matrix composites: matrices and processing. Encyclopedia of Materials: *Science and Technology, 7388-7396.*
51. Yaacob, A., Zakaria, Z. A., Zarina, M. P., Koto, J., & Kidd, P. (2015). Production process of fiberglass fast interceptor boat in Malaysia. *Journal of Ocean, Mechanical and Aerospace – Science and Engineering*, *19*, 14-20.
52. Hyer, M. W., & White, S. R. (2009). *Stress analysis of fiber-reinforced composite materials*. Lancaster, PA: DEStech Publications, Inc.
53. Selzer, R., & Friedrich, K. (1997). Mechanical properties and failure behavior of carbon fiber-reinforced polymer composites under the influence of moisture. *Composites Part A: Applied Science and Manufacturing*, *28*(6), 595-604.

54. Baldus, P., Jansen, M., & Sporn, D. (1999). Ceramic fibers for matrix composites in high-temperature engine applications. *Science, 285*(5428), 699-703.

55. Campbell F. C. (Ed.). (2003). *Manufacturing processes for advanced composites*. Oxford, ON: Elsevier.

56. Harris, B. (1991). A perspective view of composite materials development. *Materials & Design*, *12*(5), 259-272.

57. Armstrong, R. D., Jenkins, A. T. A., & Johnson, B. W. (1995). An investigation into the UV breakdown of thermoset polyester coatings using impedance spectroscopy. *Corrosion Science*, *37*(10), 1615-1625.

58. Mark, J., Ngai, K., Graessley, W., Mandelkern, L., Samulski, E., Wignall, G., & Koenig, J. (2004). *Physical properties of polymers*. Cambridge, CB: Cambridge University Press.

59. Biron, M. (2012). *Thermoplastics and thermoplastic composites*. Norwich, NY: William Andrew Publishing.

60. Pascault, J. P., Sautereau, H., Verdu, J., & Williams, R. J. (2002). *Thermosetting polymers* (Vol. 64). Boca Raton, FL: CRC press.

61. Gibson, G. (2017). Epoxy Resins. In *Brydson's Plastics Materials* (pp. 773-797). Oxford, ON: Butterworth-Heinemann.

62. Pham, H. Q., & Marks, M. J. (2000). Epoxy resins. *Ullmann's Encyclopedia of Industrial Chemistry*. Hoboken, NJ: John Wiley & Sons.

63. Chawla, K. K. (2006). Metal matrix composites. *Materials science and technology*. Hoboken, NJ: John Wiley & Sons.

64. Taya, M., & Arsenault, R. J. (2016). *Metal matrix composites: thermomechanical behavior*. Oxford, ON: Pergamon Press.

65. Kaczmar, J. W., Pietrzak, K., & Włosiński, W. (2000). The production and application of metal matrix composite materials. *Journal of materials processing technology*, *106*(1-3), 58-67.

66. Hoa, S. V. (2009). *Principles of the manufacturing of composite materials*. Lancaster, PA: DEStech Publications, Inc.

67. Mazumdar, S. (2001). *Composites manufacturing: materials, product, and process engineering*. Boca Raton, FL: CRC press.

68. Mallick, P. K. (2010). Thermoset–matrix composites for lightweight automotive structures. In *Materials, Design and Manufacturing for Lightweight Vehicles* (pp. 208-231). Sawston, CB: Woodhead Publishing.

69. Loud, S. N. (1998). Commercial and industrial applications of composites. In *Handbook of Composites* (pp. 931-956). Boston, MA: Springer.

70. Peters, S. T. (Ed.). (2011). *Composite filament winding*. Russell Township, OH: ASM International.

71. Harper, C. A., & Petrie, E. M. (2003). *Plastics materials and processes: a concise encyclopedia*. Hoboken, NJ: John Wiley & Sons.

72. Jiang, H., Ren, Y., Gao, B., Xiang, J., & Yuan, F. G. (2017). Design of novel plug-type triggers for composite square tubes: enhancement of energy-absorption capacity and inducing failure mechanisms. *International Journal of Mechanical Sciences*, *131*, 113-136.

73. Palanivelu, S., Van Paepegem, W., Degrieck, J., Van Ackeren, J., Kakogiannis, D., Van Hemelrijck, D., Wastiels, J. & Vantomme, J. (2010). Experimental study on the axial crushing behaviour of pultruded composite tubes. *Polymer testing*, *29*(2), 224-234.
74. Feraboli, P. (2006). Current efforts in standardization of composite materials testing for crashworthiness and energy absorption. In *47th AIAA/ASME/ASCE/AHS/ASC Structures, Structural Dynamics, and Materials Conference 14th AIAA/ASME/AHS Adaptive Structures Conference 7th* (p. 2217).
75. Mahdi, E., Hamouda, A. S. M., Mokhtar, A. S., & Majid, D. L. (2005). Many aspects to improve damage tolerance of collapsible composite energy absorber devices. *Composite structures*, *67*(2), 175-187.
76. Steeves, C. A., & Fleck, N. A. (2004). Collapse mechanisms of sandwich beams with composite faces and a foam core, loaded in three-point bending. Part I: analytical models and minimum weight design. *International Journal of Mechanical Sciences*, *46*(4), 561-583.
77. Chakravarty, U. K. (2010). An investigation on the dynamic response of polymeric, metallic, and biomaterial foams. *Composite structures*, *92*(10), 2339-2344.
78. Thornton, P. H. (1980). Energy absorption by foam filled structures. *SAE Transactions*, 529-539.
79. Ma, W., & Feichtinger, K. (2016). Rigid structural foam and foam-cored sandwich composites. In *Polymeric Foams* (pp. 273-332). Boca Raton, FL: CRC Press.
80. Tawfik, B. E. (2016). *Use of Composites as Alternative Materials in Ship Structures* (Doctoral dissertation, Alexandria University).

81. Leon, R. T., & Deierlein, G. G. (1996). Considerations for the use of quasi-static testing. *Earthquake spectra, 12*(1), 87-109.

82. Alkateb, M., Sapuan, S. M., Leman, Z., Jawaid, M., & Ishak, M. R. (2018). Quasi-static crush behavior of environmentally friendly kenaf/wool epoxy composites elliptical tube. *Journal of Mechanical Engineering and Sciences*, *12*(2), *3671-3688.*

83. Ramakrishna, S., & Hamada, H. (1998). Energy absorption characteristics of crashworthy structural composite materials. *Key engineering materials (Vol. 141, pp. 585-622)*. Zurich, ZH: Trans Tech Publications Ltd.

84. Xiang, Y., Yu, T., & Yang, L. (2016). Comparative analysis of the energy absorption capacity of polygonal tubes, multi-cell tubes, and honeycombs by utilizing key performance indicators. *Materials & Design*, *89*, 689-696.

85. Alkhatib, S. E., Matar, M. S., Tarlochan, F., Laban, O., Mohamed, A. S., & Alqwasmi, N. (2019). Deformation modes and crashworthiness energy absorption of sinusoidally corrugated tubes manufactured by direct metal laser sintering. *Engineering Structures, 201*, 109838.

86. Duarte, I., Krstulović-Opara, L., Dias-de-Oliveira, J., & Vesenjak, M. (2019). Axial crush performance of polymer-aluminium alloy hybrid foam filled tubes. *Thin-Walled Structures, 138*, 124-136.

87. Cao, X., Duan, S., Liang, J., Wen, W., & Fang, D. (2018). Mechanical properties of an improved 3D-printed rhombic dodecahedron stainless steel lattice structure of variable cross section. *International Journal of Mechanical Sciences, 145*, 53-63.

88. Mamalis, A. G., Robinson, M., Manolakos, D. E., Demosthenous, G. A., Ioannidis, M. B., & Carruthers, J. (1997). Crashworthy capability of composite material structures. *Composite structures*, *37*(2), 109-134.

89. Carruthers, J. J., Kettle, A. P., & Robinson, A. M. (1998). Energy absorption capability and crashworthiness of composite material structures: a review. *Applied Mechanics Reviews*, *51*(10), 635-649.

90. Reddy, S. S., Yuvraj, C., & Rao, K. P. (2015). Design, analysis, fabrication and testing of CFRP with CNF composite cylinder for space applications. *International Journal of Composite Materials*, *5*(5), 102-128.

91. Farley, G. L. (1991). The effects of crushing speed on the energy-absorption capability of composite tubes. *Journal of Composite Materials*, *25*(10), 1314-1329.

92. Sigalas, I., Kumosa, M., & Hull, D. (1991). Trigger mechanisms in energy-absorbing glass cloth/epoxy tubes. *Composites Science and Technology*, *40*(3), 265-287.

93. Schmueser, D. W., & Wickliffe, L. E. (1987). Impact energy absorption of continuous fiber composite tubes. *Trans. ASME 109*, 72-77

94. Berry, J., & Hull, D. (1984). Effect of speed on progressive crushing of epoxy glass cloth tubes. In the *Institute of physics conference series*, *70*, 463-470. New York, NY: Plenum Publishing Corp.

95. Zhu, G., Sun, G., Liu, Q., Li, G., & Li, Q. (2017). On crushing characteristics of different configurations of metal-composites hybrid tubes. *Composite Structures*, *175*, 58-69.

96. Shin, K. C., Lee, J. J., Kim, K. H., Song, M. C., & Huh, J. S. (2002). Axial crush and bending collapse of an aluminum/GFRP hybrid square tube and its energy absorption capability. *Composite structures*, *57*(1-4), 279-287.

97. Supian, A. B. M., Sapuan, S. M., Zuhri, M. Y. M., Zainudin, E. S., & Ya, H. H. (2019). Crashworthiness performance of hybrid kenaf/glass fiber reinforced epoxy tube on winding orientation effect under quasi-static compression load. *Defence Technology*.

98. Thornton, P. H. (1990). The crush behavior of pultruded tubes at high strain rates. *Journal of Composite Materials*, *24*(6), 594-615.

99. Hamada, H., & Ramakrishna, S. (1996). Impact performance of glass cloth/epoxy composite tubes with different surface treatment. *Composite Interfaces*, *4*(1), 35-44.

100. Sun, G., Wang, Z., Hong, J., Song, K., & Li, Q. (2018). Experimental investigation of the quasi-static axial crushing behavior of filament-wound CFRP and aluminum/CFRP hybrid tubes. *Composite Structures*, *194*, 208-225.

101. Mahdi, E., Hamouda, A. A., & Sebaey, T. A. (2014). The effect of fiber orientation on the energy absorption capability of axially crushed composite tubes. *Materials & Design (1980-2015)*, *56*, 923-928.

102. Chiu, L. N., Falzon, B. G., Ruan, D., Xu, S., Thomson, R. S., Chen, B., & Yan, W. (2015). Crush responses of composite cylinder under quasi-static and dynamic loading. *Composite Structures*, *131*, 90-98.

103. Jia, X., Chen, G., Yu, Y., Li, G., Zhu, J., Luo, X., Duan, C., Yang, X., & Hui, D. (2013). Effect of geometric factor, winding angle, and pre-crack angle on quasi-static crushing behavior of filament wound CFRP cylinder. *Composites Part B: Engineering*, *45*(1), 1336-1343.

104. Mahdi, E., & Sebaey, T. A. (2014). An experimental investigation into crushing behavior of radially stiffened GFRP composite tubes. *Thin-Walled Structures, 76*, 8-13.

105. Hu, D., Zhang, C., Ma, X., & Song, B. (2016). Effect of fiber orientation on energy absorption characteristics of glass cloth/epoxy composite tubes under axial quasi-static and impact crushing condition. *Composites Part A: Applied Science and Manufacturing*, *90*, 489-501.

106. Hamada, H., Coppola, J. C., Hull, D., Maekawa, Z., & Sato, H. (1992). Comparison of energy absorption of carbon/epoxy and carbon/PEEK composite tubes. *Composites*, *23*(4), 245-252.

107. Elgalai, A. M., Mahdi, E., Hamouda, A. M. S. & Sahari, B. S. (2004). Crushing response of composite corrugated tubes to quasi-static axial loading. *Composite Structures*, *66*(1-4), 665-671.

108. Yan, L., Chouw, N., & Jayaraman, K. (2014). Effect of triggering and polyurethane foam-filler on axial crushing of natural flax/epoxy composite tubes. *Materials & Design (1980-2015)*, *56*, 528-541.

APPENDIX

The following graphs were used to find the % iCFE within 0.1 from ideal values used when examining crush force efficiency performance:

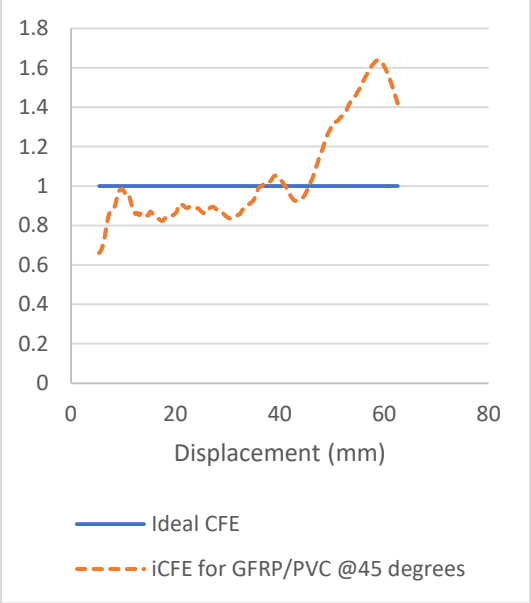

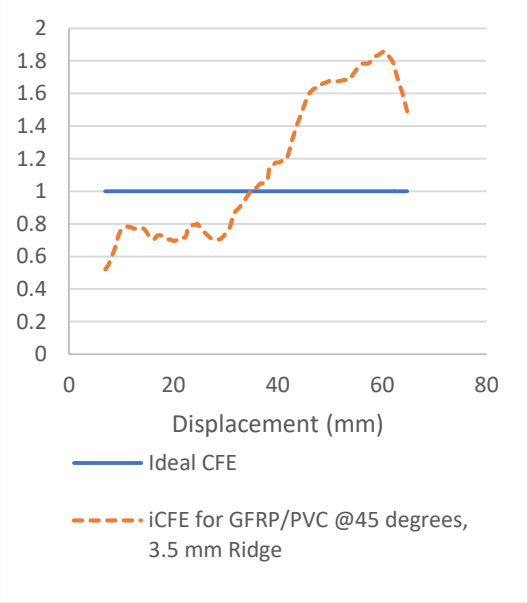

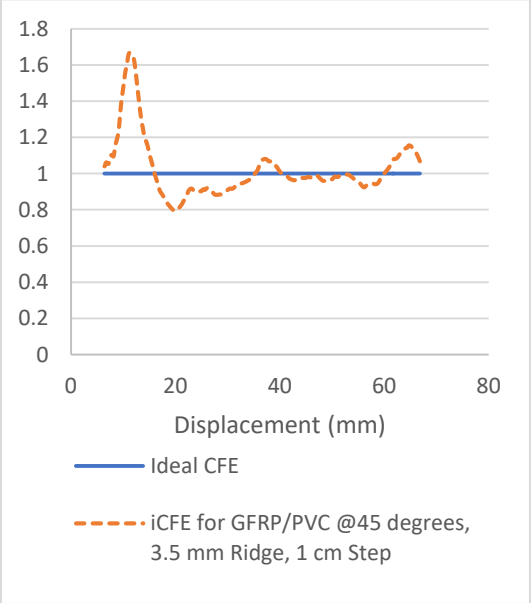

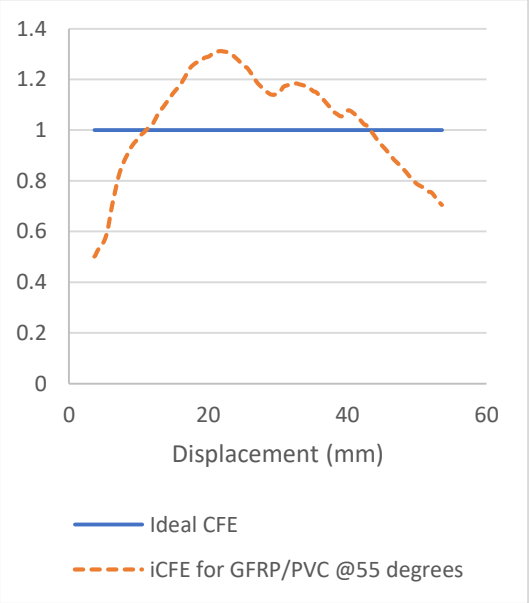

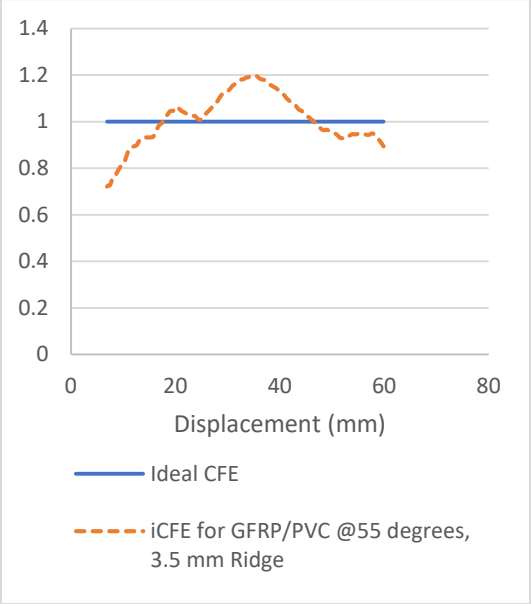
1.4
1.2
1
0.8
0.6
0.4
0.2
0
0
20
40
60
80
Displacement (mm)
Ideal CFE
iCFE for GFRP/PVC @55 degrees, 3.5 mm Ridge

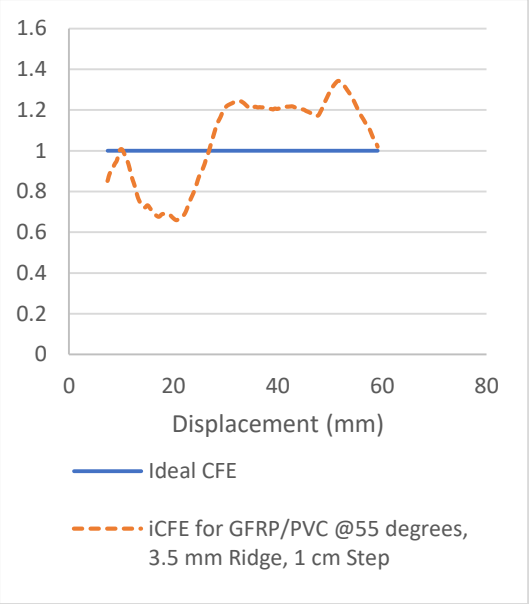
1.6
1.4
1.2
1
0.8
0.6
0.4
0.2
0
0
20
40
60
80
Displacement (mm)
Ideal CFE
iCFE for GFRP/PVC @55 degrees, 3.5 mm Ridge, 1 cm Step

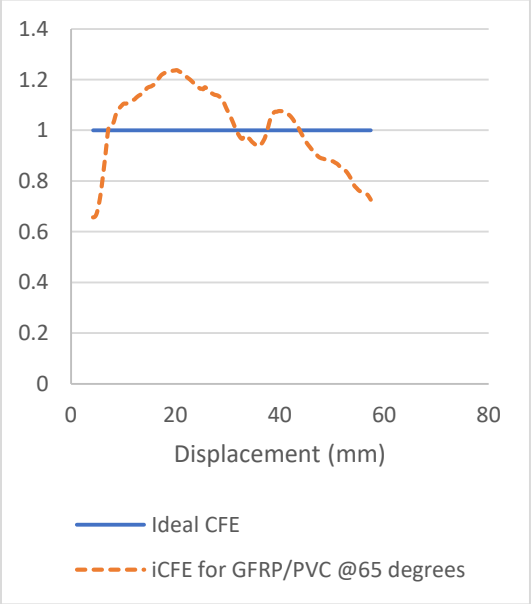
1.4
1.2
1
0.8
0.6
0.4
0.2
0
0
20
40
60
80
Displacement (mm)
Ideal CFE
iCFE for GFRP/PVC @65 degrees

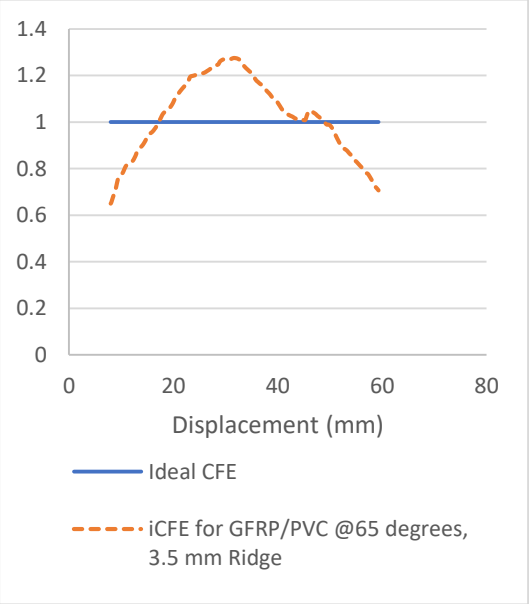
1.4
1.2
1
0.8
0.6
0.4
0.2
0
0
20
40
60
80
Displacement (mm)
Ideal CFE
iCFE for GFRP/PVC @65 degrees, 3.5 mm Ridge

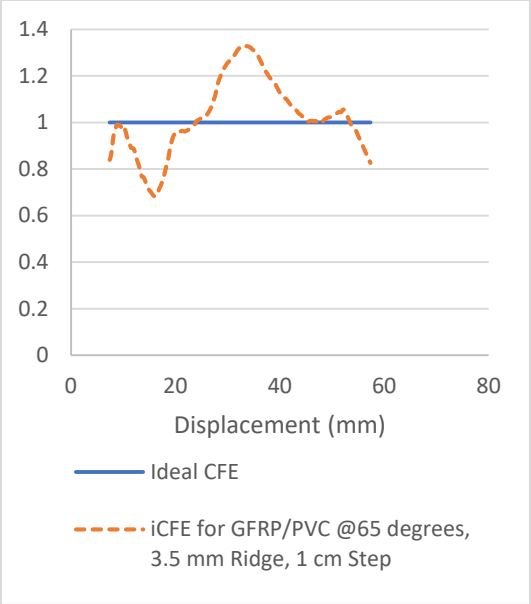
1.4
1.2
1
0.8
0.6
0.4
0.2
0
0
20
40
60
80
Displacement (mm)
Ideal CFE
iCFE for GFRP/PVC @65 degrees, 3.5 mm Ridge, 1 cm Step

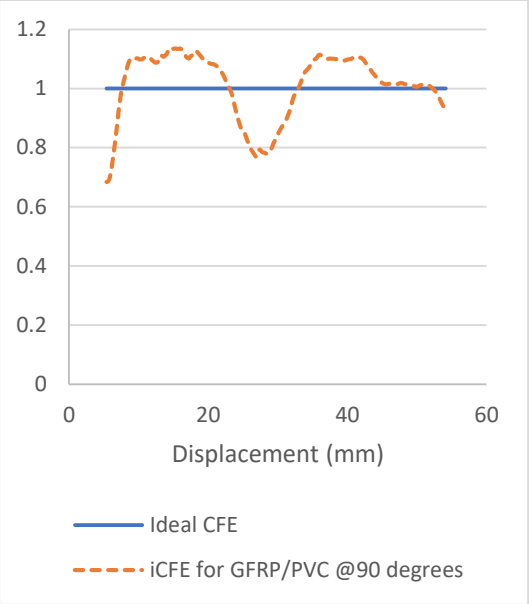
1.2
1
0.8
0.6
0.4
0.2
0
0
20
40
60
Displacement (mm)
Ideal CFE
iCFE for GFRP/PVC @90 degrees

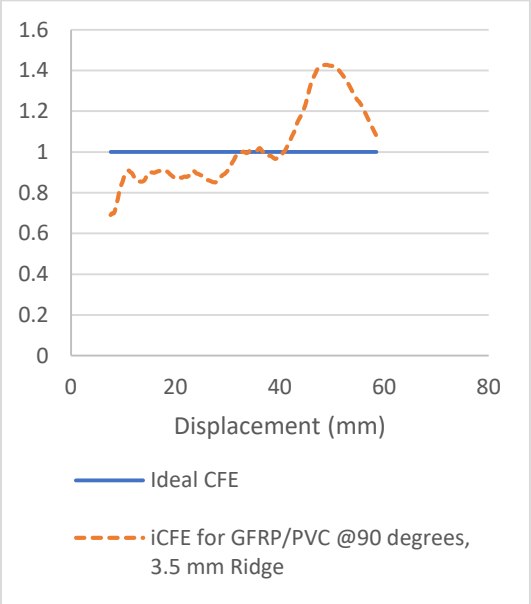
1.6
1.4
1.2
1
0.8
0.6
0.4
0.2
0
0
20
40
60
80
Displacement (mm)
Ideal CFE
iCFE for GFRP/PVC @90 degrees, 3.5 mm Ridge

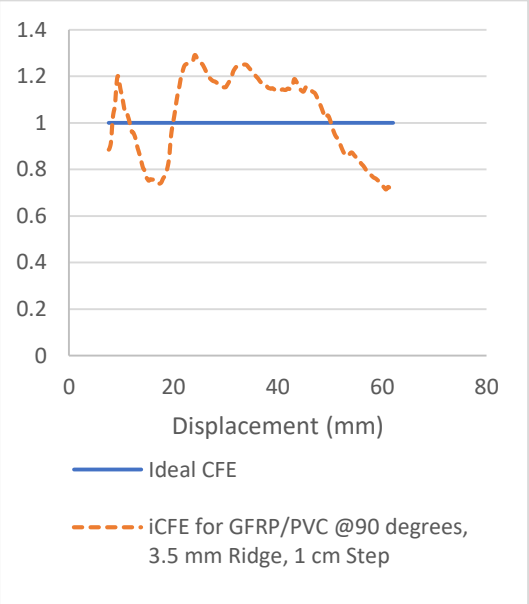
1.4
1.2
1
0.8
0.6
0.4
0.2
0
0
20
40
60
80
Displacement (mm)
Ideal CFE
iCFE for GFRP/PVC @90 degrees, 3.5 mm Ridge, 1 cm Step

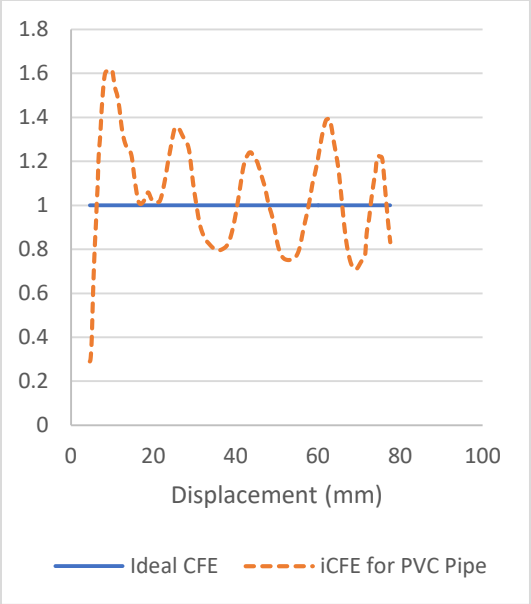
1.8
1.6
1.4
1.2
1
0.8
0.6
0.4
0.2
0
0
20
40
60
80
100
Displacement (mm)
Ideal CFE
iCFE for PVC Pipe

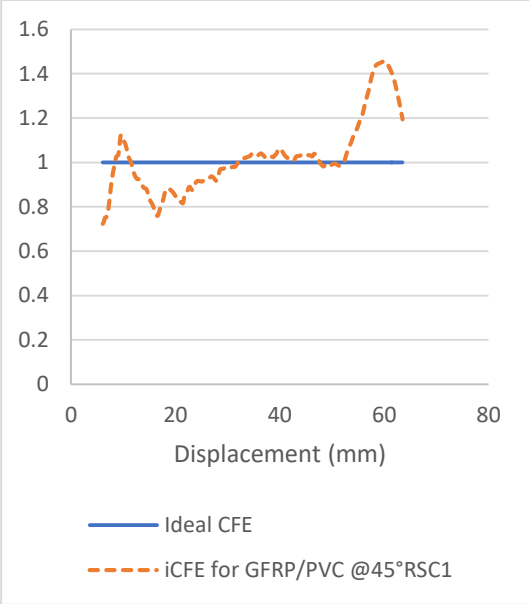
1.6
1.4
1.2
1
0.8
0.6
0.4
0.2
0
0
20
40
60
80
Displacement (mm)
Ideal CFE
iCFE for GFRP/PVC @45°RSC1

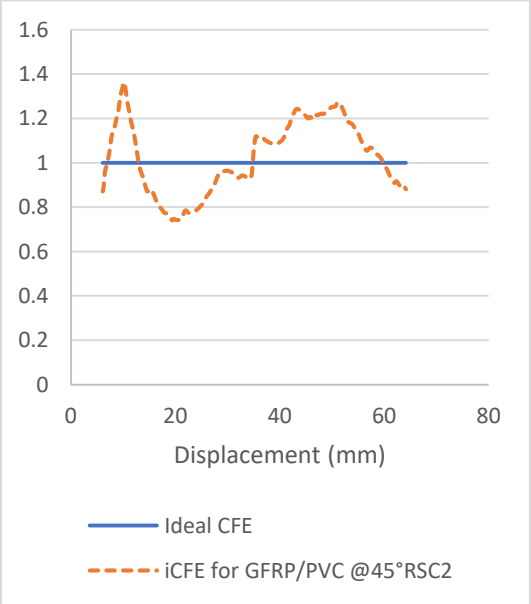
1.6
1.4
1.2
1
0.8
0.6
0.4
0.2
0
0
20
40
60
80
Displacement (mm)
Ideal CFE
iCFE for GFRP/PVC @45°RSC2

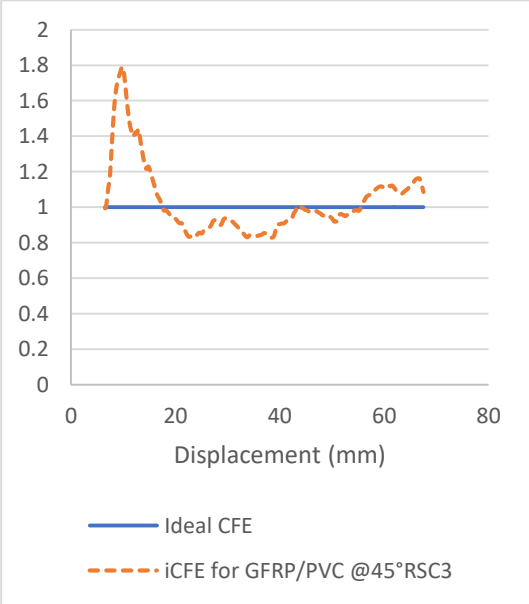
2
1.8
1.6
1.4
1.2
1
0.8
0.6
0.4
0.2
0
0
20
40
60
80
Displacement (mm)
Ideal CFE
iCFE for GFRP/PVC @45°RSC3

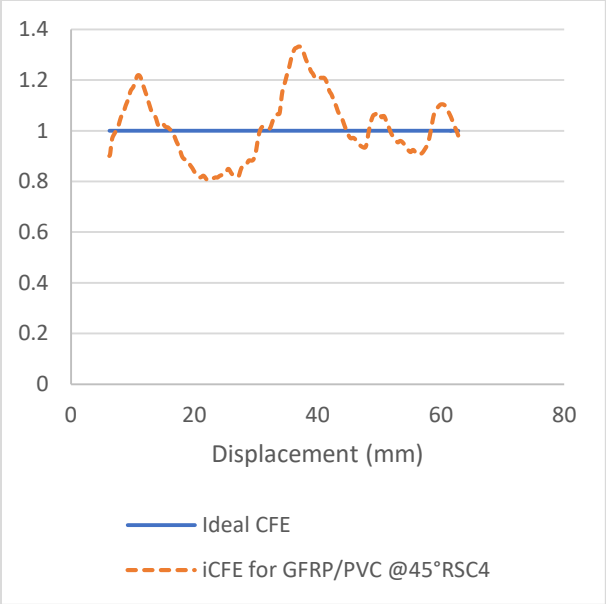
1.4
1.2
1
0.8
0.6
0.4
0.2
0
0
20
40
60
80
Displacement (mm)
Ideal CFE
iCFE for GFRP/PVC @45°RSC4